Using Lipid Biomarkers and their Isotopic Composition to reconstruct the Late Pleistocene Paleoclimate of the Amazon Basin

Dissertation zur Erlangung des Doktorgrades der Naturwissenschaften
Dr. rer. nat.

Am Fachbereich Geowissenschaften
der Universität Bremen

Vorgelegt von

Christoph Häggi

Bremen
Dezember 2016

Erstgutachter

Prof. Dr. Michael Schulz, Universität Bremen

Zweitgutachter

Dr. Boris Jansen, Universität Amsterdam

Tag des Prüfungskolloquiums

13. März 2017

Versicherung an Eides Statt

gem. § 5 Abs. 5 der Promotionsordnung vom 15.07.2015

Ich, _____
(Vorname, Name, Anschrift, ggf. Matr. -Nr.)

versichere an Eides Statt durch meine Unterschrift, dass ich die vorstehende Arbeit selbständig und ohne fremde Hilfe angefertigt und alle Stellen, die ich wörtlich dem Sinne nach aus Veröffentlichungen entnommen habe, als solche kenntlich gemacht habe, mich auch keiner anderen als der angegeben Literatur oder sonstiger Hilfsmittel bedient habe, und die zu Prüfungszwecken beigelegte elektronische Version der Dissertation mit der abgegebenen gedruckten Version identisch ist.

Ich versichere an Eides Statt, dass ich die vorgenannten Angaben nach bestem Wissen und Gewissen gemacht habe und dass die Angaben der Wahrheit entsprechen und ich nichts verschwiegen habe.

Die Strafbarkeit einer falschen eidesstattlichen Versicherung ist mir bekannt, namentlich die Strafandrohung gemäß §156 StGB bis zu drei Jahren Freiheitsstrafe oder Geldstrafe bei vorsätzlicher Begehung der Tat bzw. gemäß §161 Abs. 1 StGB bis zu einem Jahr Freiheitsstrafe oder Geldstrafe bei fahrlässiger Begehung.

_____ _____

Ort, Datum Unterschrift

Table of Contents

Abstract

The Amazon rainforest is the largest rainforest on the earth and is an important part of the global hydrologic and carbon cycles. To understand the processes controlling climate and vegetation in the Amazon Basin, a firm understanding of the past is needed. The past climate and vegetation evolution of the Amazon is, however, contested. Especially the response of the Amazonian climate to glacial conditions during the Pleistocene is still subject to debate. On the one hand, there is the view that humid conditions persisted through the late Pleistocene and that the Amazon rain forest was essentially stable during the late Pleistocene. On the other hand, there is the hypothesis that glacial conditions resulted in extensive drying in the Amazon Basin that led to partial replacement of forest with savannah vegetation. The persistence of these two competing hypothesis has multiple reasons. Firstly, there are only few climate records that represent the interior Amazon Basin and most reconstructions come from the edge of the basin, resulting in a low spatial resolution. Secondly, most of the records used for paleoclimate reconstructions have a low temporal resolution and in some cases feature hiatuses. Thirdly, most of the records are based on pollen reconstructions, which does not allow to reconstruct climate and vegetation independently.

In this study, lipid biomarkers and their isotopic composition were used to reconstruct hydroclimate and vegetation independently. To circumvent the problems of low spatial and temporal resolution, an offshore sediment core (GeoB16224-1, 6°39.38'N, 52°04.99'W) integrating the sediment input from the entire Amazon Basin was used. The core was retrieved from the continental margin off French Guiana and covers the time range from 50000 to 12800 years before present. Since core GeoB16224-1 has a constant sedimentation rate, it allows to study the Amazonian history at a better temporal resolution than previous records from the interior Amazon Basin. To find suitable biomarker proxies, sediment samples from the Amazon River and its tributaries as well as the marine deposition areas in the Atlantic Ocean were studied along with samples of suspended sediment from the Amazon Plume.

To analyze past variations in the Amazon Plume, a biomarker based salinity proxy was searched for. To this end, samples of suspended sediment from the salinity gradient induced by the Amazon Plume were used to calibrate a lipid biomarker based salinity proxy. The stable hydrogen isotope composition (δD) of sea water correlates with salinity. Hence, biomarkers that reflect δD of sea water can be used as salinity proxy. In this study, δD of alkenones and palmitic acid were tested. Alkenones are produced specifically by haptophytes, while palmitic acid is a ubiquitous organic molecule that is dominantly

produced by aquatic organisms in marine environments. Results showed that δD of alkenones did not reflect δD of sea water in most samples. This was likely caused by limited growth rates of haptophytes in response to low salinity conditions and light limitation in the Amazon Plume. Conversely, δD of palmitic acid consistently reflected δD of seawater. However, palmitic acid is easily degradable and can be produced deeper in the water column and has therefore its own limitations.

In order to have independent proxies for the precipitation and vegetation history of the Amazon Basin, the isotopic composition of long-chain *n*-alkanes was tested. Long chain *n*-alkanes are plant-wax biomarkers that constitute the wax coating of leaves. To have a measure for the precipitation intensity in the Amazon Basin, the stable hydrogen composition (δD) of long-chain *n*-alkanes was studied. δD of plant-waxes reflects the isotope composition of meteoric water, which is controlled by the amount effect in the tropics. Hence, δD of plant-waxes can be used to reconstruct past precipitation amounts. The study of sediment samples from the Amazon River and its tributaries revealed that δD of long-chain *n*-alkanes reflects the average δD composition of precipitation in each tributary. Furthermore, the results showed the values at the Amazon estuary represented an integrated signal from the tributaries. This indicates that i) the plant-waxes deposited offshore the Amazon estuary originate from the different geographical sectors of the Amazon Basin; ii) the compounds are refractory during the transport from the western parts of the basin; iii) unlike, inorganic sediment, which is mainly derived from the Andes, plant-wax biomarkers are mainly lowland sourced.

The stable carbon isotope composition ($\delta^{13}C$) of plant-waxes allows to differentiate between vegetation types using the C3 and C4 photosynthetic pathways. Since forest taxa mostly use the C3 metabolisms, while tropical savannah taxa use the C4 metabolism, this method allows to study potential shifts in dominant vegetation type. River bed sediment samples from the Amazon Basin indeed showed more depleted $\delta^{13}C$ values expected for C3 vegetation, while more enriched values from marine core tops offshore Northeastern Brazil reflected the local mixed C3/C4 vegetation.

The results of the down core *n*-alkane δD reconstruction showed that precipitation amounts during MIS 3 were comparable with present day conditions, while there was a moderate drying in the wake of full glacial conditions in MIS 2. During the deglaciation, conditions became more humid again. Model simulations using a comprehensive climate model showed that glacial drying in the Amazon was caused by the interplay of decreased precipitable water and a weakening of tropical convection. The results of the $\delta^{13}C$ based vegetation reconstruction showed that forest vegetation in the Amazon Basin persisted through the late Pleistocene. Small scale savannah intrusions were limited to Heinrich

Stadials. These results indicate that Amazon forest was resilient towards glacial drying. The savannah intrusions during Heinrich Stadials likely occurred in the north of the basin as consequence of a southward shift of the tropical rain belt. In conclusion, this thesis shows that the climate conditions in the Amazon Basin were relatively stable during the late Pleistocene. Savanna expansion during Heinrich Stadials potentially linked otherwise separated savannah patches in the Amazon forest and thereby opened migration routes, which could contribute to the explanation of the current biogeography in the tropical South America.

Zusammenfassung

Der Amazonasregenwald ist der größte Regenwald der Erde und ein wichtiger Bestandteil der globalen Wasser- und Kohlenstoffkreisläufe. Um zu verstehen welche Prozesse die zukünftige Entwicklung von Klima und Regenwald im Amazonasbecken beeinflussen, wird ein möglichst vollständiges Verständnis vergangener Entwicklungen benötigt. Wie sich Vegetation und Klima im Amazonasregenwald in der Vergangenheit entwickelt haben, ist jedoch umstritten. Insbesondere ist es nach wie vor unklar, wie das Klima im Amazonas auf die Eiszeiten während des Pleistozäns reagiert hat. Einerseits wurde ein vorwiegend feuchtes Klima, das während des gesamten Pleistozäns Bestand hatte, postuliert. Andererseits wird auch die Hypothese vertreten, dass glaziale Maxima zu ausgeprägter Trockenheit im Amazonasbecken führten, was womöglich auch eine partielle Ausbreitung von Savannenvegetation zur Folge hatte. Es gibt mehrere Gründe für diese unterschiedlichen Auffassungen. Erstens stammen die meisten Klimarekonstruktionen von den Rändern des Amazonasbeckens, während es nur sehr wenige Rekonstruktionen aus dem zentralen Amazonasbecken gibt. Zweitens verfügen die meisten dieser Rekonstruktionen über eine schlechte zeitliche Auflösung und werden zudem in verschiedenen Fällen durch Hiatus unterbrochen. Drittens basieren die meisten dieser Rekonstruktionen auf Pollenanalysen, die keine separate Analyse der Klima- und Vegetationsgeschichte ermöglichen.

In dieser Arbeit wurden Lipidbiomarker und deren Isotopenzusammensetzung verwendet um Klima und Vegetation unabhängig voneinander zu rekonstruieren. Das bisherige Problem niedriger zeitlicher und räumlicher Auflösung wurde durch einen hoch aufgelösten marinen Sedimentkern (GeoB16224-1, 6°39.38’N, 52°04.99’W) überwunden, der den Sedimenteintrag über das gesamte Amazonasbecken integriert. Der Sedimentkern wurde vom Kontinentalrand vor der Küste Französisch Guyanas genommen, wo während des Spätpleistozäns kontinuierliche Sedimentation stattfand und deckt den Zeitraum von 50000 bis 12000 Jahren vor heute ab. Aufgrund der regelmäßigen Sedimentationsraten erlaubt der Kern wesentlich genauere und höher aufgelöste Rekonstruktionen als bisher. Um geeignete Biomarkerproxies für die Niederschlags- und Vegetationsrekonstruktion zu finden, wurden sowohl Sedimentproben vom Amazonas und dessen Zuflüssen als auch marine Sedimentproben aus dem küstennahen Atlantischen Ozean analysiert. Weiter wurden Suspensionsproben von der Ausflußplume des Amazonas in den Atlantischen Ozean studiert.

Um Veränderungen in der Ausflußplume des Amazonas zu rekonstruieren, wurde nach einem Biomarker-basierten Salinitätsproxy gesucht. Dazu wurden Suspensionsproben

verwendet, die den Salinitätsgradienten vom Amazonas in den offenen Ozean abdeckten. Das Isotopenverhältnis der stabilen Wasserstoffisotope (δD) von Meerwasser korreliert mit der Salinität, weshalb ein Proxy, der δD von Meerwasser wiederspiegelt, gesucht wurde. In dieser Arbeit wurden sowohl δD von Alkenonen als auch Palmitinsäure getestet. Alkenone sind langkettige Ketone die spezifisch von Haptophyten produziert werden, während Palmitinsäure von den meisten Lebewesen synthetisiert wird und in mariner Umgebung vorwiegend von aquatischen Organismen stammt. Die Resultate zeigten, dass δD von Alkenonen in den meisten Proben keinen Zusammenhang mit δD von Meereswasser aufwiesen, was wahrscheinlich in limitierten Wachstumsraten von Haptophyten begründet liegt, die aufgrund von Lichtmangel und niedriger Salinität zustande kamen. Dagegen korrelierte δD von Palmitinsäure mit δD des Meerwassers. Die Verwendung von Palmitinsäure hat jedoch ebenfalls Nachteile, da dieses Molekül auch in größerer Wassertiefe produziert wird und damit nicht zwingend Oberflächenkonditionen widerspiegelt. Zudem ist Palmitinsäure im Gegensatz zu Alkenonen auch wesentlich weniger resistent gegen Degradation.

Zur Rekonstruktion von Niederschlagsmenge und Vegetationszusammensetzung im Amazonsbecken wurde die Isotopenzusammensetzung von langkettigen *n*-Alkanen getestet. Langkettige *n*-Alkane sind Pflanzenwachsbiomarker, welche die Wachsschicht von Blättern bilden. Als Proxy für die Niederschlagsmenge wurde δD von langkettigen *n*-Alkanen verwendet. δD von *n*-Alkanen wiederspiegelt das Isotopenverhältnis von Niederschlag, welches in den Tropen vom Mengeneffekt kontrolliert wird. Damit ist δD von *n*-Alkanen in den Tropen niederschlagsabhängig. Die Analyse von Sedimentproben aus den Amazonaszuflüssen zeigte, dass δD von langkettigen *n*-Alkanen die mittlere δD Komposition des Niederschlags im Einzugsgebiet des jeweiligen Zuflusses wiederspiegelt. *n*-Alkane von der Mündung des Amazonas in den Atlantik zeigten ein integriertes Signal der verschiedenen Zuflüsse. Dies ermöglicht folgende Rückschlüsse: i) *n*-Alkane die im Atlantik abgelagert werden stammen aus den verschiedenen Teilen des Amazonasbeckens. ii) *n*-Alkane sind refraktär während des Transports aus westlichen Teilen des Amazonasbeckens. iii) Im Gegensatz zu anorganischem Sediment, das größtenteils aus den Anden stammt, kommen *n*-Alkane mehrheitlich aus dem Tiefland.

Das Verhältnis der stabilen Kohlenstoffisotope (δ^{13}C) in langkettigen *n*-Alkanen ermöglicht es zwischen Vegetationstypen, die dominant den C3 oder den C4 Fotosynthesemetabolismus verwenden, zu differenzieren. Da Waldvegetation vornehmlich den C3 Metabolismus nutzt, während tropische Savannengräser den C4 Metabolismus verwenden, ermöglicht δ^{13}C von *n*-Alkanen die Rekonstruktion potentieller Savannenausbreitung im Amazonasregenwald. Sedimentproben aus dem Amazonas wiesen die für C3-Vegetation erwarteten δ^{13}C abgereicherte Werte auf, während für

marine Sedimentproben aus Nordost-Brasilien angereicherte Werte gemessen wurden, die für die lokale semiaride Vegetation zu erwarten war, die aus einem Mix von C3 und C4 Pflanzen besteht.

Die Resultate der auf δD von *n*-Alkanen basierten Niederschlagsrekonstruktion liefern Indizien dafür, dass der Niederschlag während dem Großteil des studierten Zeitraums mit heutigen Verhältnissen vergleichbar war. Einzig während des letzten glazialen Maximums wurden trockenere Bedingungen rekonstruiert. Während des Deglazials wurden die Klimaverhältnisse wieder feuchter. Klimamodellsimulationen zeigten auf, das die trockeneren Verhältnisse während des letzten glazialen Maximums vom Zusammenspiel von reduziertem ausfällbaren Niederschlagswasser und einer Abschwächung der tropischen Konvektion verursacht wurden. Die Resultate der $\delta^{13}C$ basierten Vegetationsrekonstruktion bestätigten die Hypothese, dass Waldvegetation im Amazonasbecken während des späten Pleistozäns Bestand hatte. Dies deutet darauf hin, dass das glaziale Maximum nur moderat trockener war, was nicht zur Verdrängung des Waldes durch Savannenvegetation führte. Hingegen fand limitierte Savannenausbreitung während Heinrich Stadialen statt. Diese Savannenausbreitung war wahrscheinlich die Folge der südwärts Bewegung der tropischen Regenzone während Heinrich Stadialen und fand daher wohl im Norden des Beckens statt. Abschließend lässt sich sagen, dass die Klima- und Vegetationsverhältnisse während des Spätpleistozäns im Amazonasbecken relativ stabil waren. Die Savannenausbreitung während Heinrich Stadialen trug womöglich zur Öffnung von Korridoren zwischen sonst getrennten Savannenflächen im Amazonasbecken bei, was zum Verständnis der heutigen Biogeographie beitragen könnte.

Acknowledgements

The three years of conducting research on the Amazon Basin have been a great and insightful experience. Therefore, I want to thank everyone who has contributed to the completion of this thesis. Especially, I want to thank Michael Schulz and Enno Schefuss for supervising this thesis and for offering me an exciting and rewarding PhD-position. Many thanks also to the members of my Thesis Committee, Gesine Mollenhauer and Stefan Mulitza. Thank you very much for many constructive meetings, which were instrumental in advancing this thesis to a satisfactory conclusion.

I want thank everyone who contributed to the AMADEUS project. Working in the framework of a larger scientific effort was very rewarding. Special thanks go to the project partners from Sao Paulo, Brazil. Thanks to Cristiano M. Chiessi for critically discussing and guiding all the manuscripts in this thesis. Many thanks go also to André O. Sawakuchi who hosted me for a two month research stay at the Geoscience Department of the University of Sao Paulo. This included two field trips to the Amazon River. Navigating most of the Brazilian Amazon River was an exciting and memorable experience for which I am immensely grateful. I also want to take Dailson Bertassoli Jr. for engaging in the sampling effort during these trips and for many ours of sample filtering on deck. Many thanks also to the fellow PhD students working within the framework of the AMADEUS project, Stefano Crivellari, Natalie Höppner, Shuwen Sun and Yancheng Zhang, for many interesting discussions on the Amazonian paleoclimate.

The laboratory work conducted in this thesis would not have been possible without the help of Jens Hefter and Ralph Kreutz whom I thank for their technical support and for keeping the GC-FID, HPLC and IRMS running. The instruction into the technicalities of biomarker analyses were very helpful. I also want to thank Ute Merkel and Matthias Prange for contributing climate modelling results, which were important for the interpretation of the paleoclimate record. Also many thanks to Hiwi Birk Stern for his assistance in the sample preparation and for many hours of sample grinding.

I thank Dierk Hebbeln and Tina Klose for administrating the GLOMAR Graduate School, which offered a diverse and helpful course program. Also many thanks to the GLOMAR-Postdoc Dana Pittauer for organizing interesting monthly research seminars. I also want to thank Nicole Hermann, Xueqin Zhao, James Collins and Friederike Grimmer for the nice atmosphere in our office and for sharing and solving the every-day problems of being a PhD-student.

Finally, I want to thank my parents and family for their support over the years.

1. Introduction

1.1. Significance of the Amazon Basin

The Amazon River is the largest river system on Earth and its runoff amounts to 15-20% of the global freshwater discharge (Dai and Trenberth, 2002). The Amazon River raises in the Peruvian and Bolivian Andes and flows along a west- east path, slightly south of the equator through an extensive lowland basin before it discharges into the western Atlantic Ocean (Fig. 1.1). The Amazon River drains large parts of tropical South America and is home to extensive floodplains, where sediment transported from the Andes is stored and deposited (Archer, 2005). The main tributaries of the Amazon are classified into white water tributaries which transport large amounts of sediment from the Andes to the lowland and clear and black water tributaries, which have their source in lowland regions and transport only small amounts of sediment. The major white water tributaries are the Solimões[1] and the Madeira Rivers, which both drain the western parts of the basin (Fig. 1.1) (Gibbs, 1967). The Solimões River is sourced in the northwestern Andes in Peru, Ecuador and Columbia, while the Madeira River is mostly sourced in the Bolivian Andes. The largest lowland tributary, the Negro River is a black water river. The black water stems from the high concentration in fulvic and humic acids from old degraded soils (Konhauser et al., 1994). Although the Negro River transports a low amount of sediment, it yields high concentrations in dissolved organic carbon. The Negro River drains the northernmost parts of the Amazon Basin and converges with Solimões River in Manaus forming the Amazon River. The two largest clear water tributaries are the Tapajos and Xingu Rivers. Both rivers drain the south eastern parts of the lowland Amazon Basin.

Most of the Amazon catchment is covered by the eponymous tropical rainforest (Fig. 1.1). Minor portions of the savanna vegetation can be found at the northern and the southern edges of the Amazon, while alpine vegetation types are present in the Andes (Figure 1.1) (Olson et al., 2001). The flood plains in the Amazon Basin are covered by Várzea forest, a mixed grassland and forest vegetation type that also features tropical grasses using the C4 photosynthetic pathway (Hamilton et al., 2004). The Amazon rainforest is home to one of the most diverse faunas and floras in the world (Da Silva et al., 2005; Wright, 2002) and is responsible for 15% of global photosynthesis and plays therefore an important role in the

[1]In some definitions the Amazon River forms at the confluence between the Maranon and Ucayali Rivers in Nauta, Peru. In this thesis, the upper part of the Amazon between Manaus and Nauta is referred to as Solimões River according to the definition mostly used in Brazil.

global carbon cycle (Li et al., 2011b). The importance of the Amazon River and rainforest for the global carbon and hydrologic cycle has led to speculation on how these cycles may change as a result to future climate variations (Gloor et al., 2015; Phillips et al., 2009).

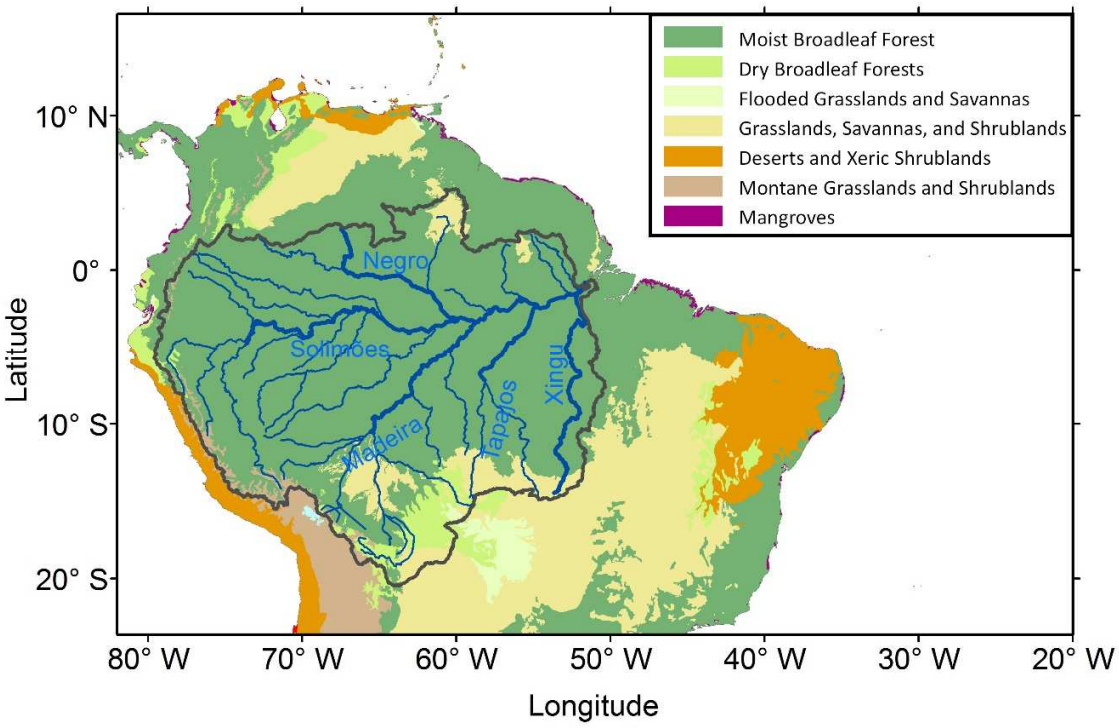

Figure 1.1. The present day potential vegetation cover in South America (Olson et al., 2001). The Amazon River and its major tributaries are marked in blue. The extent of the Amazon Basin is marked with black line. The names of the main tributaries are given in light blue.

1.2. Present day climatological setting

In most of the modern day Amazon Basin, tropical climate with humid and warm conditions can be found (Peel et al., 2007). In the lowland Basin, mean annual precipitation varies between 1500 and 3000 mm/year and mean annual temperatures are between 24 and 28°C, while drier and cooler conditions are found in the Andean parts of the basin (Hijmans et al., 2005). With exception of some northwestern parts of the Amazon Basin, which

experience year-round precipitation, most of the Amazon Basin is subject to substantial seasonal precipitation variations (Fig. 1.2). The highest precipitation amounts in the southern and central Amazon Basin are registered during the maximum of the South American Monsoon, which peaks during Austral summer in January and leads to humid conditions over most of the Amazon Basin (Garreaud et al., 2009) (Fig. 1.2A). During peak monsoonal conditions, large amounts of humid air are transported by the South American Low-Level Jet (SALLJ) along the eastern slopes of the Andes to the south (Marengo et al., 2004). Convection from the Amazon also extents to the South Atlantic Convergence Zone (SACZ) over south eastern Brazil, leading to intense local precipitation (Fig. 1.2A) (Carvalho et al., 2004). During boreal spring, convection moves northwards following the seasonal insolation maximum until it reaches its northernmost position during boreal summer (Fig. 1.2B). In July, precipitation takes mostly place in the northern parts of the basin, where it is aligned with the position of the Intertropical Convection Zone (ITCZ) (Fig. 1.2C). During October there is again a south ward shift of convection and precipitation over the central Amazon Basin and in the SACZ intensifies again (Fig. 1.2D) (Garreaud et al., 2009).

The main interannunal mode of climate variability influencing the Amazonian climate is the El Niño–Southern Oscillation (ENSO) (Brienen et al., 2012). While El Niño episodes lead to more humid conditions in the Andean parts of the basin, they result in drier conditions in the lowland Amazon Basin (Bookhagen and Strecker, 2009). Hence, El Niño episodes can lead to extensive droughts in the Amazon Basin (Jiménez-Muñoz et al., 2016). Conversely, La Niña episodes lead to wetter conditions (Bookhagen and Strecker, 2009). Compared to interannual variability, decadal variations in the South American climate are less well studied. This in part due to a lack of climate records covering multiple decadal climate cycles and in part due to the lower magnitude of variability (Garreaud et al., 2009). Nevertheless, recent studies have shown that the positive phase of the Pacific Decadal Oscillation led to an increase in precipitation in large parts of the Amazon Basin (Gloor et al., 2015).

Since the instrumental climate records maximally reach back to the 19th century, the study of climate variability on time scales exceeding a little more than a century is not possible from instrumental data. Therefore, the study of climate variability on longer time scales requires the reconstruction of past conditions based on paleoclimate proxy.

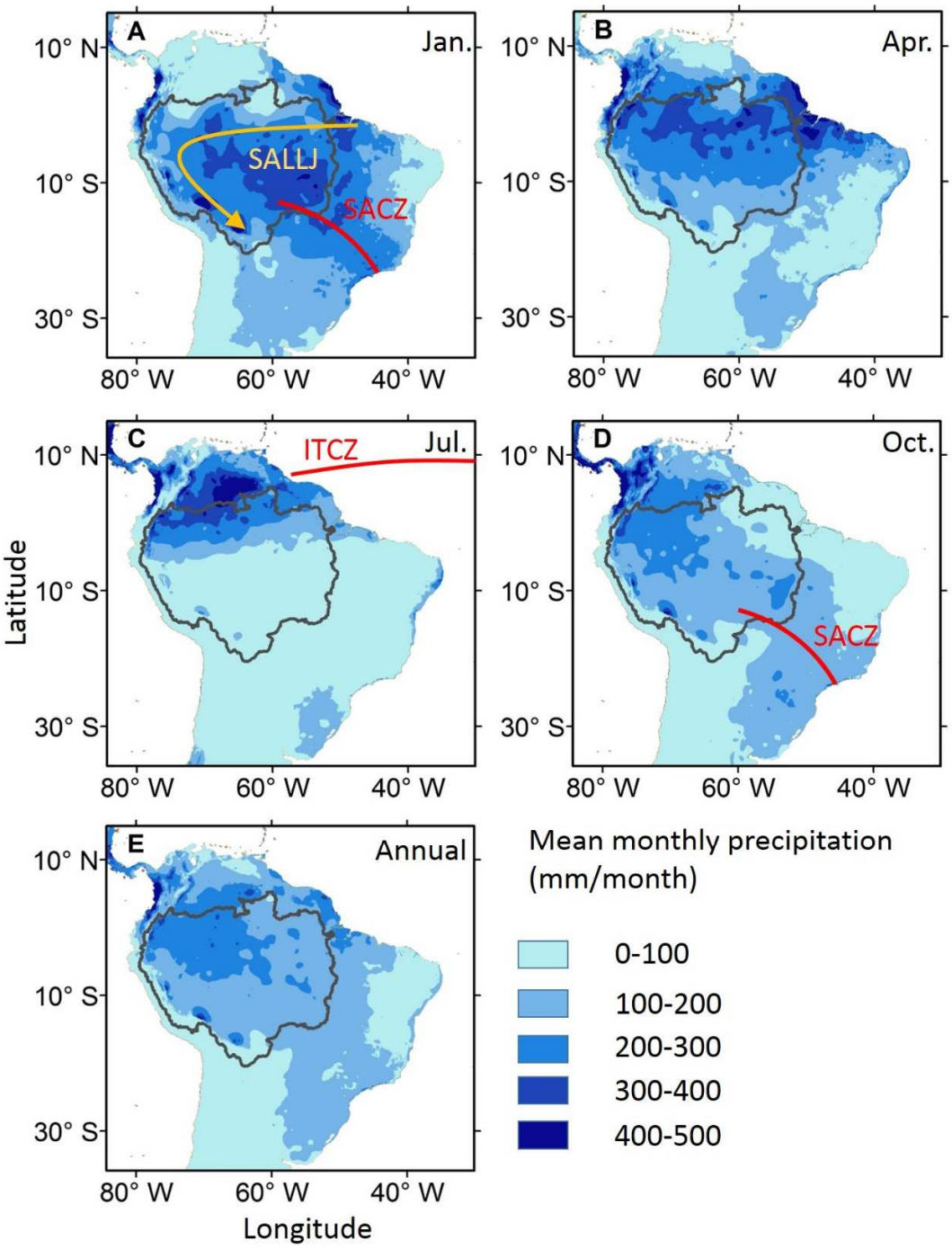

Figure 1.2. Seasonal precipitation variations in the Amazon Basin (Hijmans et al., 2005). Blue color shades represent the mean monthly precipitation for January (A), April (B), July (C) and October (D). In (E) the mean annual precipitation is given (also in mm/month). The extent of the Amazon Basin is marked with a black line. The South American Convergence Zone (SACZ), the South American Low Level Jet (SALLJ) and the Intertropical Convergence Zone (ITCZ) are marked in yellow and red lines and arrows.

1.3. Reconstructing past environmental conditions

The lack of available climate data for the time before the onset of systematical measurements has led to the development of proxy methods designed to reconstruct past climate conditions. There are various archives that hold information about past environmental conditions. Tree wood has for instance been used to reconstruct environmental conditions of the last ten millennia (i.e. the present warm time, the Holocene) (e.g. McCarroll and Loader, 2004; Reimer et al., 2013). Speleothems, corals and ice cores allow climate reconstructions on longer time scales, with some of the longest records covering most of the last million years (i.e. the current succession of multiple glacial and warm times during the late Pleistocene) (Cheng et al., 2016; Lüthi et al., 2008). To obtain information about the deep past going back millions to billions of years, sedimentary archives can be used (e.g. Zachos et al., 2001). Apart from archives that potentially allow the reconstruction of continuous time series, distinct geomorphological features like glacial moraines can be used to reconstruct past climate extremes like glacial high stands or flood events (Gosse and Phillips, 2001). The limits of these different archives are either given by available material, as is the case for tree wood and ice cores, or by limitations of the dating methods. For instance, the temporal limit for speleothems and coral reconstruction is also given by the limits U/Th dating (e.g. Cheng et al., 2016).

There is an increasing number of proxy methods that are used to retain paleoenvironmental information from abovementioned archives. The probably most frequently applied method is the analysis of the isotopic composition of ice, speleothems, corals, foraminifera shells or molecular biomarkers (e.g. Fairchild et al., 2006; Kucera, 2007; Sauer et al., 2001). Most of these isotope studies aim to reconstruct the isotopic composition of precipitation or sea water, which allows the reconstruction of precipitation, temperature, ice volume or salinity conditions or the tracing of different water masses (e.g. Dansgaard, 1964; Epstein and Mayeda, 1953; Hays et al., 1976). Other frequently applied methods include the use of pollen or dinoflagellate associations from sediment cores to reconstruct past vegetation and environmental conditions (e.g. Birks et al., 2016) or the use of the elemental composition of sediment to reconstruct past sediment provenance or weathering (e.g. Govin et al., 2012). An increasingly prominent role is the use of molecular biomarkers, which base on the observation that different organisms synthesize different organic molecules under varying environmental conditions (e.g. Eglinton and Eglinton, 2008).

One of the main problems in the use of paleoclimate proxies, is that they usually represent multiple variables, which makes the deduction of one single climate variable such as mean

annual precipitation difficult. To circumvent this problem, the application of multiple proxies in the same sample can lead to higher confidence into climate reconstructions.

1.4. Pleistocene paleoclimate

The Pleistocene represents the time period from 2.6 million years (Ma) before present (BP) until 12 thousand years (ka) BP (Cohen et al., 2013). The beginning of the period is marked by the onset of large scale northern hemisphere glaciations and the end by the beginning of the present warm period, the Holocene. First evidence for extensive past glaciations was provided by the presence of moraines and erratic boulders in the Alpine Foreland and Scandinavia (Agassiz, 1840; Venetz, 1833). Similar geomorphologic structures in North America and northern Europe revealed the past existence of large continental ice shields, coining the term ice age. The causes for the onset and demise of such glaciations remained contentious for a long time. The analysis of the oxygen isotope composition ($\delta^{18}O$) of benthic foraminifera used as a proxy for ice volume finally revealed the temporal evolution of ice age cycles (Hays et al., 1976). The study revealed that glacial-interglacial variations occurred with dominant 100 ka cycle for the last 500 ka (Fig. 1.3E)(Hays et al., 1976). This finding favored the theory that glaciations were initiated by changes in the orbital configuration, first introduced by Milankovitch (1920) (Fig. 1.3 A-E). There are three orbital cycles which interact to define insolation: The longest cycle is the 100 ka cycle of orbital eccentricity, which is caused by variations in the eccentricity of earth´s orbit around the sun (Fig. 1.3C). Changes in the tilt of earth's axis (Obliquity) occur in cycles of 40 ka. A larger axial tilt leads to stronger seasonality, while a lower axial tilt decreases seasonality (Fig. 1.3B). The shortest cycle is the 20 ka cycle of orbital precession. Orbital precession defines during which season earth is closest to the sun on its annual orbit (Fig. 1.3A). Combined, these changes in the orbital configuration, lead to variations in insolation on earth´s surface (Fig. 1.3D). Even though there are multiple competing theories, the exact chain of events translating variations in insolation to glaciations is still hotly debated (e.g. Cheng et al., 2016; Raymo and Huybers, 2008). Since the buildup of ice sheets in the arctic exerts its influence on the global circulation patters, the last glacial maximum (LGM) presents an interesting opportunity to study the reaction of different geographic regions to large-scale perturbations in the climate system.

Apart from orbital timescales there are distinct shorter term climate variations on the scale of a few centuries to millennia found during the glacial periods of late Pleistocene. On the one hand, there are large ice rafting events (Heinrich events), which led to a reduction in the Atlantic Meridional Overturning Circulation and periods of marked cooling in the

northern hemisphere (Heinrich Stadials) (Heinrich, 1988). On the other hand there are several abrupt warming events in the north Atlantic (Dansgaard-Oeschger events), which were followed by a warmer period lasting a few centuries (Dansgaard-Oeschger Interstadials) before ending with a more prolonged cooling (Fig.1.4A) (Bond et al., 1993; Dansgaard et al., 1993). The causes for Dansgaard-Oeschger events are still debated (Zhang et al., 2014). Heinrich and Dansgaard-Oeschger events led to major climate shifts around the world that are distinctly visible in various high resolution climate records (Fig. 1.4B, C) (Deplazes et al., 2013; Mosblech et al., 2012; Wang et al., 2001).

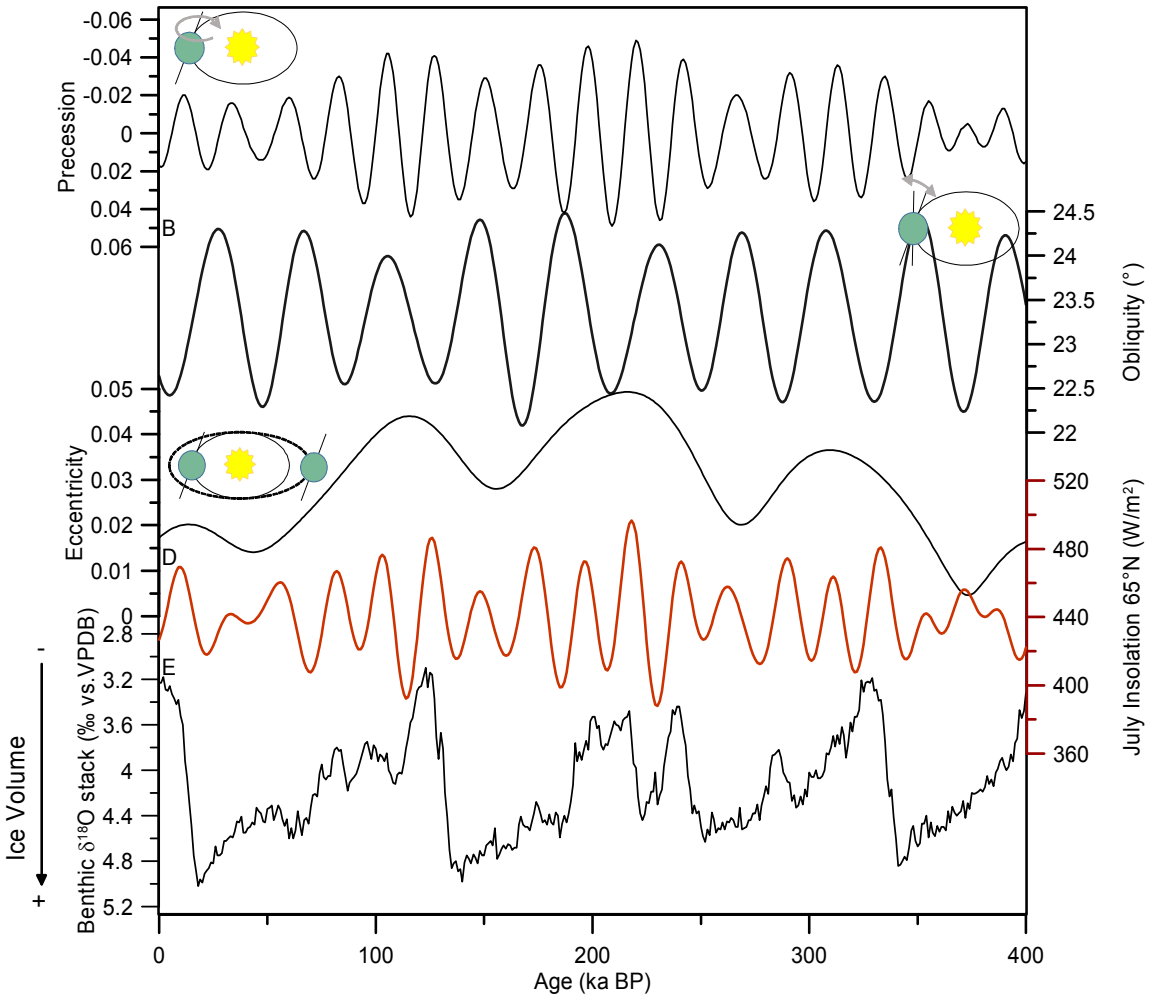

Figure 1.3. Changes in orbital precession (A), obliquity (B) and eccentricity (C) influencing the seasonal insolation on earth surface (Berger and Loutre, 1991). Variations in northern hemisphere insolation (D) (Berger and Loutre, 1991) control changes in ice volume deduced from the $\delta^{18}O$ composition of benthic foraminifera (E) (Lisiecki and Raymo, 2005).

1.5. Late Pleistocene paleoclimate in the Amazon Basin

Research on the paleoclimate in the Amazon Basin has been closely linked to the question how the biodiversity in the Amazon rainforest evolved (Fig. 1.5). The first hypothesis concerning the origin of the Amazonian biodiversity was formulated by Haffer (1969). Haffer observed that different species of birds found in the Amazon rainforest had geographically distinctly separated habitats that could not be explained by present day ecological factors. He concluded that the different bird species where formerly separated by savanna vegetation during glacial times. This would mean that during recurring glaciations of the Pleistocene, drier conditions would lead to savanna expansion that would create separated forest "refugia", where different species evolved independently. Initially, this view was supported by pollen records from lake sediment cores at the periphery of the Amazon rainforest. These records indeed showed savanna expansion during glacial times indicating an extensive drying during glacials (Absy, 1991; Absy and Van Der Hammen, 1976; van der Hammen and Absy, 1994). However, these early records where situated on the fringes of the Amazon Basin and their representativeness for the Amazon interior was questioned. Colinvaux et al. (1996) first presented results from the Hill of Six Lakes situated in north-western lowland Amazonia. Their results showed that humid conditions with tropical rainforest persisted through the LGM. This finding was later supported by pollen and biomarker studies conducted on sediment cores from the submerged Amazon delta, which were thought to integrate vegetation conditions in Amazonia (Boot et al., 2006; Haberle and Maslin, 1999; Maslin et al., 2012). Both findings were clearly contradicting the predictions made by the refugia hypothesis. Nevertheless, it was suggested that the lake sediment core sites from the Amazon interior were potentially situated in one of the forest refugia and that the signal in offshore records was probably disproportionally influenced by a gallery forest during glacial times (Berrio et al., 2000).

The onset of phylogenetic analysis raised further doubts on the validity of the refugia hypothesis. Phylogenetic studies on birds found that there was no increased speciation of birds taking place during the Pleistocene (Hoorn et al., 2010; Smith et al., 2014). Conversely, these studies suggested that the rich Amazonian biodiversity had its origin already in pre-Pleistocene times and was influenced by the Andean uplift and the establishment of the Amazon River system (Hoorn et al., 2010; Ribas et al., 2012). Recent speleothem reconstructions found that climate conditions in westernmost Amazonia were continuously humid during the late Pleistocene (Fig. 1.4C) (Cheng et al., 2013; Kanner et al., 2012; Mosblech et al., 2012). Together with the observation that species richness in western Amazonia was greater than in the eastern part of the basin(Fig. 1.5), this suggested that highest species richness was associated with long-term climate stability rather than with

swiftly changing climate conditions (Cheng et al., 2013). Such a scenario would suggest that stable climate conditions in western Amazonia allowed the occupation of niches over time. In eastern Amazonia, changes in forest structure due to late Pleistocene drying would have led to repeated extinction events which resulted in lower species richness (Cheng et al., 2013).

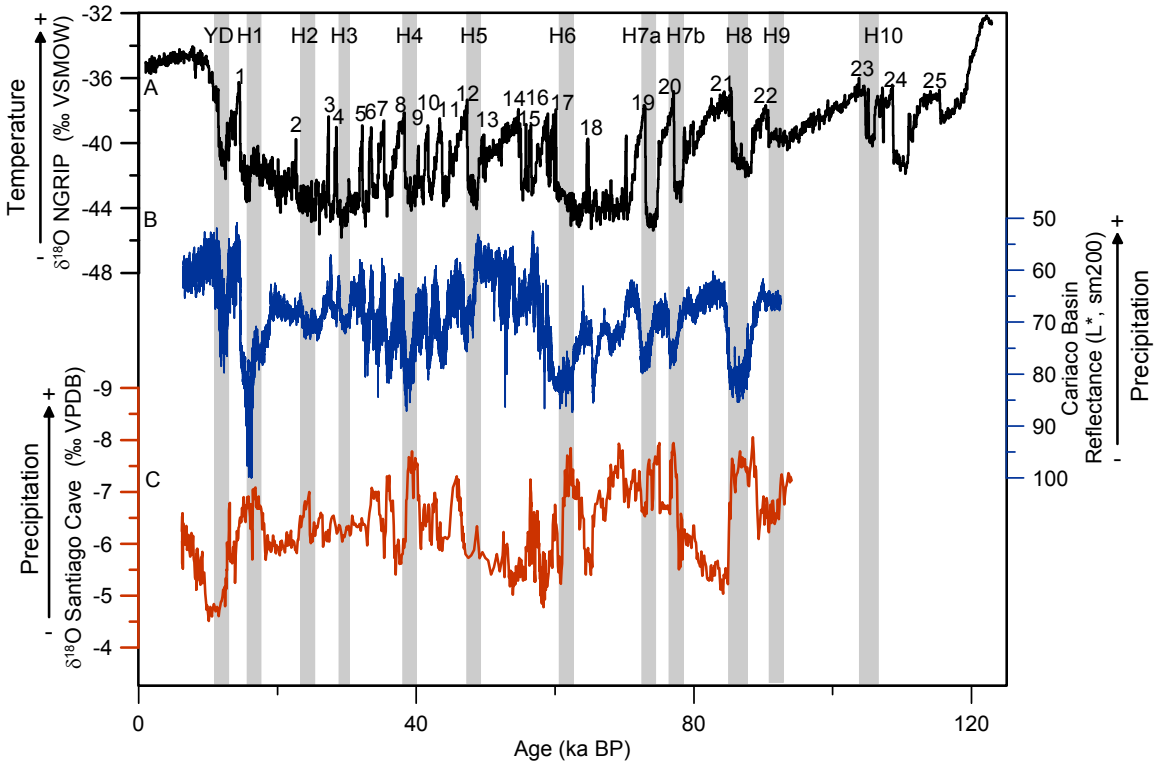

Figure 1.4. Millennial scale climate variability during the last glacial climate cycle. A) Fast temperature shifts recorded by the $\delta^{18}O$ composition of ice from Greenland ice cores (NGRIP Project members, 2004). B) Variations in color reflectance indicating changes in terrestrial input and precipitation intensity from the Cariaco Basin in northern South America (Deplazes et al., 2013). C) Variations in precipitation recorded by speleothem $\delta^{18}O$ from Santiago Cave in the Peruvian Andes (Mosblech et al., 2012). The timing of the Younger Dryas (YD) and Heinrich Stadials is given in grey bars (Rasmussen et al., 2003) and the numbers in (A) represent Dansgaard-Oeschger Interstadials (NGRIP Project members, 2004).

Even though the refugia hypothesis is no longer in the centre of the debate on the origin of the Amazonian biodiversity, the history of the extent of the Amazon rainforest is still thought to be essential for the species distribution pattern in tropical South America. For instance, it has been conjectured that the Amazon rainforest and the coastal Atlantic

forests were formerly connected by forest (Auler et al., 2004; Batalha-Filho et al., 2013; Werneck et al., 2012). Similarly, the occurrence of comparable avifauna in the savanna regions to the north and south of the Amazon basin has led to the hypothesis of a geologically recent connection during the late Pleistocene by savanna vegetation (Da Silva and Bates, 2002; Ribeiro et al., 2016). However, both the timing and exact geographical setting of such a connection are still elusive.

The availability of numerous highly resolved speleothem records from the Andean foothills in westernmost Amazonia also allowed the analysis of climate variability on shorter time scales. While climate conditions were relatively stable on orbital timescales during the late Pleistocene, the speleothem records in the Andes consistently show fast climate fluctuations with wet Heinrich Stadials and dry Dansgaard-Oeschger Interstadials (Fig. 1.4C) (Cheng et al., 2013; Kanner et al., 2012; Mosblech et al., 2012). A similar picture arises from north-east and southern Brazil (Cruz et al., 2005; Wang et al., 2004). In the north of the South American continent, the opposite signal with dry Heinrich Stadials and wet Dansgaard-Oeschger Interstadials can be found (Fig. 1.4B) (Deplazes et al., 2013; Peterson et al., 2000). This picture is commonly attributed to a south ward shift of the tropical rain belt during Heinrich Stadials and a northward movement during Dansgaard-Oeschger Interstadials. While there are now numerous highly resolved speleothem records from the westernmost, Andean part of the Amazon Basin, there are no high resolution records from the interior Amazon Basin. The low temporal resolution of the records from the Hill of Six Lakes (Bush et al., 2004a; Colinvaux et al., 1996) has also revigorated the debate on past climate conditions in lowland Amazonia(D'Apolito et al., 2013). The sections of these records covering the LGM are condensed or even absent and might therefore not fully represent LGM conditions (D'Apolito et al., 2013).

Overall, the climate picture arising from previous climate reconstructions in the Amazon Basin remains fragmentary and some of the records are still contested (Behling et al., 2009; D'Apolito et al., 2013). While there are many climate records from the edges of the Amazon Basin, especially the Andes, there are still very few records from the lowland Amazon Basin. Hence, it is still debated whether climate conditions in the central Amazon Basin were drier than today during the last glacial maximum. Furthermore, it remains unclear how the structure of the Amazon rain forest changed in response to potentially drier and cooler conditions during the last glacial maximum (Behling et al., 2009). It is still uncertain whether the Amazon rainforest was replaced by analogue forest types that are found in the Andes at higher altitudes today, by seasonally dry forest types or by vegetation without preset day analogue (Bush et al., 2004b; Pennington et al., 2004).

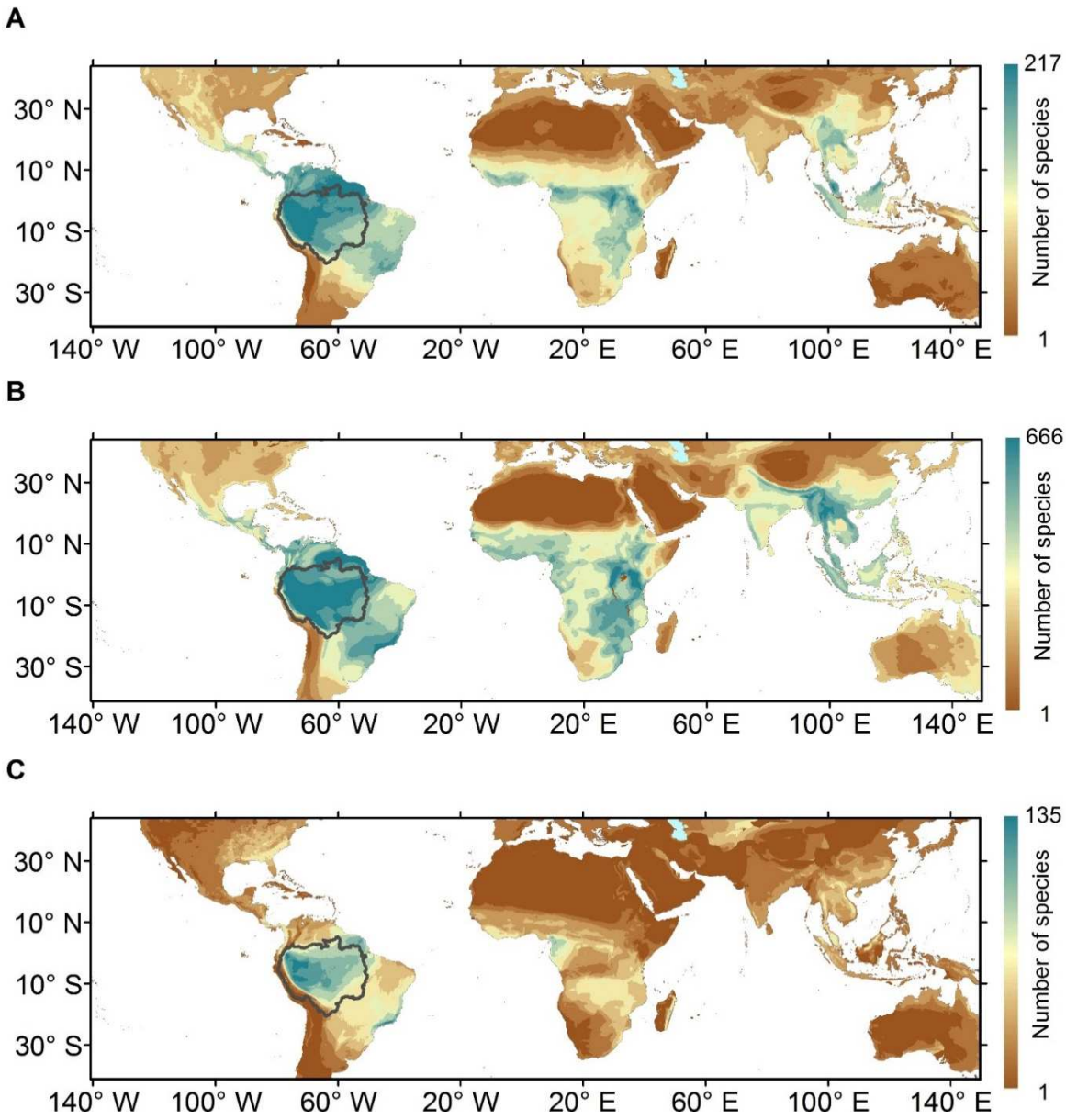

Figure 1.5. Species richness for Mammals (A), Birds (B) and Amphibians (C) (Jenkins et al., 2013). Data is based on 10 x 10 km grids. The location of the Amazon Basin is marked with a black line.

1.6. Aims of this study

As outlined above, climate and vegetation history of the Amazon Basin is still contested. Previous studies on the late Pleistocene paleoclimate of the Amazon had the following limitations: a) they had only a low spatial resolution in the lowland Amazon Basin, b) they had usually a low temporal resolution and c) they were in most cases conducted using pollen proxies that do not allow to differentiate between vegetation and climate history. This thesis aims to fill these information gaps by studying samples from a marine sediment core (GeoB16224-1), which a) integrates the Amazonian sediment and organic matter input and has b) a high temporal resolution. c) Novel biomarker proxies for precipitation intensity and vegetation are going to be applied to obtain a more detailed picture of the past climate and vegetation dynamics in the Amazon Basin. Specifically, the goals are

i) to develop a biomarker based salinity proxy to track changes in the extent of the Amazon Plume,
ii) to study the suitability of plant-wax biomarkers as proxies for the independent reconstruction of the precipitation and vegetation history in lowland Amazonia and
iii) to reconstruct the past hydrological and vegetation history of the Amazon Basin during the late Pleistocene (50-12.8 ka BP) from core GeoB16224-1 using the biomarker proxies tested before.

Within the framework of these aims the following hypotheses are going to be tested:

a) The stable hydrogen isotope composition (δD) of alkenones and palmitic acids reflects the salinity conditions in the Amazon Plume.
b) Long-chain *n*-alkanes in the Amazon Basin are mainly sourced from modern plants and are refractory during transport.
c) δD of long-chain *n*-alkanes in the Amazon tributaries reflect δD of precipitation.
d) Forest cover in the Amazon Basin persisted during the late Pleistocene.
e) Integrated climate conditions in the Amazon Basin were stable during the late Pleistocene.

1.7. Methodology

1.7.1. Plant-wax biomarkers

The primary tool employed in this thesis are plant-wax biomarkers. These biomarkers are long-chain lipid molecules constituting the wax coatings of leafs (Fig. 1.6) (Eglinton and Hamilton, 1963, 1967; Hall and Jones, 1961). The most frequently used among these molecules are long-chain *n*-alkanes and long-chain fatty acids. Both are abundant plant-wax molecules and have the advantage of being resistant against degradation during sedimentary transport and deposition.

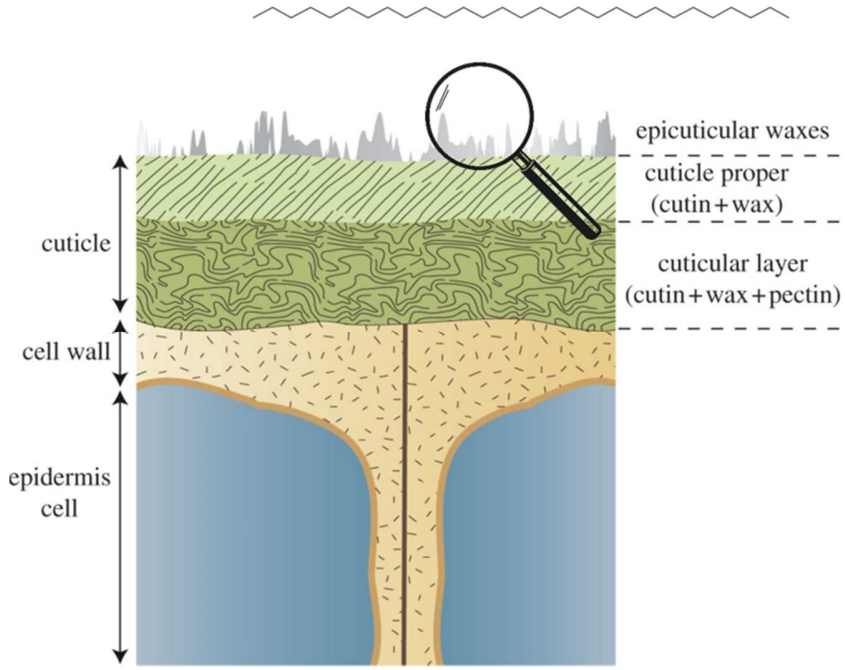

Figure 1.6. Schematic section through a leaf-cell indicating the location of plant-waxes (modified after Kourounioti et al. (2013). The molecular structure of *n*-C_{29} *n*-alkane is given as example of one of the dominant plant-wax molecules.

The relative abundance of long-chain *n*-alkanes and fatty acids can be used to obtain information about the dominant vegetation type they are originating from (e.g. Maffei, 1996). Savanna vegetation produces on average long-chain *n*-alkanes and fatty acids with a longer chain length than forest vegetation (e.g. Hughen et al., 2004; Rommerskirchen et al.,

2003). Apart from changes in dominant vegetation type, there are further factors potentially influencing the chain length of plant-waxes. Among them are changes in climate and in aquatic production (Bush and McInerney, 2015; Ficken et al., 2000). Plant-wax *n*-alkanes feature typically higher concentrations in odd-carbon number compounds and fatty acids feature higher relative amounts of compounds with an even carbon number (Cranwell, 1981; Cranwell et al., 1987). While this even or odd preference is usually dominant in pristine plant organic matter, it decreases by degradation processes and disappears entirely in heavily degraded material such as petroleum (Lichtfouse and Eglinton, 1995). Hence, the ratio of odd vs. even chain compounds can be used to monitor the degree of degradation in these compounds.

1.7.2. The isotopic composition of precipitation

The stable isotope composition of precipitation is controlled by various factors. First of all, the isotopic composition of sea water in the moisture source area plays an important role (Gat, 1996). During transport to the continental interior, the heavier stable oxygen (^{18}O) and hydrogen (^{2}H) isotopes are rained out preferentially, leading to increasing depletion with growing distance from the coast (Dansgaard, 1964). In the Amazon Basin the depletion in the heavier isotope with increasing distance to the sea is comparably week due to the extensive water recycling taking place in the Amazon Basin (Salati et al., 1979). A similar effect can also be observed with increasing altitude: Mountainous areas receive more depleted rainfall than the surrounding lowland areas. During condensation and rainout, the isotope fractionation is mainly controlled by two factors (Dansgaard, 1964). On the one hand, the temperature effect leads to precipitation enriched in the heavier isotope during warm conditions, while colder temperatures lead to more depleted precipitation. On the other hand, there is the amount effect control on the isotopic composition of precipitation. The amount effect describes the observation that the isotopic composition of precipitation in tropical and monsoonal regions is related to the precipitation amount (Dansgaard, 1964). Hence, a depletion in the heavier isotope in tropical regions such as the Amazon Basin can be interpreted to reflect an increase in the precipitation amount, while in higher latitude the temperature effect is more dominant (Salati et al., 1979; Vuille et al., 2003). Changes in altitude due to tectonic uplift or a change in the moisture source area are unlikely to have played a role over the studied time-scales in tropical Amazonia (Hoorn et al., 2010).

1.7.3. The isotopic composition of sea water

The stable isotope composition of sea water is salinity dependent (Epstein and Mayeda, 1953). Water masses with higher salinity are generally more enriched in the heavier oxygen and hydrogen isotopes than sea water with a lower salinity (McConnell et al., 2009). This is primarily caused by the effect that the isotopically lighter molecules are evaporated easier than the heavier ones. As a consequence, saline and isotopically enriched water remains in the residual. The relationship of salinity and isotopic composition can vary regionally and over time (Rohling and Bigg, 1998). Especially in front of river mouths, seasonal variations in the slope of the isotope-salinity relationship can be large (Karr and Showers, 2002). This has in part to do with variations in the composition of precipitation representing the freshwater endmember of the relationship. The stable oxygen and hydrogen isotope composition of the Amazon River shows for instance large seasonal variations. These variations are caused by changes in the isotopic composition of precipitation due to the amount effect and due to variations in discharge from tributaries from different regions of the Amazon that have a different distance from the Atlantic Ocean and are hence subject to a different continent effect (Karr and Showers, 2002).

1.7.4. δD of plant-waxes

δD of lipid biomarkers such as plant-wax biomarkers reflect the isotope composition of the water the producing organisms consume (Fig. 1.7) (Sachse et al., 2012; Sternberg, 1988). Hence, δD of plant-waxes can be used to reconstruct the past isotopic composition of precipitation in a region (Sachse et al., 2012; Schouten et al., 2002). Under certain environmental conditions there are further influences that may dominate over the initial precipitation signal. Among these factors are enhanced evaporation and water stress in arid regions, which can lead to an enrichment of δD in leaf-waxes (Farquhar et al., 2007; Kahmen et al., 2008). Furthermore, there are variations in the fractionation factor among different plant species (Feakins and Sessions, 2010; Smith and Freeman, 2006). Hence, shifts in dominant vegetation e.g. from forest to savanna should be taken into account when interpreting plant-wax isotope signals.

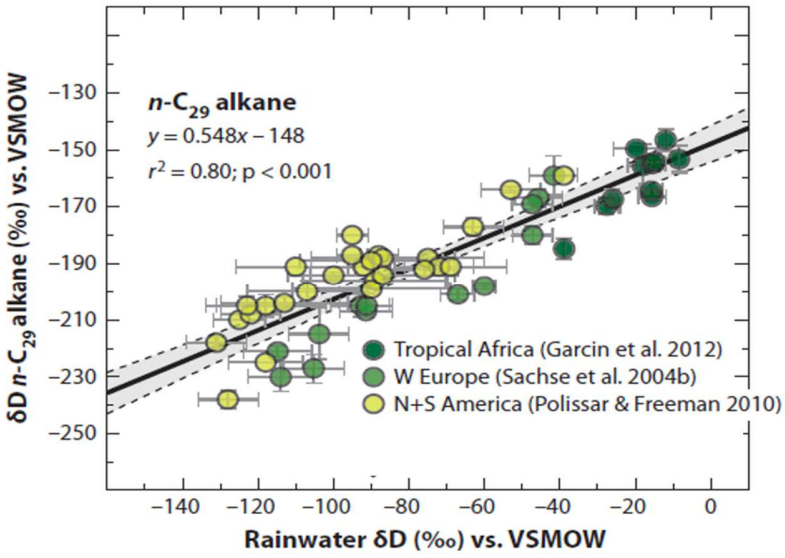

Figure 1.7. Relationship between δD of rainwater and δD of long-chain *n*-alkanes found in lacustrine samples from Europe, Africa and the Americas (Sachse et al., 2012).

1.7.5. Aquatic biomarkers

To study changes of in the aquatic environment at the core site, aquatic lipid biomarkers are used. Alkenones are long-chain, mostly di-and tri-unsaturated ketones that are produced by haptophyte algae (Fig. 1.8A) (Marlowe et al., 1984). The ratio of di- and tri-unsaturated compounds has been found to be temperature dependent (Conte et al., 1998; Prahl and Wakeham, 1987). Due to their temperature sensitivity and low degradability, alkenones are a frequently used biomarker in paleoceanography. δD of alkenones has also been used as tool for sea surface salinity reconstructions (Englebrecht and Sachs, 2005; Schouten et al., 2006). One of the main drawbacks of the use of alkenones as proxies is that alkenones produced by coastal and open marine species have a different temperature relationship and also a different δD fractionation factor (M'Boule et al., 2014; Versteegh et al., 2001).

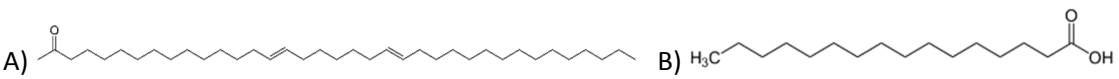

Figure 1.8. A) Molecular structure of the $C_{37:2}$ alkenone (Marlowe et al., 1984) and (B) Palmitic acid (Rustan and Drevon, 2001).

In contrast to the specifically known source of alkenones, palmitic acid is a ubiquitous organic molecule (Fig. 1.8B). In marine environments it is mostly produced by phytoplankton in the surface layer. δD of palmitic acid has also been employed to reconstruct δD of water and salinity (Huang et al., 2002; Smittenberg et al., 2011). Palmitic acid is less frequently used to reconstruct δD of sea water than alkenones, since palmitic acid is less resistant towards degradation and might also be produced deeper in the water column.

1.7.6. $\delta^{13}C$ of plant-wax biomarkers

The stable carbon isotope composition ($\delta^{13}C$) of plant-waxes and plant organic matter is influenced by the photosynthetic pathway of plants (Rieley et al., 1991). The C3 photosynthetic pathway leads to a stronger isotopic fractionation during carbon fixation and therefore more depleted $\delta^{13}C$ values. The C4 and CAM photosynthetic pathways exhibit less isotopic fractionation and therefore lead to typically more enriched $\delta^{13}C$ values (Fig. 1.9) (O'Leary, 1981). Since the C3 metabolism is used by most forest taxa, while the C4 and CAM metabolisms are typically used by tropical and subtropical savanna species, $\delta^{13}C$ of plant-waxes can be used to differentiate between dominant savanna and forest vegetation (Huang et al., 2001).

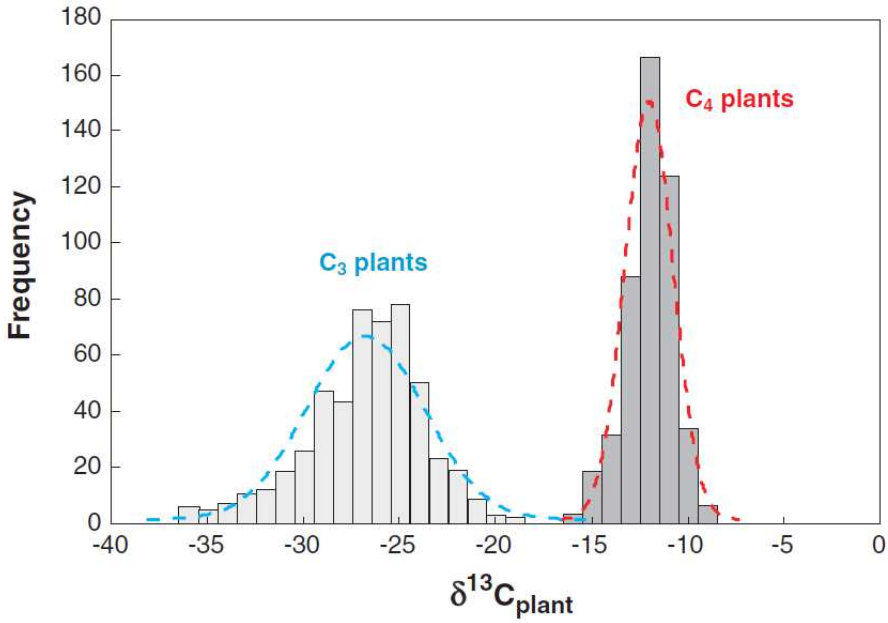

Figure 1.9. $\delta^{13}C$ of plant organic matter from C3 and C4 plants (Tipple and Pagani, 2007). The figure illustrates the differences in $\delta^{13}C$ for plants using different photosynthetic metabolisms.

1.7.7. Sample Material

The sample material used in this thesis is composed of samples of suspended sediment from the Amazon Plume, collected during cruise MSM 20/3, samples of river bed sediment from the Amazon River and its tributaries, core-tops samples from the coastal regions offshore the Amazon estuary and samples from sediment core GeoB16224-1 retrieved from the continental margin off French Guiana (6°39.38'N, 52°04.99'W) (Mulitza et al., 2013). The suspended sediment samples are used for the calibration of aquatic biomarkers and cover the salinity gradient induced by Amazon River freshwater into the tropical Atlantic Ocean. The river bed- and core-top samples are used for the study of origin and transport of plant-wax biomarkers in the Amazon River. The sample set comprises river bed samples from the major Amazon tributaries as well as samples from the Amazon estuary. Core-top samples were collected from the submerged Amazon delta, shelf areas offshore northeastern South America and from the continental margin. The sample set allows to study the deposition areas of organic matter from the Amazon River. Core GeoB16224-1 is used to reconstruct past climate conditions during the late Pleistocene (12.8-50 ka BP). The sediment core was taken at 2510 m water depth and has a core length of 760 cm. The core site received constant sedimentation from the Amazon River during the late Pleistocene until sedimentation shifted to the shelf during the deglacial sea level rise (Zhang et al., 2015). Due to the constant sedimentation rate, the core allows to reconstruct the environmental conditions of the Amazon Basin at a high temporal resolution.

2. Thesis outline and author contributions

This thesis is presented in cumulative form and consists of three manuscripts that are either published (Häggi et al., 2015; Häggi et al., 2016), or submitted to international peer-reviewed scientific journals. A short outline of the manuscripts and the individual author contributions as well as a detailed description of own contributions are given in the following:

2.1. Manuscript outline

Chapter 3: Testing the D/H ratio of alkenones and palmitic acid as salinity proxies in the Amazon Plume

Christoph Häggi, Cristiano M. Chiessi and Enno Schefuß

Published in *Biogeosciences* 2015, Vol. 12, pages 7239-7249.

E.S., C.M.C. and C.H. designed the study. E.S. and C.M.C conducted the sample collection. C. H and E.S. performed laboratory work and analyzed the data. C.H. wrote the manuscript with contributions from both co-authors.

This manuscript deals with the calibration of a biomarker δD based salinity proxy. To this end the δD composition of alkenones and palmitic acid was measured along the salinity gradient induced by the Amazon Plume. Results show that δD of alkenones does not faithfully record δD of sea water, while δD of palmitic shows a strong correlation with δD of sea water.

Chapter 4: Origin, transport and deposition of leaf-wax biomarkers in the Amazon Basin and the adjacent Atlantic

Christoph Häggi, André O. Sawakuchi, Cristiano M. Chiessi, Stefan Mulitza, Gesine Mollenhauer, Henrique O. Sawakuchi, Paul A. Baker, Matthias Zabel and Enno Schefuß

Published in *Geochimica et Cosmochimica Acta*, 2016, Vol. 192 pages 149-165.

E.S., S.M., C.M.C and C.H. designed the study. A.O.S, C.M.C, ES, S.M, H.O.S, and P.A conducted the sample collection. C.H and M.Z. performed laboratory work. C.H. wrote the manuscript with contributions from all co-authors.

In this manuscript, the origin of plant-waxes transported by the Amazon River is studied by analyzing the δD and $\delta^{13}C$ composition of long-chain *n*-alkanes from river bed and marine core-top sediments. Results show that biomarkers transported by the Amazon River are C3 plant derived. Geographically, the signal at the Amazon estuary integrates contributions from the different sub catchments of the lowland basin. The depleted δD at the Amazon estuary also indicates that compounds are transported from the western parts of the basin and are hence comparably resistant against degradation.

Chapter 5: Response of the Amazon rainforest to late Pleistocene climate variability

Christoph Häggi, Cristiano M. Chiessi, Ute Merkel, Stefan Mulitza, Matthias Prange, Michael Schulz and Enno Schefuß

E.S., S.M. and C.M.C. designed the study. S.M., C.M.C., and E.S collected the samples. C.H performed the laboratory work. U.M., M.P. and M.S. provided the model data. C.H. wrote the manuscript with contributions from all co-authors.

In this manuscript, the late Pleistocene vegetation and precipitation history of the lowland Amazon Basin are reconstructed from a marine sediment core using the $\delta^{13}C$ and δD composition of long-chain *n*-alkanes. Results show that forest vegetation persisted through the late Pleistocene and was only reduced during Heinrich Stadials, when savanna intrusions occurred in the northern parts of the Basin. The δD based precipitation reconstruction showed that humid conditions persisted through much of the late Pleistocene and that moderate drying was limited to full glacial conditions.

2.2. Description of own contributions

All the above mentioned manuscripts were written by myself with comments and contributions by the co-authors. The allocation of the datasets to the different manuscript was also largely done by myself. A detailed overview of my contributions on the sampling and laboratory work is given in the following:

For the first manuscript addressing the establishment of a biomarker δD based salinity proxy, I conducted the methylation and two cleaning steps of the fatty acid fraction and

conducted the subsequent Gas Chromatography (GC-FID) and Isotope Ratio Mass Spectrometry (IRMS) measurements. The sample drying, the lipid extraction and separation as well as alkenone GC-FID and IRMS measurements had been conducted earlier by Ana C. R. de Albergaria-Barbosa and Enno Schefuß. The water isotope data was measured by Enno Schefuß. The sample collection was conducted during *RV Maria S. Merian* cruise MSM20/3 by Cristiano M. Chiessi and Enno Schefuß.

For the second manuscript on leaf-wax transport in the Amazon River, I conducted the laboratory preparation and biomarker measurements for all samples. This included the lipid extraction of the samples, the compound separation using column chromatography and cleaning steps for the removal of unsaturated compounds and conducting GC-FID and IRMS measurements. Help during the extraction was provided by Birk Stern, a student helper. XRF measurements were conducted by Matthias Zabel. Total organic carbon (TOC) data was measured by Brit Kockisch. The water isotope data was measured by Enno Schefuß. River bed samples were provided by André and Henrique O. Sawakuchi, while core-top samples were provided by Paul A. Baker as well as the *RV Maria S. Merian* cruise MSM20/3.

For the third manuscript on the climate and vegetation reconstruction of the late Pleistocene Amazon Basin, I collected samples from core GeoB16224-1 with help of Birk Stern. The samples were ground by Birk Stern. Lipid extraction was again conducted by myself with help of Birk Stern. I conducted the full lipid separation and cleaning process for all samples and conducted all the GC-FID and IRMS measurements. The CCSM3 climate model runs presented in this manuscript were provided by Ute Merkel, Matthias Prange and Michael Schulz.

3. Testing the D/H ratio of alkenones and palmitic acid as salinity proxies in the Amazon Plume

C. Häggi[1], C. M. Chiessi[2] and E. Schefuß[1]

[1]MARUM – Center for Marine Environmental Sciences, University of Bremen, Germany

[2]School of Arts, Sciences and Humanities, University of São Paulo, Brazil

Published in *Biogeosciences* 2015, Vol. 12, pages 7239-7249.

Abstract

The stable hydrogen isotope composition of lipid biomarkers, such as alkenones, is a promising new tool for the improvement of paleosalinity reconstructions. Laboratory studies confirmed the correlation between lipid biomarker δD composition (δD_{Lipid}), water δD composition (δD_{H_2O}) and salinity. Yet, there is limited insight into the applicability of this proxy in oceanic environments. To fill this gap, we test the use of the δD composition of alkenones (δD_{C37}) and palmitic acid (δD_{PA}) as salinity proxies using samples of surface suspended material along the distinct salinity gradient induced by the Amazon Plume. Our results indicate a positive correlation between salinity and δD_{H_2O}, while the relationship between δD_{H_2O} and δD_{Lipid} is more complex: δD_{PA} correlates strongly with δD_{H_2O} (r^2=0.81) and shows a salinity dependent isotopic fractionation factor. δD_{C37} only correlates with δD_{H_2O} in a small number (n=8) of samples with alkenone concentrations >10 ng L^{-1}, while there is no correlation if all samples are taken into account. These findings are mirrored by alkenone based temperature reconstructions, which are inaccurate for samples with low alkenone concentrations. Deviations in δD_{C37} and temperature are likely to be caused by limited haptophyte algae growth due to low salinity and light limitation imposed by the Amazon Plume. Our study confirms the applicability of δD_{Lipid} as a salinity proxy in oceanic environments. But it raises a note of caution concerning regions where low alkenone production can be expected due to low salinity and light limitation, for instance, under strong riverine discharge.

3.1. Introduction

The precise reconstruction of past ocean salinity is still a pending issue in paleoclimatology (Rohling, 2007). Until recently, most paleosalinity studies have relied on foraminifera based reconstructions of the stable oxygen isotope composition of seawater, which correlates with salinity (Epstein and Mayeda, 1953). However, temperature also controls the oxygen isotope composition of foraminifera, making corrections in the estimation of paleosalinity necessary (Lea et al., 2000; Rostek et al., 1993). The imprecision associated with this approach has led to the search for alternative salinity proxies. The use of the hydrogen isotopic composition of algal lipids (δD_{Lipid}) for the reconstruction of the stable hydrogen composition of water (δD_{H_2O}) is one of such recent developments (Schouten et al., 2006; Sessions et al., 1999). As outlined in a theoretical framework by Rohling (2007), this method has the potential to lead to more precise reconstructions of surface water salinity in combination with foraminifera based $\delta^{18}O$.

So far, efforts to apply δD_{Lipid} as a salinity proxy have mainly involved the use of long-chain alkenones. Long-chain alkenones have the advantage of being exclusively produced by specific haptophyte algae, and of showing good preservation over geologic timescales (Marlowe et al., 1990; Marlowe et al., 1984). Laboratory studies have confirmed the correlation of the D/H ratio of the C_{37} alkenones (δD_{C37}) with δD_{H_2O} (Englebrecht and Sachs, 2005; Schouten et al., 2006). Furthermore, the D/H fractionation factor between alkenones and water ($\alpha_{C_{37}}$)

$$\alpha_{C37} = \frac{\delta D_{C37} + 1000}{\delta D_{H_2O} + 1000} \tag{3.1}$$

was found to be salinity dependent, leading to a potentially twofold way to reconstruct salinity (Schouten et al., 2006). There are, however, potential factors that may compromise the use of δD_{C37} and $\alpha_{C_{37}}$ as salinity proxies. $\alpha_{C_{37}}$ is, for instance, inconsistent among different haptophyte algae species. Species preferring shelf environments have a higher $\alpha_{C_{37}}$ than species favoring open marine habitats (M'Boule et al., 2014). In some situations $\alpha_{C_{37}}$ has shown a small temperature dependency (Zhang and Sachs, 2007). Furthermore, $\alpha_{C_{37}}$ is also dependent on algal growth phase and rate (Chivall et al., 2014b; Schouten et al., 2006; Wolhowe et al., 2009). All these factors potentially exceed the effects of salinity and may impede the use of δD_{C37} as a paleosalinity proxy. Nevertheless, paleoclimate studies have made successful use of δD_{C37} as a paleosalinity proxy (Giosan et al., 2012; Pahnke et al., 2007; Schmidt et al., 2014; van der Meer et al., 2007; van der Meer et al., 2008).

However, in some cases, factors like species variability complicated δD_{C37} based salinity reconstructions (Kasper et al., 2015).

Apart from alkenones, there is a variety of other algal lipids which feature a distinct δD_{H_2O} – δD_{Lipid} relationship (Nelson and Sachs, 2014; Sauer et al., 2001; Zhang et al., 2009). Among these less frequently used compounds is palmitic acid. Palmitic acid is a saturated fatty acid, which is highly abundant in most aquatic environments. The infrequent use of palmitic acid is mainly due to its ubiquitous occurrence, which does not allow linkage to a single group of producing species. Furthermore, palmitic acid is less resistant to degradation than alkenones (Sun and Wakeham, 1994). Nevertheless, δD of palmitic acid (δD_{PA}) has been successfully used as a paleoclimate indicator in several studies (Huang et al., 2002; Shuman et al., 2006; Smittenberg et al., 2011).

Although there are numerous laboratory and paleoclimate studies confirming the applicability of δD_{Lipid} to reconstruct the past isotopic composition of water, there have been only few calibration studies in oceanic environments (Schwab and Sachs, 2009; Schwab and Sachs, 2011; Wolhowe et al., 2015). To fill this gap, we analyzed δD_{C37} and δD_{PA} of suspended particle samples along the salinity gradient induced by the Amazon freshwater plume and tested their applicability as salinity proxies (Fig. 3.1). Along with the hydrogen isotope analyses, we also tested the accuracy of the $U_{37}^{k'}$ temperature proxy (Müller et al., 1998) under the influence of the Amazon Plume. Potential impact of haptophyte species variability was monitored using the C_{37}/C_{38} ratio (Rosell-Mele et al., 1994), as defined below.

$$C_{37}/C_{38} = \frac{C_{37:3}Me + C_{37:2}Me}{C_{38:3}Et + C_{38:3}Me + C_{38:2}Et + C_{38:2}Me} \quad (3.2)$$

3.2. Methods

3.2.1. Study area

The study area is situated offshore northern Brazil and French Guyana close to the Amazon estuary (Fig. 3.1). A large portion of the research area is influenced by freshwater outflow from the Amazon River, which induces a steep salinity gradient (Lentz and Limeburner, 1995). The freshwater plume is generally transported northwestwards by the North Brazil Current along the coastline of northern Brazil and French Guyana, while areas to the southeast of the Amazon River Estuary are largely unaffected by the Amazon freshwater discharge (Geyer et al., 1996). The geometry and transport of the freshwater plume are

subject to large seasonal variations. The plume reaches its maximum extent during peak Amazon discharge in boreal summer (Molleri et al., 2010), while its northwestward transport is controlled by wind-stress along the shelf (Geyer et al., 1996).

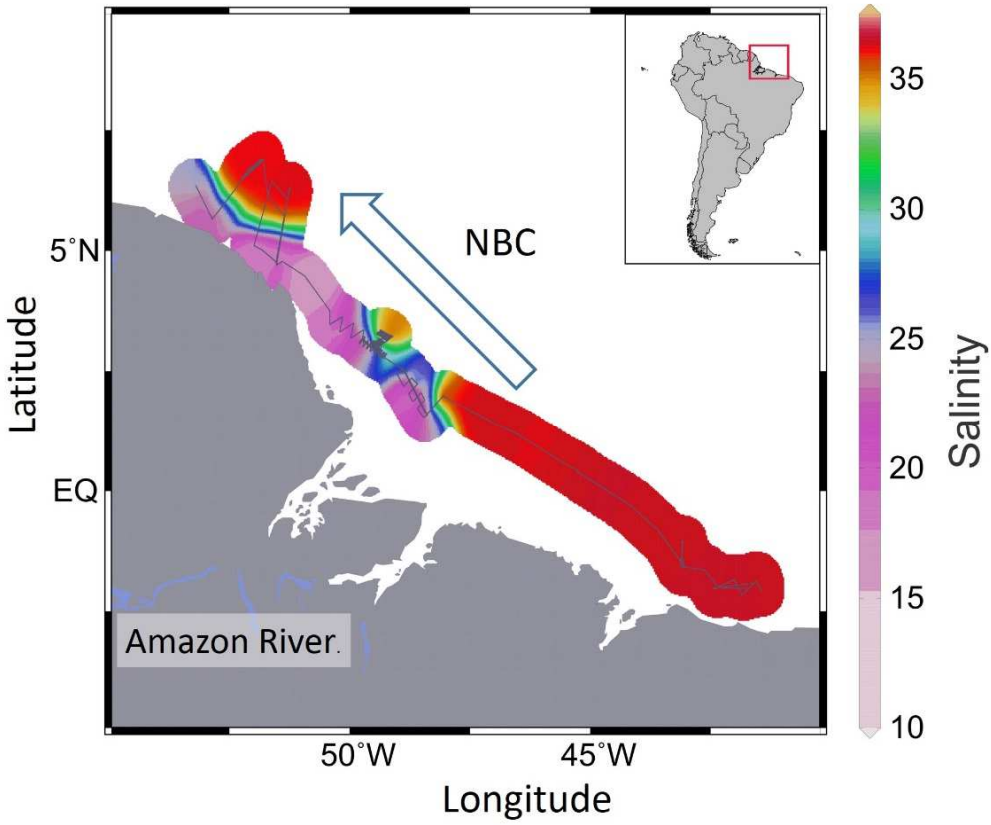

Figure 3.1. Map of the low salinity plume of the Amazon River outflow derived from the interpolation of onboard salinity measurements. The grey line shows RV Maria S. Merian cruise track MSM20/3 (Mulitza et al., 2013). The blue arrow depicts the North Brazil Current (NBC).

3.2.2. Sampling

Sampling was conducted during the RV *Maria S. Merian* cruise MSM20/3 from February 21th to March 9th 2012 (Mulitza et al., 2013). Samples of suspended particles were collected along a southeast to northwest transect off northeastern South America across the Amazon Plume (Fig. 3.1). Samples were taken via the ships seawater inlet at about 6 meters below sea level operated by a diaphragm pump. Between 100 and 500 litres of water were filtered over a period of 30 to 150 minutes on pre-combusted GFF filters. After sampling, filters were wrapped in pre-combusted aluminium foil and stored at -20°C. Along with the

suspended particle samples, water samples were collected at the beginning and at the end of each filtering period. Water samples were sealed with wax and stored at 4°C before analysis. On-board salinity and temperature measurements were conducted in one second intervals by a SeaBird Electronics SBE 45 Micro thermosalinograph (accuracy 0.002°C and 0.005 psu).

3.2.3. Stable isotope analysis of water

The stable hydrogen isotope composition of seawater samples was determined at MARUM – Center for Marine Environmental Sciences, University of Bremen, with a Thermal-Conversion/Elemental-Analyser operated at 1400°C coupled to a ThermoFisher Scientific MAT 253 mass-spectrometer. Measurements were repeated ten times for each seawater sample. Four in-house water standards used for calibration were calibrated against IAEA standards VSMOW, GISP and SLAP. The maximum deviation from the calibration slope was 1.6 ‰ vs. VSMOW and the average deviation was 0.7 ‰ vs. VSMOW.

3.2.4. Lipid analysis

Suspended particle samples were freeze-dried in a Christ Alpha 1-4 freeze-dryer. Lipids were extracted in a DIONEX Accelerated Solvent Extractor (ASE 200) using a dichloromethane (DCM): methanol (MeOH) 9 : 1 solution at 1000 psi and 100 °C for three cycles lasting 5 minutes each. Prior to extraction 2-nonadecanone and erucic acid were added as internal standards for the ketone and acid fractions, respectively. After extraction, samples were dried in a Heidolph ROTOVAP system. The extracts were saponified using 0.1 mol KOH in MeOH, yielding neutral and acid fractions. The neutral fraction was separated in three fractions using activated silica gel chromatography (1% H_2O). The first fraction was eluted with hexane, yielding saturated and unsaturated hydrocarbons. The second fraction was eluted with (DCM), yielding ketones, including alkenones. The third fraction was eluted with DCM:MeOH 1:1, yielding polar compounds. The acid fraction was methylized with MeOH of known isotopic composition (-156 ± 2 ‰ vs. VSMOW), yielding the corresponding fatty acid methyl esters (FAMEs). The FAMEs were subsequently cleaned over pipet columns containing two centimeters of silica. In order to remove unsaturated compounds, further cleaning over columns of two centimeters of $AgNO_3$ was conducted. Ketones and FAMEs were analyzed using a ThermoFisher Scientific Focus gas chromatograph equipped

with an Rxi-5ms 30x column (30 m, 0.25 mm, 0.25 µm) and a flame ionization detector. Compounds were quantified by comparing the integrated peak areas of the compounds to external standard solutions. Precision of compound quantification is about 5% and precision of $U_{37}^{k'}$ reconstructions is 0.38°C based on multiple standard analyses. Compound-specific isotope analyses was carried out on a ThermoFisher Scientific MAT 253 Isotope Ratio Mass Spectrometer coupled via a GC Isolink operated at 1420°C to a ThermoFisher Scientific Trace GC equipped with a HP-5ms column (30 m, 0.25 mm, 1 µm). For each sample duplicate injections of C_{37} and palmitic acid were conducted. Measurement accuracy was controlled by *n*-alkane standards of known isotopic composition every six measurements and by the daily determination of the H_3^+ factor using H_2 as reference gas. H_3^+ factors varied between 5.6 and 6.2, while the mean absolute deviation of external standards was 2.2‰. In order to prevent a bias introduced by variable alkenone distribution, the δD of alkenones was analyzed for $C_{37:2}$ and $C_{37:3}$ together rather than separately (van der Meer et al., 2013). δD values for palmitic acid were corrected for the methyl group added during methylation.

3.3. Results

Onboard sea surface temperature measurements resulted in uniform values of 28.5 ± 0.5 °C, while salinity varied between 10 and 36 psu (Fig. 3.1; Table 3.1). The hydrogen isotope analyses of seawater samples yielded δD values between 6 and -15 ‰ (all isotope values are given vs. VSMOW). The values correlated linearly with sea surface salinity (Fig. 3.2a). The suspended particle samples yielded C_{37} alkenone concentrations between 0.2-65.3 ng L^{-1} (Table 3.1). Samples with a salinity >25 psu showed variable concentrations (0.2-65.3 ng L^{-1}), while samples with a salinity <25 psu had concentrations consistently lower than 10 ng L^{-1}. There were little to no alkenones (concentration <1 ng L^{-1}) in filter samples with a salinity <15 psu (Fig. 3.2c, Table 3.1). The fatty acid analysis yielded almost exclusively short chain compounds, of which palmitic acid had concentrations between 1.4 and 27 µg L^{-1} (Fig. 3.2d). Variations in palmitic acid concentrations showed a weak inverse correlation with salinity (Fig. 3.2d). For samples with alkenone concentrations >10 ng L^{-1}, sea surface temperature reconstructions agreed within the calibration error of 1.5°C with onboard temperature measurements (Fig. 3.2b, Table 3.1). Samples with a concentration <10 ng L^{-1} featured a larger scatter with deviations from onboard measurements of up to 10°C (Fig. 3.2b). The ratio of the C_{37}/C_{38} alkenones resulted in values between 0.9 and 1.7 (Table 3.1), indicating the prevalence of open ocean haptophyte contribution throughout the transect (Rosell-

Mele et al., 1994). The $C_{37:4}$ alkenone, sometimes used as a salinity proxy, was not present in our samples.

Due to the absence of alkenones in the low salinity samples, isotope analysis of the C_{37} alkenone was only possible in samples with a salinity > 15 psu. For these samples, δD_{C37} varied between -176 ‰ and -205 ‰ (Fig. 3.3a, Table 3.1). When all samples are taken into account, δD_{C37} and δD_{H_2O} do not correlate (Fig. 3.3a). If only the samples with an alkenone concentration >10 ng L^{-1} were considered, linear regression yielded a correlation between δD_{C37} and δD_{H_2O} with a slope of 1.36 ‰ δD_{C37} per 1‰ δD_{H_2O} ($r^2 = 0.51$, $p < 0.05$; Fig. 3.3a). $\alpha_{C_{37}}$ varied between 0.79 and 0.84 and showed no significant salinity dependence (Fig. 3.3c). In contrast to δD_{C37}, δD_{PA} strongly correlates with δD_{H_2O}, regardless of lipid concentration ($r^2 = 0.81$, $p < 10^{-7}$; Fig. 3.3b). The slope of the linear regression is 1.72 ‰ δD_{PA} per 1 ‰ δD_{H_2O}. The fractionation factor between palmitic acid and water (α_{PA}) yielded values between 0.79 and 0.83, featuring a significant salinity dependency with an increase of 0.001 per salinity unit (Fig. 3.3d).

Table 3.1. Average geographic position, average measured sea surface temperature (SST), average sea surface salinity (SSS), C_{37} concentration, palmitic acid (PA) concentration, $U_{37}^{k'}$, C_{37}/C_{38} ratio, δD of water (δD_{H_2O}), δD of C_{37} (δD_{C37}) and δD of palmitic acid (δD_{PA})for each sample. Values for salinity and temperature are the average of onboard measurements taken in one second intervals during each filtering period. Errors represent the standard deviation of these measurements. δD values of water represent the mean of two samples taken at the beginning and the end of each filtering period, each sample represents the mean of ten replicate injections. Errors represent the propagated standard deviation of these measurements. δD values of C_{37} and palmitic acid are the means of duplicate measurements. Errors represent the range between the duplicate measurements.

Sample	Lat.	Long.	SST (C°)	SSS (psu)	Conc. C_{37} (ng L^{-1})	Conc. PA (µg L^{-1})	$U_{37}^{k'}$	C_{37}/C_{38}	δD_{H_2O}	δD C_{37}	δD PA
PP10	1.9035	-48.4169	28.37 ± 0.03	36.2 ± 0.09	47.7	1.3	0.98	1.46	4.8 ± 0.9	-190.1 ± 0.5	-170.8 ± 1
PP11	1.7587	-48.2568	28.99 ± 0.04	34.72 ± 0.51	54.2	N/A	0.96	1.56	6.6 ± 1.2	-189.2 ± 3.7	N/A
PP12	1.7123	-48.2975	29.28 ± 0.05	31.65 ± 1.1	65.3	6	0.95	1.45	2.3 ± 1.1	-185.4 ± 2.2	-183.5 ± 0.8
PP13	1.6655	-48.3388	29.31 ± 0.18	28.06 ± 1.2	20.6	16.6	0.96	1.47	-2.6 ± 1.6	-200.8 ± 1.9	-193.2 ± 1.7
PP14	1.6197	-48.3791	29.17 ± 0.03	25.79 ± 0.51	5.7	12.3	0.94	1.42	-4.1 ± 1.1	-206.3 ± 1.3	-197.5 ± 0.4
PP15	1.5724	-48.421	29.28 ± 0.05	22.86 ± 0.47	8.6	19.4	0.95	1.44	-6.7 ± 1	a	-205.4 ± 0.9
PP16	1.5676	-48.4632	29.23 ± 0.05	20.91 ± 0.47	1.4	13.9	0.89	1.33	-9.2 ± 0.9	a	-209.7 ± 0.6
PP17	1.6199	-48.5119	29.02 ± 0.07	20.55 ± 0.41	1.5	8.7	0.89	1.19	-11.8 ± 1.4	-176.9 ± 0.3	-205.9 ± 0
PP19	2.0306	-48.759	28.67 ± 0.02	17.84 ± 0.55	3.8	N/A	0.71	2.52	-14.5 ± 1.3	a	N/A
PP20	2.0858	-48.7282	28.73 ± 0.03	21.15 ± 1.38	2.6	N/A	0.81	1.08	N/A	a	N/A
PP21	2.1431	-48.6728	28.82 ± 0.02	26.22 ± 1.63	1.3	N/A	0.79	1.12	N/A	a	N/A
PP22	2.1815	-48.6369	28.82 ± 0.05	30.76 ± 1.2	2.8	N/A	0.91	1.44	N/A	a	N/A
PP23	2.2205	-48.6038	28.9 ± 0.02	33.25 ± 0.5	2.8	N/A	0.95	1.43	N/A	a	N/A

Sample	Lat.	Long.	SST (C°)	SSS (psu)	Conc. C_{37} (ng L^{-1})	Conc. PA (µg L^{-1})	$U_{37}^{k'}$	C_{37}/C_{38}	δD_{H_2O}	δD C_{37}	δD PA
PP24	2.259	-48.6055	28.93 ± 0.02	33.89 ± 0.11	4.9	N/A	0.97	0.99	3.8 ± 0.9	-191.8 ± 1.9	N/A
PP25	2.3389	-48.7336	28.84 ± 0.04	27.45 ± 1.27	5.1	N/A	0.87	0.92	N/A	a	N/A
PP26	2.2984	-48.7711	28.82 ± 0.03	23.96 ± 1.09	0.4	N/A	0.87	1.25	N/A	a	N/A
PP27	2.2674	-48.7995	28.71 ± 0.04	20.8 ± 0.71	0.4	N/A	0.65	0.98	N/A	a	N/A
PP33	2.0652	-48.5919	28.6 ± 0.04	17.44 ± 0.24	1.1	N/A	0.68	1.01	N/A	a	N/A
PP34	1.9301	-48.5528	28.63 ± 0.04	16.02 ± 0.12	6.6	N/A	0.78	1.27	N/A	a	N/A
PP35	1.7071	-48.4395	28.45 ± 0.04	18.21 ± 0.39	0.8	N/A	0.76	1.03	N/A	a	N/A
PP36	1.6196	-48.4013	28.55 ± 0.06	24.34 ± 0.4	2.2	16.5	0.85	1.17	-9.1 ± 1.2	a	-204.3 ± 0.2
PP37	1.7662	-48.4925	28.37 ± 0.03	17.63 ± 1.27	0.6	N/A	0.76	1.2	N/A	a	N/A
PP38	2.0088	-48.6108	28.35 ± 0.05	14.14 ± 0.76	0.7	N/A	0.64	1.02	-17.4 ± 0.9	a	N/A
PP40	2.8827	-49.4089	28.73 ± 0.03	33.54 ± 0.06	4.0	N/A	0.81	0.99	N/A	a	N/A
PP41	2.8566	-49.3425	29.08 ± 0.06	29.34 ± 1.32	0.2	2.1	0.81	1.8	0.2 ± 0.9	a	-188 ± 1.1
PP42	2.8342	-49.3151	29.04 ± 0.03	26.65 ± 1.52	0.2	2.0	0.86	1.25	-2.2 ± 1.1	a	-197.1 ± 0.7
PP43	3.1391	-49.3335	28.46 ± 0.04	36.16 ± 0.11	16.7	5.5	0.97	1.55	5.9 ± 1.3	-180.3 ± 0.6	-183.4 ± 0.8
PP44	3.0999	-49.3064	28.23 ± 0.03	34.89 ± 0.45	59.1	N/A	0.98	1.54	6.3 ± 1.1	-189 ± 1.4	N/A
PP45	3.0627	-49.4272	28.51 ± 0.02	32.83 ± 0.8	33.3	N/A	0.98	1.63	4.1 ± 0.9	-190.8 ± 0.4	N/A
PP46	3.0911	-49.4337	28.68 ± 0.04	33.1 ± 0.65	9.2	N/A	0.96	1.42	N/A	a	N/A
PP47	3.0554	-49.4321	28.49 ± 0.01	29.2 ± 0.08	6.1	16.4	0.96	1.29	0 ± 0.9	-177.2 ± 1.4	-201.6 ± 0.7
PP48	2.915	-49.3347	28.03 ± 0.02	23.42 ± 0.27	7.7	7.2	0.88	1.14	-9.2 ± 1.4	-197.9 ± 0.5	-202.3 ± 1.6

Sample	Lat.	Long.	SST (C°)	SSS (psu)	Conc. C_{37} (ng L^{-1})	Conc. PA (µg L^{-1})	$U_{37}^{k'}$	C_{37}/C_{38}	δD_{H_2O}	δD C_{37}	δD PA
PP49	2.8972	-49.4713	28.07 ± 0.03	21.86 ± 0.46	1.3	16.2	0.89	1.23	-8.4 ± 1	a	-211.7 ± 0.3
PP51	3.1025	-49.7931	28.3 ± 0.06	18.31 ± 0.21	2.2	N/A	0.74	1.04	N/A	a	N/A
PP52	3.098	-49.6761	28.68 ± 0.03	24.91 ± 0.16	0.6	27.0	0.86	1.23	-10 ± 1.3	a	-204.9 ± 1.6
PP53	3.5031	-50.1667	28.25 ± 0.08	20.33 ± 1.93	1.0	N/A	0.85	1.38	N/A	a	N/A
PP54	3.5576	-50.3623	28.2 ± 0.1	18.63 ± 0.6	0.3	11.9	0.82	1.05	N/A	a	N/A
PP55	3.9688	-50.5373	28.27 ± 0.16	16.94 ± 1.38	0.7	N/A	0.75	1.04	-16 ± 0.8	a	N/A
PP57	4.4874	-51.2401	28.04 ± 0.05	15.88 ± 0.09	0.1	17.7	0.82	b	-18.2 ± 0.7	a	-220.3 ± 0.8
PP60	6.1499	-51.2679	28.09 ± 0.03	36.16 ± 0.01	2.0	2.7	0.99	b	5.8 ± 0.8	-183.2 ± 1.2	-182.4 ± 0.6
PP61	5.5698	-51.8561	27.93 ± 0.09	32.19 ± 1.28	23.4	N/A	0.98	1.11	2.1 ± 1.3	-191.1 ± 2.7	N/A
PP62	5.3201	-51.9255	27.9 ± 0.04	22.72 ± 1.32	3.4	23.2	0.97	1.1	-8.3 ± 0.9	-192 ± 5.4	-209.7 ± 1.4
PP65	4.766	-51.5166	27.55 ± 0.08	17.58 ± 4.51	1.1	20.2	0.97	1.05	N/A	a	N/A
PP66	6.658	-52.8391	28.09 ± 0	36.06 ± 0	7.1	4.01	0.96	1.2	6.2 ± 0.7	-195.5 ± 0.1	-188.9 ± 0.5
PP67	5.9423	-52.6319	27.91 ± 0.07	25.25 ± 1.1	9.2	13.4	0.97	1.32	-4.9 ± 1.2	-183.7 ± 2	-206.7 ± 0
PP68	5.79	-52.7484	27.53 ± 0.06	23.4 ± 0.17	4.6	N/A	0.96	1.16	-7.1 ± 1.2	-192.5 ± 0.4	N/A
PP69	6.0839	-53.601	27.47 ± 0.03	22.69 ± 0.24	2.5	N/A	0.8	1.45	N/A	a	N/A
PP70	6.2821	-53.1561	27.64 ± 0.03	24.96 ± 0.74	2.4	N/A	0.96	1.03	N/A	a	N/A

[N/A] No measurements conducted

[a] C_{37} yield was not high enough for isotope analysis

[b] No clear peak distinction for C_{38}

3.4. Discussion

3.4.1. Lipid sources

3.4.1.1. Alkenone sources

The C_{37}/C_{38} ratio was used for the assessment of the dominant alkenone source (Conte et al., 1998). Open marine species like *Emiliana huxleyi* and *Gephyrocapsa oceanica* produce alkenones with a C_{37}/C_{38} between 0.5 and 1.5 (Conte et al., 1998). Coastal species like *Isochrysis galbana* and *Chrysotila lamellosa* produce alkenones with a C_{37}/C_{38} ratio >2, sometimes even >10 (M'Boule et al., 2014; Marlowe et al., 1984; Prahl et al., 1988). The C_{37}/C_{38} ratio of the samples from the Amazon Plume varied between 0.9 and 1.7 and alkenone production was therefore likely dominated by open marine species (Conte et al., 1998). Since some of the samples feature values at the upper limit for open marine species, some (probably small) contribution by coastal haptophytes cannot be ruled out (Kasper et al., 2015). Alternatively, the small variations in the C_{37}/C_{38} ratio could also be the effect of species variability within open marine haptophytes (Conte et al., 1998). In contrast to previous laboratory and field studies (Chu et al., 2005; Ono et al., 2009), we do not find a correlation between salinity and the C_{37}/C_{38} ratio (not shown here).

3.4.1.2. Palmitic acid sources

Palmitic acids are not exclusively produced by aqueous organisms and are also synthesized by terrestrial plants and bacteria (Eglinton and Eglinton, 2008). Unlike aqueous organisms, terrestrial plants also synthesize long-chain fatty acids (Eglinton and Hamilton, 1967), which were not present in the filter samples. This indicates that the palmitic acids found in the Amazon Plume are exclusively produced by aquatic organisms. Also, the fast turnover rates of palmitic acid makes a contribution by riverine compounds unlikely. Furthermore, previous studies have generally confirmed that palmitic acids in marine environments are predominantly produced by marine algae (Pearson et al., 2001).

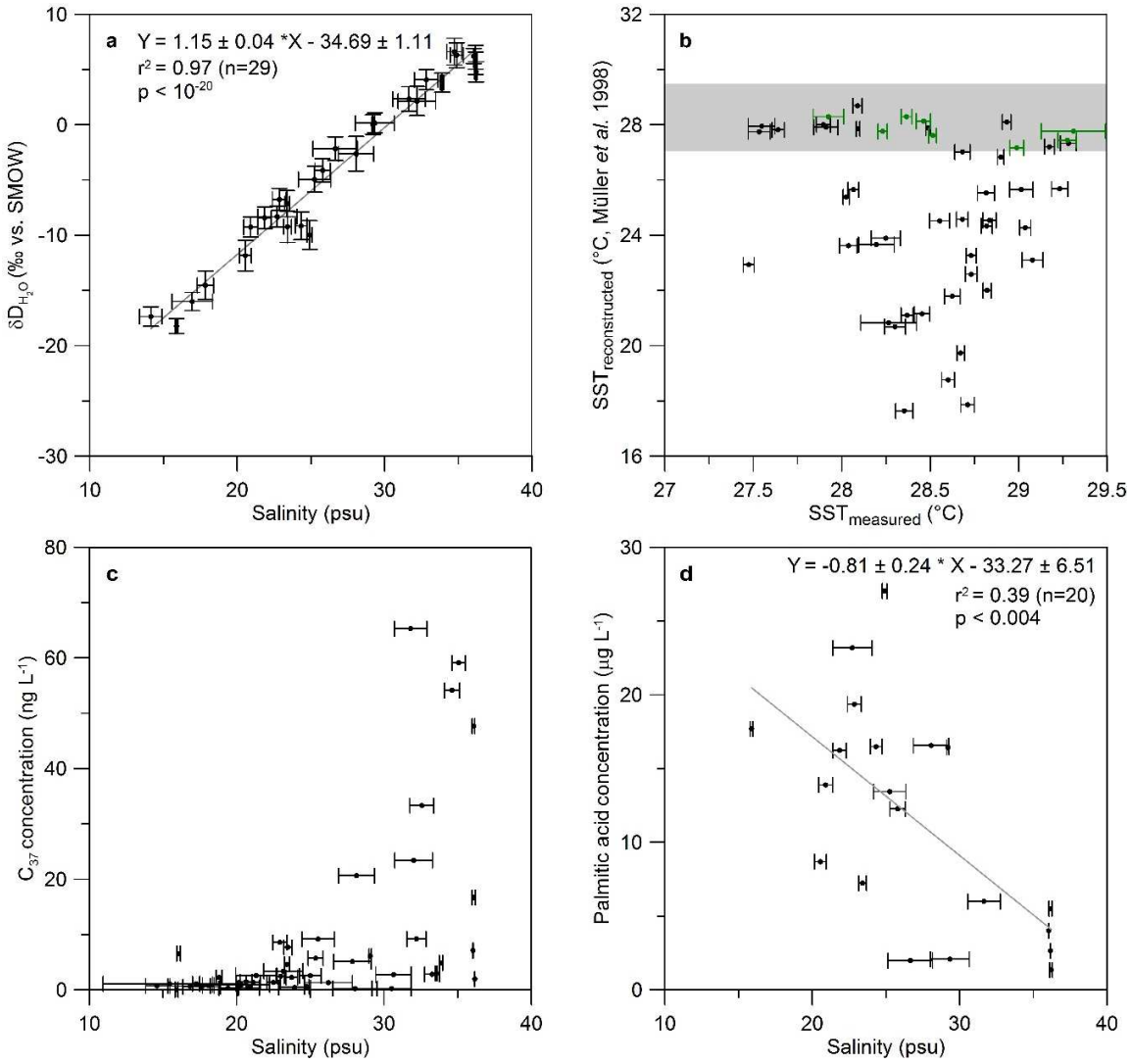

Figure 3.2. a) δD_{H_2O} plotted against salinity; b) $U^{k'}_{37}$ based sea surface temperature (SST) reconstruction using the calibration by Müller et al. (1998) plotted against measured temperature. Green data points represent samples with a C_{37} concentration > 10 ng L^{-1}. The grey bar indicates the range of measured SST; c) Concentration of the C_{37} alkenones plotted against salinity; d) Palmitic acid concentration plotted against salinity.

3.4.2. Temperature reconstruction

Oceanic temperature reconstructions based on alkenones are a widely used tool in paleoclimatology (Bard et al., 1997; Rühlemann et al., 1999). The global calibrations in use are based on open marine haptophyte species (Müller et al., 1998; Prahl and Wakeham, 1987). Our reconstructed temperatures show deviations of up to 10°C from instrumentally measured temperature for samples with alkenone concentration <10 ng L^{-1} (Fig. 3.2b). These anomalous, generally lower than expected values, could be caused by different processes. First, coastal species bear a temperature-$U^{k'}_{37}$ relationship with a markedly lower slope than open marine species (Sun et al., 2007; Versteegh et al., 2001). Hence, a larger alkenone contribution by coastal haptophyte species would lead to the observed lower temperatures. Second, lower salinity is reported to cause metabolic stress in alkenone producers leading to anomalous reconstructed temperatures (Harada et al., 2003). Third, variations in haptophyte growth rate due to nutrient or light limitation could also lead to variations in reconstructed temperatures (Epstein et al., 1998; Versteegh et al., 2001). The latter two points would also lead to lower alkenone concentrations and thus enhance the possibility of overprint by advection of allochthonous alkenones.

Variations in haptophyte algae composition recorded by changes in the C_{37}/C_{38} ratio do not show a correlation with the residue

$$T_{residue} = T_{measured} - T_{reconstructed} \quad (3.3)$$

of the temperature reconstruction (not shown here). Hence, variations in species composition are likely insufficient to account for the $T_{residue}$. Conversely, there is a correlation between $T_{residue}$ and salinity (Fig. 3.4a). Salinity might therefore be an important cause for the large $T_{residue}$ (Harada et al., 2003). The riverine waters of the Amazon Plume are generally nutrient rich (Santos et al., 2008), which makes a scenario of nutrient limitation unlikely to impact temperature control of $U^{k'}_{37}$ in our study area. The high sediment load delivered by the Amazon River, however, leads to light limitation in the study area (Smith and Demaster, 1996). Light limitation is indeed reported to lower reconstructed $U^{k'}_{37}$ temperatures by up to 7°C (Versteegh et al., 2001). Since diminished alkenone production due to low salinity and light limitation would lead to smaller alkenone concentrations, this would also explain why high concentration samples feature no temperature deviation (Fig. 3.4b). The advection of allochthonous alkenones biasing temperature reconstructions has been suggested in other studies (Benthien and Müller, 2000; Rühlemann and Butzin, 2006). In our samples, $U^{k'}_{37}$ overprint by advected alkenones

can be considered less likely, since there are no nearby areas where alkenones with a lower temperature signal could originate from.

In conclusion, there are multiple potential factors influencing the $U_{37}^{k'}$ deviation in the Amazon Plume. Given that low alkenone concentrations are consistently associated with large negative temperature deviations, reduced alkenone production due to low salinity and light limitation in the Amazon Plume might be the most important factor for the temperature deviations (Fig. 3.4a, b) (Harada et al., 2003; Versteegh et al., 2001).

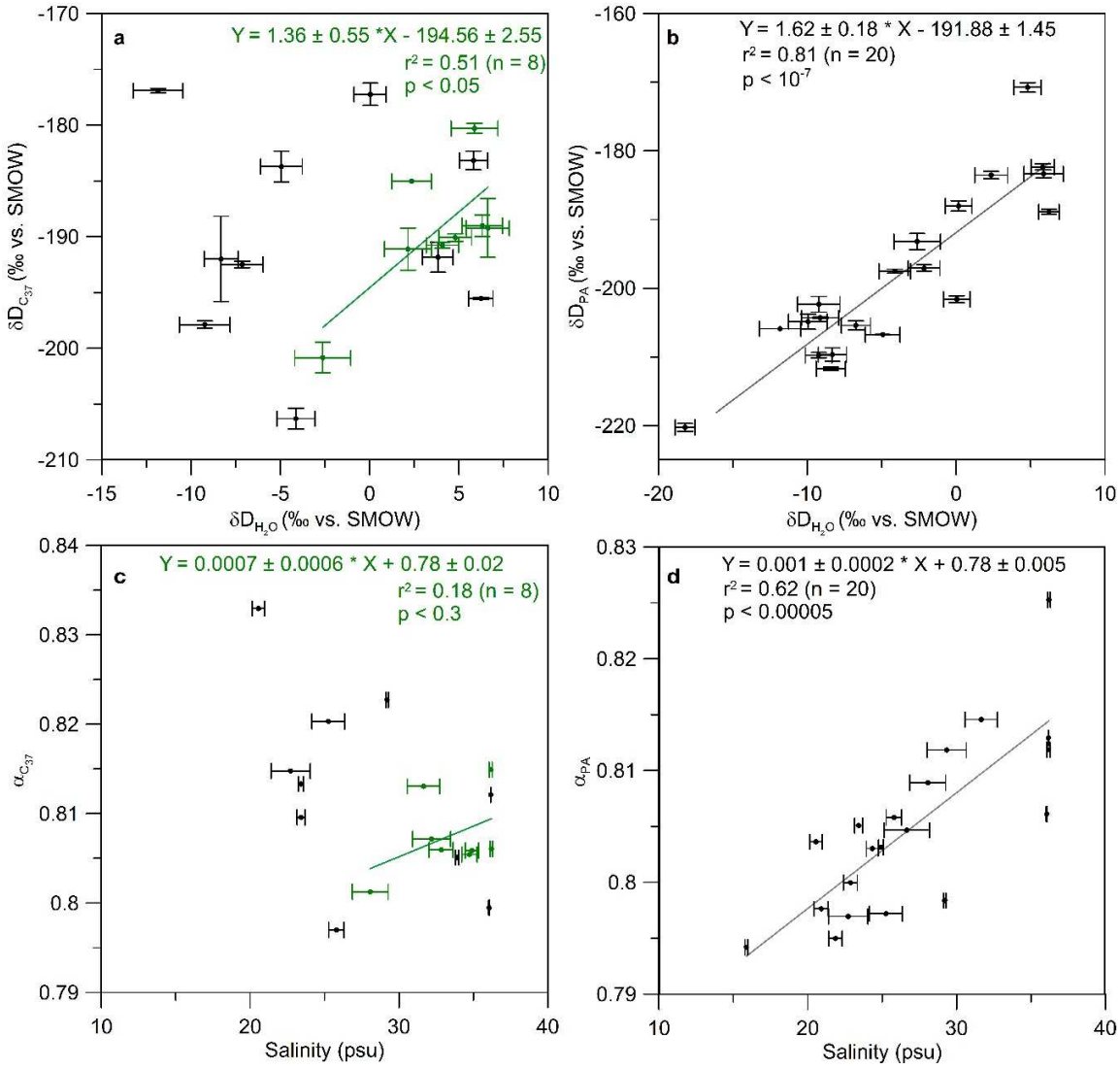

Figure 3.3. Results of the δD_{lipid} analysis. a) $\delta D_{C_{37}}$ plotted against δD_{H_2O}. Green data points represent samples with a C_{37} concentration > 10 ng L^{-1}; b) δD_{PA} against δD_{H_2O}; c) $\alpha_{C_{37}}$ against salinity. Green data points represent samples with a C_{37} concentration > 10 ng L^{-1}; d) α_{PA} against salinity.

3.4.3. Stable hydrogen isotope signals

3.4.3.1. Alkenone δD

If all samples are considered, there is no correlation between δD_{C37} and δD_{H_2O} (Fig. 3.3a). Given the relationship between C_{37} concentration, $T_{residue}$ and salinity (Fig. 3.4a, b), we also tested whether there would be a better fit between δD_{C37} and δD_{H_2O} for high C_{37} concentration samples. There is indeed a correlation between δD_{C37} and δD_{H_2O} for samples with a C_{37} concentration >10 ng L^{-1} (Fig. 3.3a). However, with a p-value of 0.05 and a low sample number of n=8, this relationship has to be viewed with caution. Nevertheless, we consider it to be an important information to study the potential factors leading to the deviation between δD_{C37} and δD_{H_2O}. Especially, since this relation reflects a generally constant α_{C37} of 0.81 and agrees with results obtained for open marine species cultured at different salinities (M'Boule et al., 2014). For a potential impact on δD_{C37}, factors similar to those considered for the temperature deviations have to be scrutinized: synthesis by coastal haptophyte species (M'Boule et al., 2014), changes in growth rate and phase (Schouten et al., 2006; Wolhowe et al., 2009), overprint by advected material and variations in salinity (Schouten et al., 2006). Since temperature is more or less uniform over the entire study area, a temperature effect as reported by Zhang and Sachs (2007) is not expected to play a role.

As previously mentioned, variations in the C_{37}/C_{38} ratio imply only limited variation in haptophyte species composition. Moreover, the values of α_{C37} are between 0.795 and 0.835 and are only slightly higher than observed in laboratory experiments studying open marine haptophytes (Schouten et al., 2006), but are markedly lower than observed for coastal haptophytes (M'Boule et al., 2014). This again suggests that the studied alkenones are predominantly of open marine haptophyte origin. Although there are no signs for a full scale change from open marine to coastal haptophytes, the variability in habitat preference may still be sufficient to have a significant influence on α_{C37}. The C_{37}/C_{38} variability found in a sediment core collected offshore Mozambique by Kasper et al. (2015) was similar to the one found in our samples and the associated species variability was likely large enough to significantly influence δD_{C37}. In our samples, the C_{37}/C_{38} ratio does however not correlate with α_{C37} and species variations alone are therefore unlikely to be the dominant cause for the absent correlation between δD_{C37} and δD_{H_2O} in low salinity samples. In contrast to laboratory studies (Schouten et al., 2006), we find no clear relationship between salinity and fractionation factor (Fig. 3.3c). The absence of a salinity-α_{C37} relationship was also reported in a field study by Schwab and Sachs (2011) who explained their findings by the presence of additional factors such as species variability and temperature, which may have

counteracted the effects of salinity. If the relation between δD_{C37} and δD_{H_2O} for high concentration samples is used to calculate the residue for each sample,

$$\delta D_{res\ C37} = \delta D_{\ C37} - (1.358\ \times \delta D_{H_2O} - 194.558) \quad (3.4)$$

it becomes apparent that low concentration samples have higher residuals (Fig. 3.4d). Furthermore, $\delta D_{res\ C37}$ correlates with salinity, which indicates that $\delta D_{res\ C37}$ is largely influenced by the input of low salinity Amazon freshwater (Fig. 3.4c). This observation would also fit with the assumption that the lower C_{37} concentration in those samples were a result of lower growth rate, because lower growth rate leads to a higher fractionation factor (M'Boule et al., 2014; Sachse and Sachs, 2008; Schouten et al., 2006). Since the steep salinity gradient of the Amazon Plume leads to a wide range of surface water isotopic composition over a short geographic distance, we cannot exclude some influence of advected alkenones in samples with low or absent in situ alkenone production. As this effect is insufficient to explain the large $T_{residue}$, advection is likely not the main factor responsible for the absence of a correlation between δD_{C37} and δD_{H_2O}. Although the deviation in δD_{C37} cannot be tied to a single factor, low alkenone production associated with the low salinity, suspension rich Amazon waters is likely the most important factor (Wolhowe et al., 2015). Thus, the temperature- and δD_{C37} deviations are likely caused by similar effects (Fig. 3.4a-d).

3.4.3.2. Palmitic acid δD

In contrast to δD_{C37}, δD_{PA} correlates well with δD_{H_2O} (Fig. 3.3b). Furthermore, α_{PA} correlates with salinity (Fig. 3.3d) and thus confirms the relationship between salinity and α observed in various laboratory and field studies for palmitic acid and other lipids (Chivall et al., 2014a; M'Boule et al., 2014; Schouten et al., 2006). Our findings imply that the limiting factors potentially leading to variations in α_{C37} do not influence α_{PA}. The factors that could potentially influence δD_{PA} are largely similar to those influencing δD_{C37} (Chivall et al., 2014a). Unlike for alkenones there is, however, no clear evidence for a growth rate dependence of α_{PA} (Zhang et al., 2009).

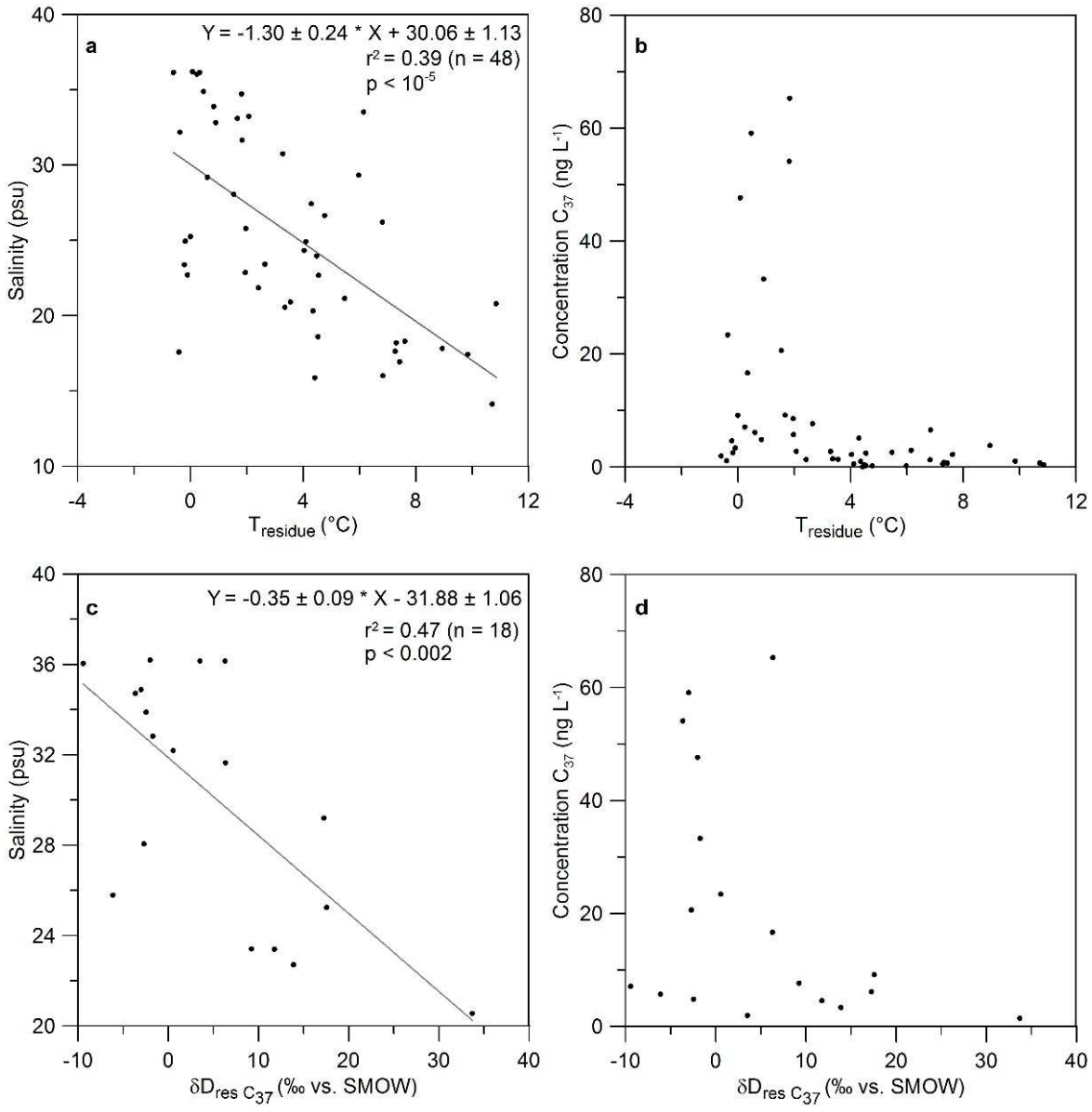

Figure 3.4. Residues of the $U_{37}^{k'}$ based SST reconstruction plotted against salinity (a) and C_{37} concentration (b). Residues of the $\delta D_{C_{37}}$ measurement plotted against salinity (c) and C_{37} concentration (d).

One striking difference between palmitic acid and alkenones in our samples is the different abundance of the two compounds. Palmitic acid concentrations were about three orders of magnitude higher than alkenone concentrations (Fig. 3.2c, d). This is unsurprising, since palmitic acid is typically very abundant in marine environments (Pearson et al., 2001). In further contrast to the C_{37} concentration, the palmitic acid concentration was not lower in low salinity samples, but featured a trend towards higher concentrations. This indicates that

palmitic acid producing organisms were not negatively affected by the low salinity, sediment rich Amazon input like haptophyte algae, but rather benefited from the high nutrient supply by the Amazon (Santos et al., 2008). This marked difference supports the notion that low alkenone production rates in parts of the study area were responsible for the α_{C37} deviations. Furthermore, the high palmitic acid concentrations also limit the influence of a possible overprint of the in situ signal by allochthonous compounds. Apart from that, the high turnover rate of palmitic acid may further impede the influence of allochthonous compounds. This is also in contrast to alkenones, which are comparably stable towards degradation (Sun and Wakeham 1994). Therefore, the lower turnover rate of alkenones renders these compounds more susceptible to overprint by older, allochthonous compounds.

Our study shows that α_{PA} remains relatively stable over a range of varying environmental conditions. This finding is similar to one reached by studies along a lake transect from Southern Canada to Florida, which found a good agreement between δD_{PA} and δD_{H_2O} over a variety of ecological environments (Huang et al., 2002, 2004). The α_{PA} of 0.82 observed in those studies is also in the range of α_{PA} observed in the Amazon Plume (0.79-0.83). This further indicates that species composition and other factors are not influencing α_{PA} to a large extent on an ecosystem level. Potential variations of α_{PA} from different contributors are either small or levelled out by integration over ecosystems. A surprising constancy in δD_{PA} has also been observed in a sediment core from the Santa Barbara Basin (Li et al., 2009). There, the δD_{PA} remained constant even in the presence of heterotrophic palmitic acid producers. This could indicate that the constancy in α_{PA} is not only limited to phototrophic organisms as observed here and by Huang et al. (2004), but also extends to heterotrophic organisms. The constancy could be caused by the very similar biosynthetic pathway for palmitic acid in bacteria and eukaryotes (Li et al., 2009).

Although there are multiple lacustrine studies successfully applying δD_{PA} as paleoenvironmental proxy (Shuman et al., 2006; Smittenberg et al., 2011) and δD_{PA} faithfully records δD_{H_2O} in our study, there are still multiple factors that could overprint a surface δD_{PA} signal. Especially in open oceanic environments, palmitic acid production deeper in the water column could alter the signal recorded at the surface. After deposition, bacterial activity in the sediment could also overprint the original upper water column signal (Perry et al., 1979).

3.5. Conclusions

Our study shows that δD_{PA} in suspended particle samples from the Amazon Plume salinity gradient records variations in salinity. For δD_{C37}, this correlation is only present in samples above a C_{37} concentration of 10 ng L^{-1}. The low alkenone concentrations are likely caused by the sediment-rich freshwater input of the Amazon River impeding haptophyte growth and affecting α_{C37}. Hence, the ubiquitous nature of palmitic acid proved to be highly beneficial in the study area. Moreover, palmitic acid bears the advantage of easier isotopic measurement and a high availability in most environments. The use of δD_{PA} as a standalone salinity proxy has to be considered with caution. Potential disadvantages of palmitic acid include post depositional degradation, compound synthesis deeper in the water column, which may not record surface conditions and the bacterial overprint in the sediment. A possible way to circumvent these limitations, as well as the problems encountered for δD_{C37}, could be the alongside use of δD_{PA} and δD_{C37}. δD_{PA} is not sensitive to the low concentration issues encountered in this study, while δD_{C37} is only produced in surface waters and not susceptible to synthesis or degradation deeper in the water column or sediments. Therefore, the combined study of compound-specific hydrogen isotope composition of more than one compound could yield important information on influences in δD_{Lipid} other than salinity.

Acknowledgements

We would like to acknowledge funding through the DFG-Research Center / Cluster of Excellence „The Ocean in the Earth System“ at MARUM- Center for Environmental Sciences. CH thanks GLOMAR – Bremen International Graduate School for Marine Sciences for support and CMC acknowledges financial support from FAPESP (grant 2012/17517-3). We thank the *RV Maria S. Merian* cruise MSM20/3 crew for technical support during sampling, and Ralph Kreutz and Ana C. R. de Albergaria-Barbosa for laboratory support. Helpful comments by two anonymous reviewers greatly improved the manuscript.

4. Origin, transport and deposition of leaf-wax biomarkers in the Amazon Basin and the adjacent Atlantic

Christoph Häggi[a], André O. Sawakuchi[b], Cristiano M. Chiessi[c], Stefan Mulitza[a], Gesine Mollenhauer[a,d], Henrique O. Sawakuchi[e], Paul A. Baker[f,g], Matthias Zabel[a] and Enno Schefuß[a]

[a] *MARUM – Center for Marine Environmental Sciences, University of Bremen, Leobener Str., 28359 Bremen, Germany*

[b] *Institute of Geosciences, University of São Paulo, Rua do Lago, 562, São Paulo, SP 05508-080, Brazil*

[c] *School of Arts, Sciences and Humanities, University of São Paulo, Av. Arlindo Bettio 1000, São Paulo SP 03828-000, Brazil*

[d] *Alfred Wegener Institute – Helmholtz Centre for Polar and Marine Research, Am Handelshafen 12, 27570 Bremerhaven, Germany*

[e] *Center of Nuclear Energy in Agriculture, University of São Paulo, Av. Centenário 303, Piracicaba SP 13400-970, Brazil*

[f] *Division of Earth and Ocean Sciences, Duke University, Durham, NC 27708, USA*

[g] *School of Geological Sciences and Engineering, Yachay Tech University, San Miguel de Urcuqui, Hacienda San Jose, Imbabura, Ecuador*

Published in *Geochimica et Cosmochimica Acta*, 2016, Vol. 192, pages 149-165.

Abstract

Paleoenvironmental studies based on terrigenous biomarker proxies from sediment cores collected close to the mouth of large river systems rely on a proper understanding of the processes controlling origin, transport and deposition of biomarkers. Here, we contribute to the understanding of these processes by analyzing long-chain *n*-alkanes from the Amazon River system. We use the δD composition of long-chain *n*-alkanes from river bed sediments from the Amazon River and its major tributaries, as well as marine core-top samples collected off northeastern South America as tracers for different source areas. The $\delta^{13}C$ composition of the same compounds is used to differentiate between long-chain *n*-alkanes from modern forest vegetation and petrogenic organic matter. Our $\delta^{13}C$ results show depleted $\delta^{13}C$ values (-33 to -36‰) in most samples, indicating a modern forest source for most of the samples. Enriched values (-31 to -33‰) are only found in a few samples poor in organic carbon indicating minor contributions from a fossil petrogenic source. Long-chain *n*-alkane δD analyses show more depleted values for the western tributaries, the Madeira and Solimões Rivers (-152 to -168‰), while *n*-alkanes from the lowland tributaries, the Negro, Xingu and Tocantins Rivers (-142 to -154‰), yield more enriched values. The *n*-alkane δD values thus reflect the mean annual isotopic composition of precipitation, which is most deuterium-depleted in the western Amazon Basin and more enriched in the eastern sector of the basin. Samples from the Amazon estuary show a mixed long-chain *n*-alkane δD signal from both eastern lowland and western tributaries. Marine core-top samples underlying the Amazon freshwater plume yield δD values similar to those from the Amazon estuary, while core-top samples from outside the plume showed more enriched values. Although the variability in the river bed data precludes quantitative assessment of relative contributions, our results indicate that long-chain *n*-alkanes from the Amazon estuary and plume represent an integrated signal of different regions of the onshore basin. Our results also imply that *n*-alkanes are not extensively remineralized during transport and that the signal at the Amazon estuary and plume includes refractory compounds derived from the western sector of the Basin. These findings will aid in the interpretation of plant-wax-based records of marine sediment cores collected from the adjacent ocean.

4.1. Introduction

The past climate evolution of the Amazon Basin and its implications for the global carbon cycle are the subjects of ongoing debate (Cheng et al., 2013; D'Apolito et al., 2013; Gloor et al., 2015; Phillips et al., 2009). For an improved understanding of past Amazonian climates, environmental archives such as marine sediment cores are of great importance. Terrestrial organic matter (OM) transported by rivers and deposited offshore can provide valuable

information on the continental climate and vegetation history. The analysis of specific molecular plant-wax compounds such as long-chain *n*-alkanes has proven useful for the reconstructions of past vegetation and climate conditions (e.g. Pancost and Boot, 2004; Rieley et al., 1991). For example, the hydrogen isotopic composition (δD) encoded in plant-wax compounds can be used to infer the isotopic composition of meteoric water, assuming that other variables are controlled for (e.g. Fornace et al., 2014; Sachse et al., 2012; Sauer et al., 2001; Schefuß et al., 2005; Tierney et al., 2008). The stable carbon isotope composition ($\delta^{13}C$) from the same compounds varies among vegetation types that utilize either the C3 or the C4 photosynthetic pathways and can be used as an indicator of the relative contributions of these two types of vegetation (e.g. Bird et al., 1995; Huang et al., 2001). Alternatively, $\delta^{13}C$ enrichment in long-chain *n*-alkanes may also signal the presence of highly degraded compounds derived from fossil petrogenic sources (Lichtfouse and Eglinton, 1995). In extensive river catchments like the Amazon Basin, a thorough insight into the sources and the transport processes of OM is necessary to appropriately interpret the signal encoded in plant-waxes accumulated in sediment archives. Apart from sourcing from plant organic matter, either directly or via soils, long-chain *n*-alkanes biomarkers can also be of petrogenic origin from eroded sedimentary rocks (Ishiwatari et al., 1994). Biological degradation during transport can alter and overprint the isotopic signal recorded by plant-waxes, biasing primary climate- and vegetation-related signals (Galy et al., 2011). The source region of plant-waxes may also be unevenly distributed in a river catchment (Galy et al. 2011). Additionally, the source region may vary temporally and contribute compounds from different sectors of a catchment depending on the seasonality of rainfall (Ponton et al. 2014).

So far, knowledge on sources and transport of plant-waxes in the Amazon River and its major tributaries is restricted to the Andean headwaters. In the Madre de Dios River, an Andean tributary of the Madeira River, Ponton et al. (2014) found that δD of long-chain fatty acids reflect an integrated signal along an altitudinal gradient. Their findings imply that leaf waxes accumulated downstream and that the sourcing of leaf-waxes is independent of the provenance of inorganic sediment. Similar findings have also been reported by studies using $\delta^{13}C$ analyses of bulk particulate organic carbon (POC) and lignin from Andean and lowland tributaries (e.g. Hedges et al., 2000; McClain and Naiman, 2008). $\delta^{13}C$ analyses of POC also revealed mixed contributions from Andean (30-50%) as well as lowland (50-70%) OM sources (Hedges et al., 2000; McClain and Naiman, 2008; Quay et al., 1992). Both findings suggest that unlike inorganic sediment that is mainly sourced in the Andes, OM might be mainly lowland sourced (Bouchez et al., 2014; Meade et al., 1985). Radiocarbon dating of POC revealed that while lowland sourced OM is modern, Andean sourced material contains up to 80% of old petrogenic material derived from sediments (Bouchez et al., 2014; Clark et al., 2013; Mayorga et al., 2005; Townsend-Small et al., 2007). During transport, a

considerable amount of OM is remineralized to CO_2 and CH_4 (e.g. Mayorga et al. 2005, Sawakuchi et al. 2015). The study of lignin, for instance, revealed that up to 90% of lignin transported in the Amazon is remineralized during transport (Ward et al., 2013). This raises the question whether leaf waxes in the Amazon River are also mainly lowland or Andean sourced, whether they are partially of petrogenic origin and whether compounds from the western sectors of the Amazon Basin are remineralized during transport to the Amazon estuary.

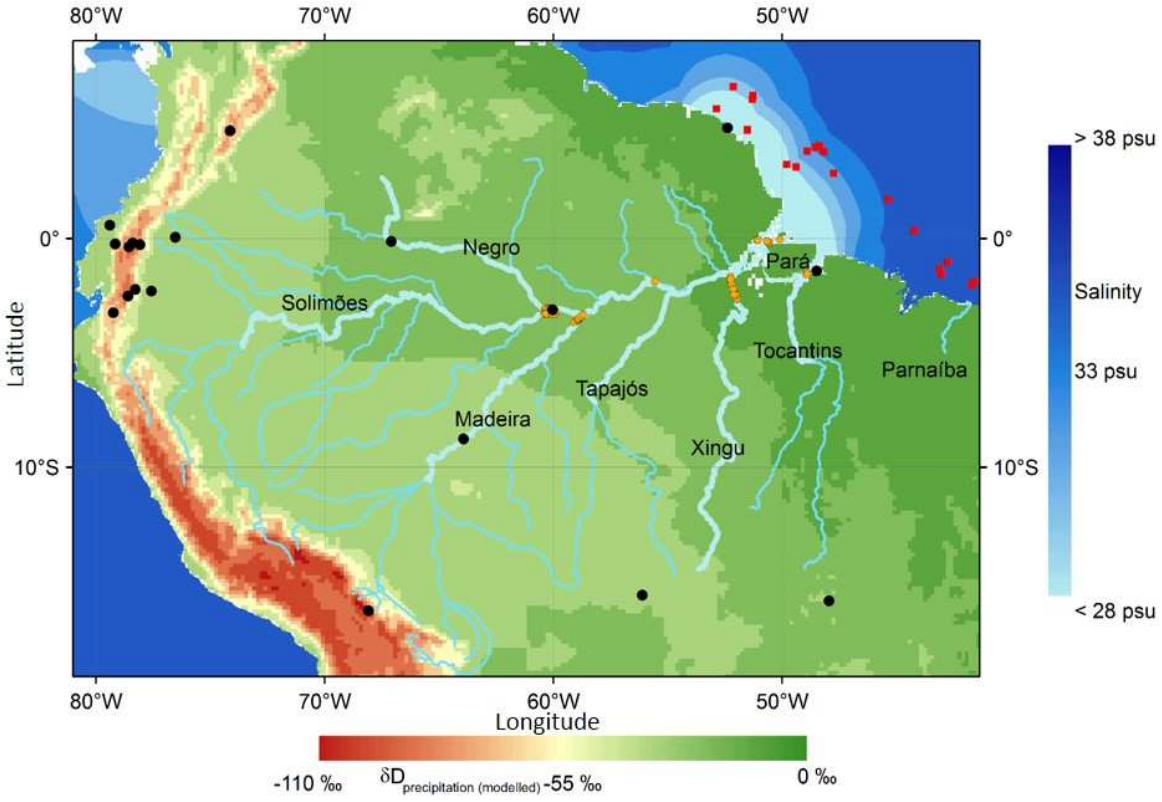

Figure 4.1. Modelled mean annual isotopic composition of precipitation in the Amazon Basin (Bowen and Revenaugh, 2003) and minimal ocean salinity during the annual cycle indicating the maximal extent of the Amazon freshwater plume (Sbrocco and Barber, 2013). Main tributaries are marked with light blue lines, river sediment samples are marked with orange dots, marine core-top samples are marked with red squares and the GNIP stations serving as base for the isotope model are marked with black dots (Bowen and Revenaugh, 2003).

Here we evaluate the stable isotopic composition (δD and $\delta^{13}C$) of long-chain *n*-alkanes from river bed sediment samples to study their source regions and transport mechanisms. Furthermore, we use the Al/Si ratio as a grain size proxy (Bouchez et al., 2011) and the Fe/K ratio to trace the origin of inorganic sediment in some samples (Govin et al., 2014). Finally, we study the offshore deposition of plant-waxes from the Amazon Basin using marine core-top samples to identify suitable areas for paleoclimate studies.

4.2. Materials and methods

4.2.1. Study area

The Amazon is the largest drainage basin on Earth. With its most remote sources located in the high Andes, the Amazon River eventually discharges some 3000 km farther east into the western equatorial Atlantic Ocean (Fig. 4.1). The Amazon River drains large parts of tropical South America, and its catchment is mostly covered by rainforest. The large western tributaries, the Madeira River and the Solimões River are generally classified as white water rivers carrying vast quantities of suspended sediment mostly derived from the Andes (Gibbs, 1967). The Negro River, the largest lowland tributary, is a black water river with little suspended sediment but a high dissolved organic carbon (DOC) load (Konhauser et al., 1994). The next two largest lowland tributaries, the Tapajós River and the Xingu River are clear water rivers which carry little organic and inorganic sediment (Moreira-Turcq et al., 2003). According to some definitions, the Tocantins River (located to the east of Xingu River) is included as a further clear water tributary of the Amazon. The estuary of the Tocantins River (called Pará River) is situated about 200 kilometers to the south of the Amazon estuary and receives some contribution from the main-stem Amazon. After its discharge into the Atlantic Ocean, Amazon river water and its suspended sediments are transported in the Amazon Plume that is entrained northwestwards along the continental margin by the North Brazil Current (Geyer et al., 1996; Muller-Karger et al., 1988). During northward transport, a portion of the Amazon sediment load is deposited on mud banks situated on the coastal shelf of Macapá, Brazil, and French Guiana (Kineke and Sternberg, 1995).

4.2.2. Sampling

River bed sediments and river water samples were collected during two field trips to the Amazon Basin in September and October 2011 (dry season) and May 2012 (wet season). The river bed samples were raised from water depths between 0.7 and 45 m from the

Madeira, Solimões, Negro, Xingu and Pará Rivers, and also from the Amazon estuary (Table 4.1, Fig. 4.1). The sampling of river bed sediment from different depths of the river allowed the collection of samples with a wide range of grain sizes and total organic carbon (TOC) content. The samples are representative of the major deposition settings of the studied rivers and comprise sediments from areas dominated by deposition of suspended sediments (floodplain margin) as well as areas dominated by bed load deposition (channel thalweg). The sampling was conducted close to the confluence of each tributary to the Amazon main stem and in the Amazon estuary in order to assess the integrated signal of each sub-catchment (Fig. 4.1). Samples were taken either with a Van Veen bottom sampler or from the uppermost four centimetres of mini-cores. All samples were stored in plastic bags. Twenty-four river water samples were collected from the Madeira, Solimões, Negro and Xingu Rivers (Table 4.1, Fig. 4.1). The water samples were pumped from 2/3 of the maximum water depth of the channel at each sampling site (i.e. between 2 and 52 m) with an in-situ Shurflo pump coupled to a hose. Water samples were stored in glass vials, sealed with Parafilm, and subsequently frozen.

Marine core-tops were collected during *RV Maria S. Merian* cruise MSM20/3 in February and March 2012 (Mulitza et al., 2013) and during the *RV Knorr* cruise KNR/97-4 in February and March 2010. The 20 selected cores were raised from water depths between 34 and 2850 m, and cover the latitudinal range from 2°S to 6°N off northeastern South America (Table 4.1, Fig. 4.1). Samples were taken from the uppermost centimetre of the MSM20/3 multicores and the uppermost ten centimetres of the KNR/97-4 multicores. All samples were stored in pre-combusted glass petri-dishes and were subsequently frozen. Core-top samples collected from the Amazon shelf (i.e. under the direct influence of the modern Amazon discharge plume) can be expected to be modern (Kineke and Sternberg, 1995), while samples from the continental slope off northeastern South America (i.e. outside the direct influence of the Amazon discharge plume) have lower accumulation rates and are therefore expected to have an integrated Holocene age (Zhang et al., 2015).

4.2.3. Methodological approach

4.2.3.1. Differentiation between modern plant and petrogenic *n*-alkanes

To differentiate between pristine plant-derived *n*-alkanes and degraded, possibly petrogenic compounds, the $\delta^{13}C$ composition of long-chain *n*-alkanes was analyzed along with the relative abundance of compounds with different chain length. *n*-Alkanes derived from petrogenic sources are ^{13}C enriched compared to C3 forest vegetation and the $\delta^{13}C$ composition can therefore be used to detect petrogenic sourcing of *n*-alkanes (Ishiwatari et

al., 1994; Lichtfouse and Eglinton, 1995). Compounds derived from C4 or CAM vegetation would also show enrichment in $\delta^{13}C$ (Castañeda and Schouten, 2011; Collister et al., 1994; Rieley et al., 1991). Since C3 forest vegetation is dominant in the Amazon Basin and there are only minor C4 sources, a dominant influence of C4 plants is considered unlikely (Hamilton et al. 2004). Degradation of long chain *n*-alkanes can be detected from the ratio of odd- vs. even-numbered carbon-chain homologues (Cranwell, 1981). An increase in the fraction of even-numbered chain length leads to lower values in the Carbon Preference Index (CPI) and hints at enhanced degradation:

$$CPI_{27-33} = 0.5 \times \left(\frac{nC_{27} + nC_{29} + nC_{31} + nC_{33}}{nC_{26} + nC_{28} + nC_{30} + nC_{32}} + \frac{nC_{27} + nC_{29} + nC_{31} + nC_{33}}{nC_{28} + nC_{30} + nC_{32} + nC_{34}}\right) \quad (4.1)$$

The input of petrogenic *n*-alkanes can also be detected using the relative distribution of long chain *n*-alkanes. *n*-Alkanes from petrogenic sources are on average shorter chained than compounds from modern plant sources (Jeng, 2006). Hence, the average chain length (ACL) of long-chain *n*-alkanes can be used to differentiate between petrogenic and modern plant sources:

$$ACL_{27-33} = \frac{27 \times nC_{27} + 29 \times nC_{29} + 31 \times nC_{31}\ 33 \times nC_{33}}{nC_{27} + nC_{29} + nC_{31} + nC_{33}} \quad (4.2)$$

The ACL also varies among different vegetation types. Savanna-dominated vegetation (in Africa) typically produces compounds with longer chain lengths than found in tropical forest vegetation (Feakins et al., 2016; Rommerskirchen et al., 2003; Vogts et al., 2012). For South America no ACL values for tropical savanna-dominated vegetation are available. Apart from variations in dominant vegetation type, variations in temperature and aridity can also impact ACL (Bush and McInerney, 2015). Warmer climate conditions are for instance reported to lead to higher ACL (Bush and McInerney, 2015).

4.2.3.2. Differentiation between geographic regions

The δD of long-chain *n*-alkanes was utilized to differentiate between different source regions (Ponton et al., 2014). The isotopic composition of precipitation in the Amazon Basin becomes more depleted towards the west due to the continental and the altitudinal effects on precipitation (Fig. 4.1) (Gonfiantini et al., 2001; Salati et al., 1979). In the lowland Amazon Basin, this gradient amounts to approximately 35‰. The δD of leaf-wax biomarkers mainly reflects the deuterium composition of meteoric water, but is also subject to secondary effects such as variations among different photosynthetic pathways and plant life forms (Hou et al., 2008; Sachse et al., 2012). As the vegetation in lowland Amazonia is dominated by forest tree taxa (Houghton et al., 2001) and the humid climate minimizes the effects of evapotranspiration, secondary effects are only playing a minor role in the Amazon (Feakins et al., 2016). Since the δD of precipitation and *n*-alkanes varies among different geographic regions, the δD of long-chain *n*-alkanes can be used as a marker to differentiate between source areas in the western and eastern Amazon Basin. To estimate the average isotopic composition of precipitation in the studied tributary catchments, we used a spatial 10′ x 10′ model of isotopic composition in precipitation by Bowen and Revenaugh (2003) (Fig. 4.1) and obtained precipitation δD values for each catchment by averaging catchment-wide δD values using ArcGIS 2010. The isotope model considers topographical and meteorological patterns as well as rainfall isotope data collected by GNIP stations, which are relatively sparse in the Amazon Basin (Fig. 4.1). The 95% confidence interval of the model is between 0 and 10‰ in the lowland Amazon Basin, with a narrower confidence interval (i.e. 0- 5‰) in the eastern sector of the basin (Bowen and Revenaugh, 2003). As a further measure of the isotopic composition of precipitation in each sub-catchment, we also analyzed the isotopic composition of river water from each tributary during the dry and wet seasons to test if the east-west gradient in precipitation isotopy was also reflected in the river water.

4.2.4. Analytics

4.2.4.1. Stable hydrogen isotope analyses of river water

The stable hydrogen isotope composition of river water samples was determined at MARUM – Center for Marine Environmental Sciences, University of Bremen, with a Thermal-Conversion/Elemental-Analyser operated at 1400°C coupled to a ThermoFisher Scientific MAT 253 isotope ratio mass-spectrometer. Measurements were repeated ten times for each water sample. The in-house water standards were calibrated against IAEA standards VSMOW, GISP and SLAP. The maximum deviation from the calibration slope was

0.9‰ vs. VSMOW and the average deviation was 0.3‰ vs. VSMOW. For each tributary, six samples were analyzed (except for Negro River and Xingu River with 5 and 7 samples respectively), three collected during the dry season in September and October 2011 and three sampled during the wet season in May 2012 (Table 4.1).

4.2.4.2. TOC and *n*-alkane analyses

River bed and core-top sediments were freeze-dried in a Christ Alpha 1-4 LDplus freeze dryer. Subsequently, the samples were ground using an agate mortar and pestle. TOC analyses were performed on aliquots of 60-70 mg of sediment using a LECO CS 200 CS-Analyzing System. Prior to analysis carbonates were removed using 12.5% HCl. Total lipid extracts were obtained with an ASE200 accelerated solvent extractor using a dichloromethane (DCM): methanol (MeOH) 9: 1 solution at 1000 psi and 100 °C for three cycles lasting 5 minutes each. Squalane was added as internal standard for the alkane fraction prior to extraction. After lipid extraction, solvent was removed in a Heidolph ROTOVAP system. Asphaltenes were removed over pipette columns consisting of 4 cm of Na_2SO_4 using DCM and hexane as solvents. The lipid extracts were subsequently saponified using 0.1M KOH in MeOH solution, yielding neutral and acid fractions. Compounds in the neutral fraction were separated using columns with deactivated silica (1% H_2O). Subsequent elution with hexane, DCM and DCM: MeOH 1:1 yielded the *n*-alkane, ketone and polar fractions. The *n*-alkane fraction was further cleaned by elution with hexane over 4 cm of $AgNO_3$-coated SiO_2 to remove unsaturated compounds. *n*-Alkanes were analyzed in a ThermoFisher Scientific Focus gas chromatograph equipped with an Rxi-5ms 30x column (30 m, 0.25 mm, 0.25 µm) and a flame ionization detector. *n*-Alkanes of different chain length were quantified by comparing peak areas of the compounds to external standard solutions and to the internal squalane standard. Precision of compound quantification is about 5% based on multiple standard analyses.

Compound-specific stable hydrogen isotope analyses of the C_{29} and C_{31} *n*-alkanes were carried out on a ThermoFisher Scientific MAT 253 isotope ratio mass spectrometer coupled via a GC Isolink operated at 1420°C to a ThermoFisher Scientific Trace GC equipped with a HP-5ms column (30 m, 0.25 mm, 1 µm). Each sample was analyzed in duplicate. δD compositions were measured against calibrated H_2 reference gas. Measurement accuracy was monitored by interspersing internal laboratory *n*-alkane standards of known isotopic composition every six measurements. Laboratory-internal *n*-alkane standards were measured routinely against offline-determined standards (‘Arndt B2’ obtained from Arndt Schimmelmann, Indiana University, USA) and revealed isotopic offsets within analytical error. Daily determination of the H^+_3 factor varied between 5.4 and 6.0 over the

measurement period. Long-term mean absolute deviation based on the external *n*-alkane standard was 2.8‰. All δD values are reported in ‰ against VSMOW. Compound-specific stable carbon isotope analyses were carried out on a ThermoFisher Scientific MAT 252 isotope ratio mass spectrometer coupled via a GCC combustion interface with a nickel catalyzer operated at 1000°C to a ThermoFisher Scientific Trace GC equipped with a HP-5ms column (30 m, 0.25 mm, 0.25 µm). $\delta^{13}C$ values were calibrated against CO_2 reference gas of known isotopic composition and all carbon isotope values are given in ‰ against VPDB. Duplicate injections were conducted for each sample and measurement accuracy was controlled by interspersing *n*-alkane standards of known isotopic composition every six measurements. Similar to δD analysis, laboratory internal *n*-alkane standards were routinely checked against offline-determined standards ('Arndt B2') and yielded isotopic offsets within analytical error. Long-term mean absolute deviation of external standards was 0.15‰.

4.2.4.3. XRF Analysis

Aluminium, silicon, iron and potassium concentrations in surface sediments were detected by using energy dispersive polarization X-ray Fluorescence (EDP-XRF) spectroscopy. Bulk samples were freeze-dried, powdered and homogenized. Then 3-4 g of dry sediment powder were measured with a PANalytical Epsilon -3XL instrument. Analytical quality was assessed by repeated analyses of the certified standard reference material MAG-1. The measured values were within 1% of the accepted value for Al, Si, Fe and K. The standard deviation of replicates was less than 0.6%.

4.3. Results

Lipid analyses from river sediment and core-top samples yielded dominantly odd-numbered long-chain *n*-alkanes with a CPI > 3. The most abundant homologues were the C_{29} and C_{31} *n*-alkanes (nC_{29} and nC_{31}), which were present in similar concentrations (± 10%, in a few cases ± 20%). Stable carbon and hydrogen isotope values of nC_{29} and nC_{31} were similar to each other. Since there are no substantial differences between nC_{29} and nC_{31}, isotopic values and concentrations are reported as amount weighted averages of nC_{29} and nC_{31} ($nC_{29\text{-}31}$).s

4.3.1. River water

Stable hydrogen isotopic analyses of river water samples yielded the most depleted values for the Andean-sourced Madeira and Solimões Rivers, with respective values of -53.2 ± 1.1‰ and -52.5 ± 1.0‰ for the wet season and -35.2 ± 1.2‰ and -33.3 ± 1.1‰ for the dry season (Table 4.1, Fig. 4.2). The lowland tributaries are more deuterium-enriched, with the most enriched values found for the Xingu River (wet season: -19.6 ± 1.6‰; dry season: -15.9 ± 1.3‰). These trends generally confirm the modelled mean annual precipitation δD (Fig. 4.1), which also yield more depleted values for the western areas of the Amazon Basin (Table 4.1). The seasonal variation of isotopic values for the lowland rivers Negro and Xingu Rivers is markedly lower than for Madeira River and Solimões River. For Xingu River, the difference of δD between wet and dry season is almost within the propagated standard deviation of the measurements. Given that we have only two data points over the entire annual hydrologic cycle, the differences in seasonality should be taken with caution.

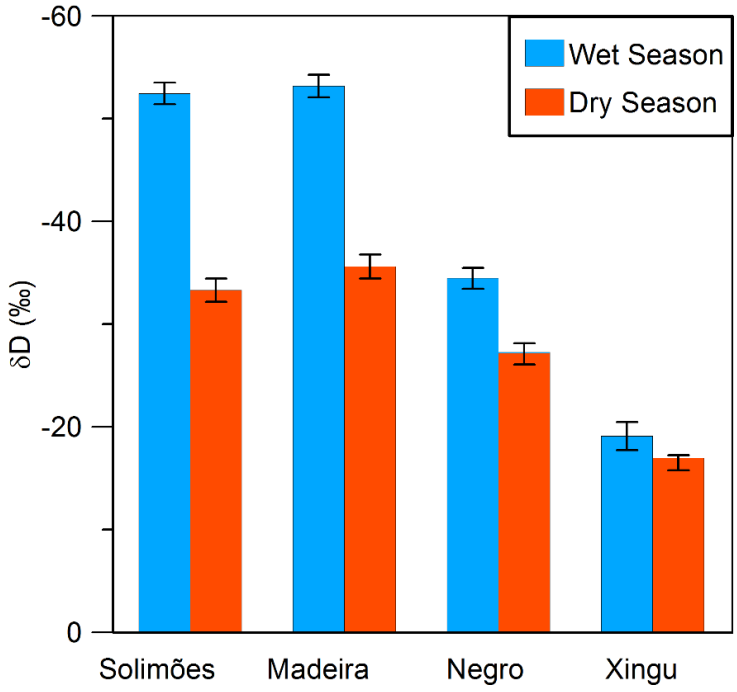

Figure 4.2. Hydrogen isotope composition of wet (blue) and dry (red) season water samples from the major Amazon River tributaries. Wet season sampling was undertaken during May while dry season sampling was undertaken during September and October. With the exception of the dry season for Negro River and the wet season for Xingu River, each value consists of three individual samples which were analyzed separately in ten replicate measurements. Errors represent the propagated standard deviation of the measurements.

4.3.2. River bed sediments

Values for the Al/ Si ratio varied between 0.1 and 0.56 (Table 4.2, Fig. 4.3). Samples with a low Al/Si ratio indicating a coarser grain size have a low TOC content, while samples with higher Al/Si values indicating finer grain sizes ratios were associated with higher TOC content (Fig. 4.3). Concentrations of nC$_{29\text{-}31}$ in river bed sediments varied between 9 and 2000 ng g^{-1} dry weight sediment (Table 4.2). The lowest concentrations (9 - 350 ng g^{-1}) were found in the white water tributaries (Solimões River and Madeira River), while maximum concentrations (280-2000 ng g^{-1}) were found in the samples from lowland tributaries (Xingu River and Negro River). The extremely low nC$_{29\text{-}31}$ concentrations in some of the white river sediment samples resulted in *n*-alkane amounts insufficient for δD analysis (Table 2). Compound-specific δ^{13}C nC$_{29\text{-}31}$ analyses of the river bed sediments yielded values between -30.8‰ and -36.0‰ (Fig. 4.4a, Table 4.2). δ^{13}C nC$_{29\text{-}31}$ enrichment > -35‰ was found in samples from white water rivers, while more depleted values < -35‰ were found in black and clear water rivers (Fig. 4.4a, b). There is no systematic offset between wet and dry season samples (Table 4.2). δ^{13}C nC$_{29\text{-}31}$ enrichment is also associated with a low ACL (r^2 = 0.62; $p < 10^{-9}$), while ACL values are consistently higher in the δ^{13}C nC$_{29\text{-}31}$ depleted lowland tributary samples (Fig. 4.5a). In contrast, CPI values do not differ significantly between white, clear, and black water tributaries (Fig. 4.5b). Here, low values are also present in samples from the lowland tributaries (Fig. 4.5b). Compound-specific δD nC$_{29\text{-}31}$ analyses of river bed sediments yielded values between -142‰ and -168‰ and correlate with the modeled average isotopic composition of precipitation in each catchment (Table 4.2, Fig. 4.6, r^2 = 0.56; $p < 10^{-8}$). Deuterium depleted values were found in the Madeira and Solimões Rivers, while the eastern tributaries, the Xingu and Negro Rivers, were more enriched (Fig. 4.6). δD nC$_{29\text{-}31}$ of river bed samples from the Pará River also showed values falling within the range of lowland tributaries (Fig. 6). δD nC$_{29\text{-}31}$ from the Amazon estuary samples ranged between the values of white water and lowland tributaries (Fig. 4.6). There is substantial variability, up to 15‰, of δD nC$_{29\text{-}31}$ within each of the river catchments. However, the median values for the samples for each tributary fit well with the average modelled isotopic composition of precipitation in each catchment (Fig. 4.6, r^2 = 0.93; $p < 0.003$). Only the samples from the Solimões River are more enriched than predicted by the model (Fig. 4.6). There, the variability is associated with TOC content, with more δD enriched values in lower TOC samples (Fig. 4.7). In the Xingu River, samples close to the confluence with the main-stem Amazon are more δD nC$_{29\text{-}31}$ depleted (Fig. 4.8). Likewise, Fe/K ratios exhibit a similar pattern, with main-stem Amazon values similar to those in the Xingu River confluence. For δD nC$_{29\text{-}31}$, there is again no systematic difference between the wet and dry season river bed samples (Table 4.2, Fig. 4.6).

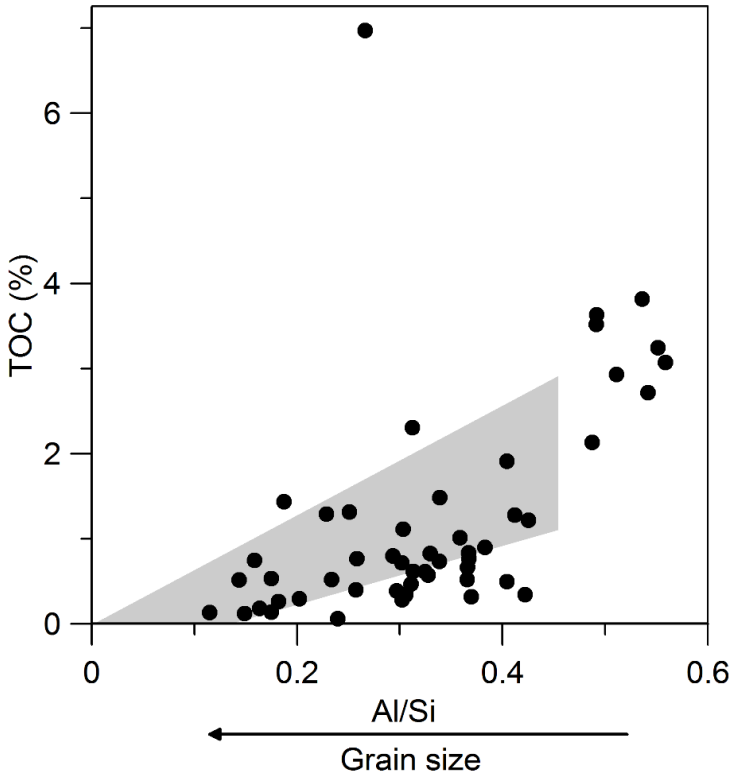

Figure 4.3. Al/Si data as an indicator of grain size distribution vs. total organic carbon (TOC) content. The grey area indicates the range of values found in a previous study (Bouchez et al., 2011) using suspended and river bed sediment samples from water depth profiles from the Solimões and Madeira Rivers.

4.3.3. Marine core-tops

Concentrations of $nC_{29\text{-}31}$ in marine core-top sediments collected offshore the Amazon estuary and the Brazilian Northeast varied between 18 and 200 ng g^{-1} dry weight. Highest concentrations (70-200 ng g^{-1}) were found underlying the Amazon freshwater plume (Table 3). Core-tops collected to the south of the Amazon estuary and from the continental slope exhibited lower concentrations (18-68 ng g^{-1}). $\delta^{13}C$ $nC_{29\text{-}31}$ values of core-tops are around -33.5‰ on the continental shelf under the influence of the Amazon freshwater plume (Fig. 4.9, Table 4.3). South of the estuary, $\delta^{13}C$ values are more enriched with values up to -27‰ (Fig. 4.9). There is also a distinct gradient from the continental shelf under the influence of the freshwater plume towards more enriched values farther offshore on the continental slope. δD $nC_{29\text{-}31}$ values of around -155‰ in samples underlying the Amazon freshwater plume are similar to the ones found in the Amazon estuary (Fig. 4.10, Table 4.3). In a similar

way as noted for $\delta^{13}C$, samples collected south of the estuary are more deuterium-enriched (up to -135‰) and there is also an offshore gradient to more deuterium-enriched values towards the continental slope (Fig. 4.10).

4.4. Discussion

4.4.1. Grain size distribution and contribution of petrogenic compounds

River bed samples from the Amazon main stem and its major tributaries featured a wide range of average grain sizes and TOC contents. This distribution includes the range of grain sizes and TOC values reported in a previous study that used suspended sediments and river bed samples along water column profiles in Solimões River, Madeira River (i.e., white water tributaries) and the Amazon main stem (Bouchez et al., 2011) (Fig. 4.3). Additionally, our sample set also features samples from the black and clear water tributaries, which are finer grained and have a higher TOC content in their downstream sectors before the confluence with the Amazon River. Thus, our sample set reflects a representative overview of sediment transported in the Amazon River and its tributaries.

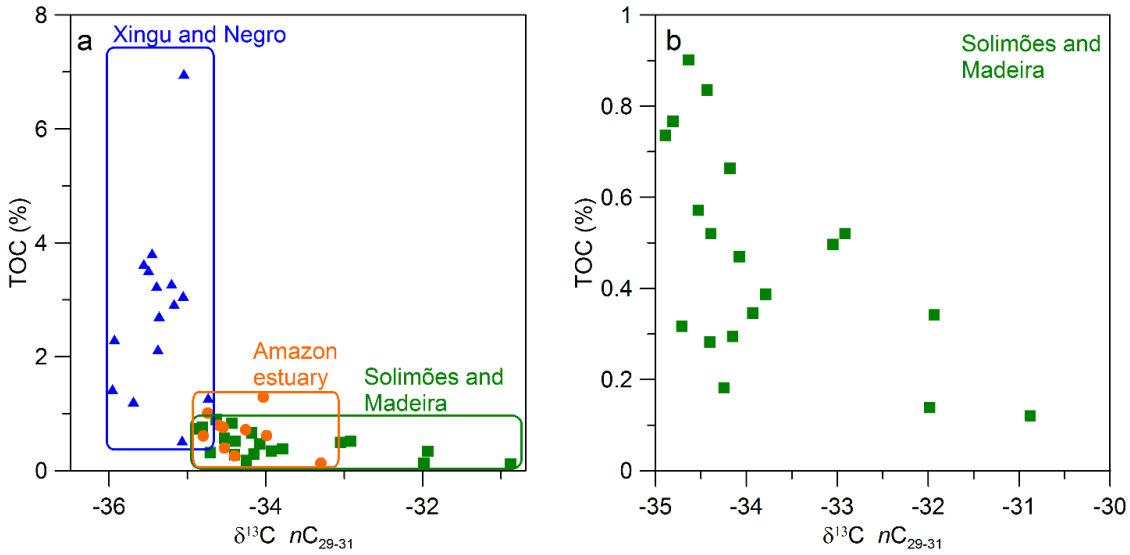

Figure 4.4. a) Total organic carbon (TOC) content of river bed sediments vs. $\delta^{13}C$ nC_{29-31} for samples from different Amazon River tributaries and the estuary. River bed samples from the lowland tributaries, the Negro and Xingu Rivers, are marked with blue triangles. Samples from the white water tributaries, the Madeira and Solimões Rivers, are marked with green squares. Samples from the Amazon River estuary are marked with orange dots. b) TOC vs. $\delta^{13}C$ nC_{29-31} for samples from the Madeira and Solimões Rivers.

The $\delta^{13}C$ $nC_{29\text{-}31}$ of most samples is in the range expected for modern C3 tropical rainforest (i.e. values between -33 and -37‰, Fig. 4.4a). This indicates that the $nC_{29\text{-}31}$ are predominantly sourced from C3 vegetation. The enrichment present in the low TOC and coarse-grained samples from the bottom of the river channel points to an additional, minor source for $nC_{29\text{-}31}$ (Fig. 4.4a, b). Earlier studies indicate contributions from a petrogenic source to bulk OM in the Amazon Basin detected by radiocarbon analysis (Bouchez et al., 2014; Clark et al., 2013; Mayorga et al., 2005). Such contributions were particularly evident in low TOC (TOC<0.5%) samples from the white water tributaries that also exhibited ^{13}C enrichment in bulk TOC (Bouchez et al., 2014; Clark et al., 2013; Mayorga et al., 2005). Since our results also show $\delta^{13}C$ $nC_{29\text{-}31}$ enrichment in low TOC samples from the Solimões and Madeira Rivers, this enrichment is most likely due to contributions from a petrogenic $nC_{29\text{-}31}$ source (Fig. 4.4 b).

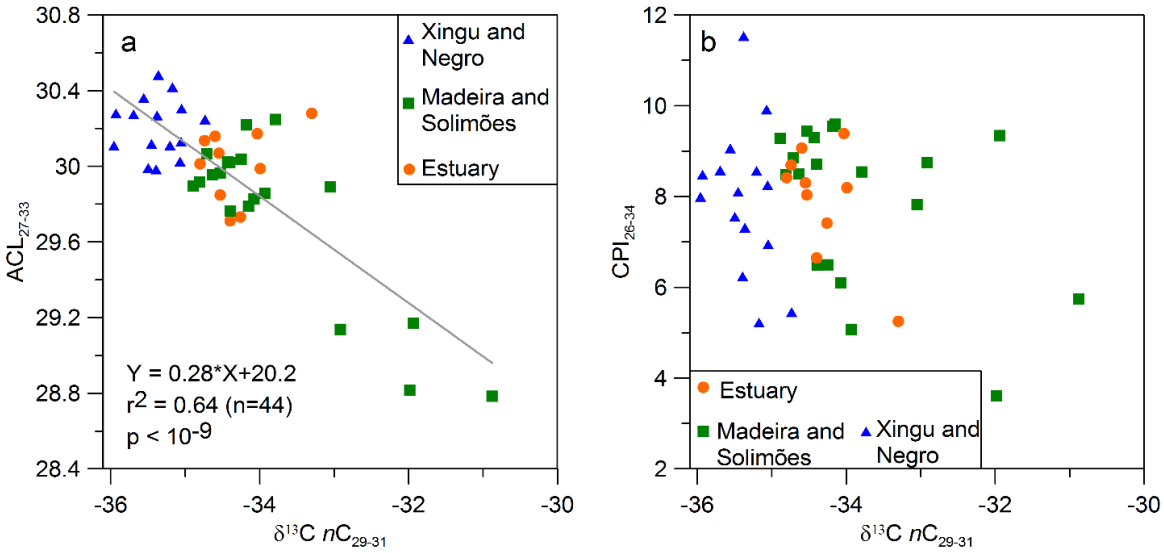

Figure 4.5. $\delta^{13}C$ $nC_{29\text{-}31}$ vs. average chain length (ACL) a) and carbon preference index (CPI) b). Green squares represent samples from the white water tributaries, the Solimões and Madeira Rivers, blue triangles represent samples from the lowland tributaries, the Negro and Xingu Rivers, and orange dots represent samples from the Amazon estuary.

The presence of old, degraded *n*-alkanes in low TOC samples from the white water rivers is corroborated by low ACL values, which are consistently associated with enriched $\delta^{13}C$ $nC_{29\text{-}31}$ values of the white water tributaries, indicating the partial petrogenic sourcing of $nC_{29\text{-}31}$ (Jeng, 2006) (Fig. 4.5a). In contrast, if the $\delta^{13}C$ $nC_{29\text{-}31}$ enrichment would have been caused by a contribution of C4 plants (e.g. by the C4 grasses present in the *Várzea* vegetation in

floodplains of the Madeira and Solimões Rivers), an increase of the ACL with $\delta^{13}C$ $nC_{29\text{-}31}$ enrichment would be expected (Hamilton et al., 2004; Rommerskirchen et al., 2003), which is not observed. CPI values for some of the clear water samples are as low as the values from Andean samples featuring $\delta^{13}C$ $nC_{29\text{-}31}$ enrichment. (Fig. 4.5b). The lower CPI values of those samples are likely caused by biodegradation due to high microbial activity in the lowland tributaries or due to high OM degradation in tropical soils (Moreira-Turcq et al., 2003; Richey et al., 1990). It is also possible that the storage of these sediments in the flooded *Ria* valleys at the mouths of the Negro, Tapajós and Xingu Rivers renders them susceptible to degradation. *Ria*s have lake-like sedimentary dynamics (Archer, 2005), favouring planktonic activity and trapping of upstream sediments. Since the petrogenic *n*-alkane source was only detected in low concentration samples, it represents only a minor contribution to the long-chain *n*-alkanes in the entire Amazon Basin. This finding is consistent with radiocarbon dating of POC, which implies a maximum fraction of petrogenic POC of 10% (Bouchez et al., 2014). The petrogenic *n*-alkanes likely originate from the Andes, where organic-rich sediments in the Solimões and Madeira Rivers head waters present a conceivable source for petrogenic POC (Putzer, 1984). POC studies in mountainous tributaries have indeed found a locally large petrogenic POC contribution of up to 80% (Clark et al., 2013). Miocene to Pleistocene sedimentary units under erosion in channel margins of the Solimões and Madeira catchments are also potential *n*-alkanes sources (Campbell Jr et al., 2006; Nogueira et al., 2013). A more quantitative assessment on the exact proportion of petrogenic $nC_{29\text{-}31}$ could be achieved by compound-specific radiocarbon dating of samples from the different tributaries and the Amazon River main stem.

Table 4.1. Position, sampling season, tributary, sampling depth and δD values for the water samples collected in this study. The isotope measurements represent the mean of ten replicates per sample. Errors are the standard deviation of these measurements.

Sample	Long. (°E)	Lat. (°N)	Season	River	Sampling depth (m)	δD (‰)	Error
MAO 72	-60.4	-3.29	wet	Solimões	28	-52.7	0.8
MAO 77	-60.04	-3.31	wet	Solimões	18	-51.9	0.5
MAO 80	-59.88	-3.22	wet	Solimões	20	-52.8	0.5
MAO 81	-60.44	-3.02	wet	Negro	11	-32.9	0.6
MAO 83	-60.29	-3.06	wet	Negro	52	-34.3	0.6
MAO 93	-60	-3.18	wet	Negro	17	-36.2	0.6
MAO 38	-59.07	-3.66	wet	Madeira	14	-53.1	0.6
MAO 42	-58.9	-3.52	wet	Madeira	12	-53.3	0.8
MAO 45	-58.79	-3.42	wet	Madeira	17	-53.2	0.4
XA 39	-52.14	-3.22	wet	Xingu	9-4	-18.9	0.3
XA 49	-51.97	-3.4	wet	Xingu	3	-19.3	0.8
XA 53	-51.97	-2.63	wet	Xingu	2	-19.3	0.8
XA 73	-52.16	-2.22	wet	Xingu	9	-18.9	0.7
MAO 02f	-60.35	-3.05	dry	Negro	15	-27.4	0.5
MAO 03c	-60.21	-3.08	dry	Negro	15	-27.1	0.7
MAO 05d	-60.02	-3.29	dry	Solimões	4	-33.1	0.8
MAO 10d	-60.29	-3.27	dry	Solimões	9	-32.6	0.7
MAO 13d	-59.89	-3.2	dry	Solimões	13	-34.2	0.5
MAO 22b	-59.02	-3.64	dry	Madeira	7	-35.8	0.6
MAO 22c	-59.02	-3.63	dry	Madeira	16	-35.4	0.8
MAO 28c	-58.8	-3.44	dry	Madeira	22	-35.6	0.6
XA 23	-51.69	-3.49	dry	Xingu	3	-16.2	0.8
XA 26	-51.98	-2.65	dry	Xingu	2	-15.8	0.7
XA 28	-51.85	-3.01	dry	Xingu	10	-15.9	0.7

4.4.2. Relative contribution of the major Amazon River tributaries

The median δD $nC_{29\text{-}31}$ of the major tributaries shows more enriched values for the eastern tributaries and more depleted values for western tributaries and thus features the same trend as the modelled mean isotopic precipitation composition of the respective catchments (Fig. 6)(Bowen and Revenaugh, 2003). This trend is also mirrored by the isotope composition of river waters, which show more depleted δD values for the western tributaries and more enriched values for the eastern tributaries (Fig. 4.2). δD $nC_{29\text{-}31}$ values from the Amazon estuary were intermediate to values of the western and eastern tributaries and the median δD $nC_{29\text{-}31}$ at the Amazon estuary also correlates with the modelled average precipitation δD of the entire Amazon Basin (Fig. 4.6). This observation supports the notion that δD $nC_{29\text{-}31}$ at the Amazon estuary reflects a mixed signal of western white water tributaries and eastern clear and black water tributaries, and thus represents an integrated signal of the main Amazon tributaries. The δD $nC_{29\text{-}31}$ values from the Pará River also correlate to the average precipitation composition of the Tocantins River catchment (Fig. 4.6). This suggests that the Pará River mainly receives $nC_{29\text{-}31}$ input from the Tocantins River and that the contributions from the main-stem Amazon River are minor.

While samples from the Solimões River with a higher TOC content (0.5-1%) show δD $nC_{29\text{-}31}$ values similar to those of the Madeira River (Fig. 4.6), samples with a lower TOC have more enriched δD values (Fig. 4.7). This enrichment is likely the result of a higher contribution of petrogenic compounds in low TOC samples (Fig. 4.7). Petrogenic *n*-alkanes tend to be more δD-enriched than pristine biogenic material (Schimmelmann et al., 2006). Hence, petrogenic contributions to sediment samples have been reported to lead to variations in δD $nC_{29\text{-}31}$ values (Li et al., 2011a). In the Madeira River, the samples with the lowest TOC, did not yield enough material for δD $nC_{29\text{-}31}$ measurement, consequently a similar relation could not be detected for that tributary (Table 4.2).

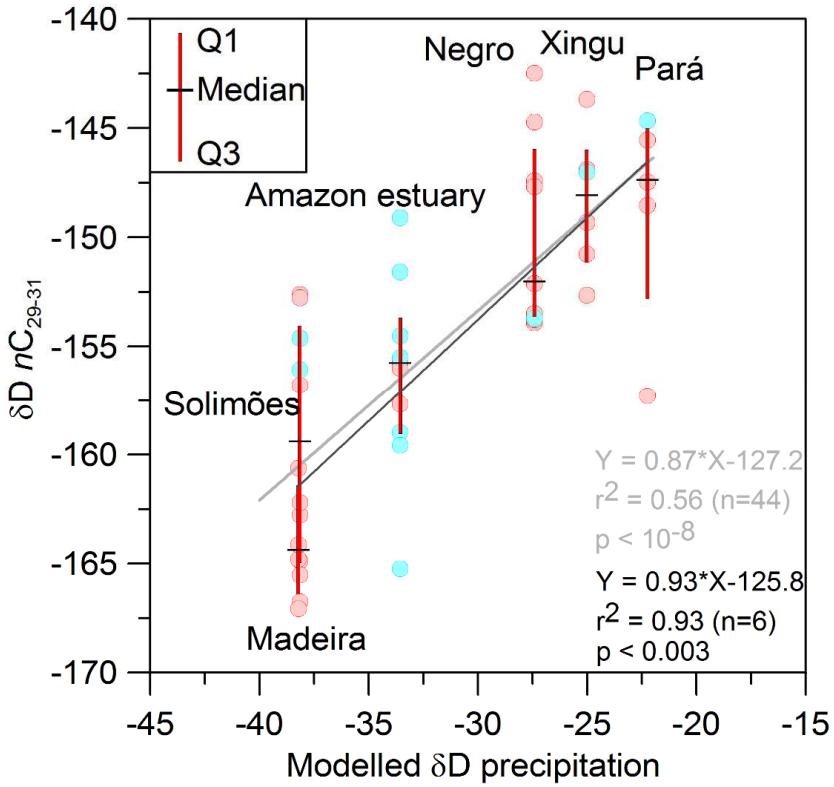

Figure 4.6. δD $nC_{29\text{-}31}$ of river bed sediments vs. modelled mean annual precipitation δD in each catchment from Bowen and Revenaugh (2003). Red vertical bars indicate the range between the upper and lower quartile for each tributary and black horizontal bars indicate the median value. Blue data points reflect samples taken during the wet season. Red data points indicate dry season samples. The black regression line uses the median values for each tributary and the grey regression line the single data points. Samples close to the Amazon confluence are omitted from the Xingu River data set as discussed in section 4.3.

Although the median δD $nC_{29\text{-}31}$ values from the Amazon tributaries correlate well with the average isotope composition of precipitation, the data is subject to a large variability (Fig. 4.6). This variability is similar to that reported from calibration studies using lacustrine sediment and riverine suspension samples (Garcin et al., 2012; Polissar and Freeman, 2010; Ponton et al., 2014; Sachse et al., 2004). Variability can stem from grain size sorting and incomplete mixing of *n*-alkanes from different sources or varying degrees of degradation during soil formation. Due to the variability, the detection of a potential regional bias is not straightforward. We cannot infer the precise relative contributions of individual tributaries and it remains unclear whether there are biases within the different catchments. In the latter regard, the case of the Andean-sourced white water tributaries is of special interest. In terms of covered area, the Solimões and Madeira catchments are largely situated in lowland Amazonia, while the bulk of their suspended sediment load is derived from the

Andes (McClain and Naiman, 2008). If the *n*-alkanes transported by the white water tributaries represented a pure Andean signal, they would be expected to yield a high amount of petrogenic material (Clark et al., 2013) or, alternatively, much more δD depleted values in their *n*-alkanes, as Andean precipitation is much more depleted than that for the average basin of Solimões or Madeira (Fig. 4.1). Given the wide range of isotopic composition and TOC content observed in the different samples (Fig. 4.3), it seems likely that there is a wide variety of sources of the compounds in the different samples from the same tributary, which are not mixed or sorted before deposition. Samples with low TOC content likely contain a higher proportion of petrogenic material from the Andes (Bouchez et al., 2014; Clark et al., 2013). Organic-rich samples are likely predominantly sourced from lowland soils or represent material that was reworked on the floodplains where modern organic matter accumulated i.e. in the form of plant-wax *n*-alkanes (Mayorga et al., 2005; Quay et al., 1992). In terms of bias towards certain tributaries, there might be a higher $nC_{29\text{-}31}$ input by the white water tributaries, which have high POC fluxes and drain large floodplain areas (McClain and Naiman, 2008; Moreira-Turcq et al., 2003). Conversely, clear water rivers like the Xingu River mainly drain bedrock areas and yield smaller POC fluxes and may also provide a lower $nC_{29\text{-}31}$ input (Archer, 2005; McClain and Naiman, 2008). However, the contribution of the clear water tributaries, the Xingu and Tapajós Rivers, is too low to significantly influence the δD $nC_{29\text{-}31}$ found at the Amazon estuary to an extent exceeding the sample variability.

The finding that the Amazon River estuary receives significant $nC_{29\text{-}31}$ input from lowland sources contrasts with the dominant Andean sourcing of its inorganic sediments (Meade et al., 1985). These results are in line with previous studies using bulk $\delta^{13}C$, lignin and long-chain fatty acids as tracers for the origin of OM, which detected a mixing of Andean and lowland OM sources (Hedges et al., 2000; McClain and Naiman, 2008; Ponton et al., 2014; Quay et al., 1992). The finding that leaf-wax biomarkers can have distinctly different sources than inorganic sediment is supported by a similar study from the Ganges-Brahmaputra Rivers (Galy et al., 2011). This study also found that leaf-waxes partly originate from lowland sources in the Ganges valley, unlike inorganic sediment that is mainly sourced from the Himalayas. In addition, Galy et al. (2011) detected a strong seasonal variation associated with enhanced monsoonal precipitation during boreal summer. In our river bottom sediments obtained by grab sampling seasonality is likely not resolved, as these sediments may contain signals deposited over several years.

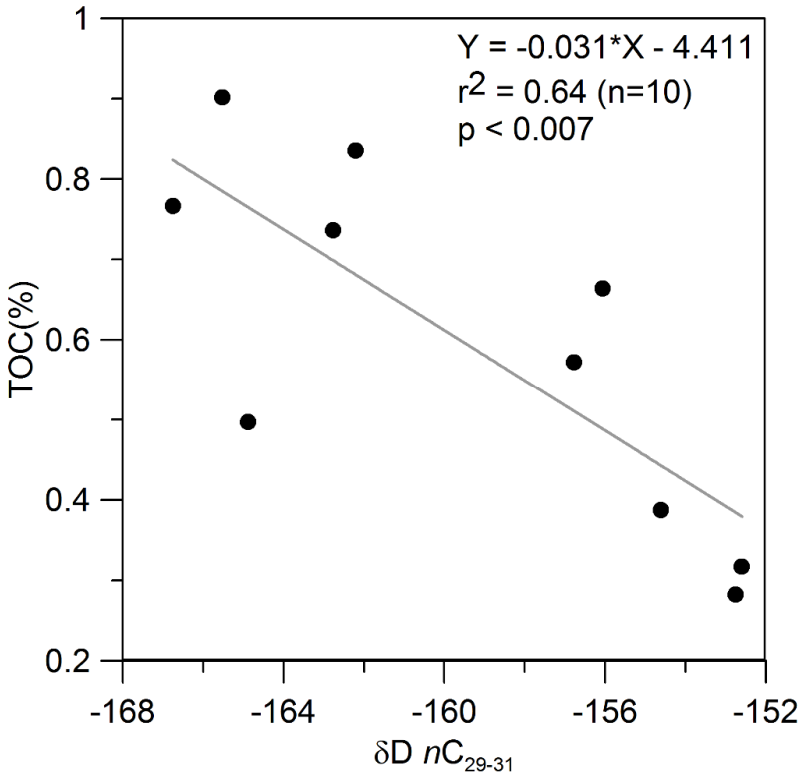

Figure 4.7. δD $nC_{29\text{-}31}$ vs. TOC for river bed samples from the Solimões River.

Table 4.2. Position, sampling season, tributary, water depth, TOC content, $nC_{29\text{-}31}$ concentration, ACL, CPI, $\delta^{13}C$ $nC_{29\text{-}31}$, δD $nC_{29\text{-}31}$ and Al/Si ratio of the river bed samples collected for this study. Positions where no measurements were conducted are marked with N/A.

Sample	Long.(°E)	Lat.(°N)	Sea-son	River	Water depth (m)	TOC (%)	Conc. $nC_{29\text{-}31}$ (ng g^{-1})	ACL	CPI	$\delta^{13}C$ $nC_{29\text{-}31}$ (‰)	δD $nC_{29\text{-}31}$ (‰)	Al/Si
MAO 02c	-60.3628	-3.0807	Dry	Negro	12	1.28	283.1	30.2	5.5	-34.74	-153.9	0.41
MAO 02d	-60.3561	-3.0720	Dry	Negro	9	1.44	398.9	30.1	8.0	-35.96	-144.7	0.19
MAO 02e	-60.3498	-3.0607	Dry	Negro	16	2.93	871.9	30.4	5.2	-35.17	-153.5	0.51
MAO 02f	-60.3465	-3.0530	Dry	Negro	22	1.22	660.3	30.3	8.6	-35.69	-147.4	0.43
MAO 03a	-60.1995	-3.0511	Dry	Negro	0.7	2.13	425.4	30.3	11.5	-35.38	-147.7	0.49
MAO 03h	-60.1961	-3.0544	Dry	Negro	13	0.53	489.0	30.0	9.9	-35.07	-152.1	0.17
MAO 3	-60.2154	-3.0859	Dry	Negro	0.7	2.72	1296.7	30.5	7.3	-35.36	-153.8	0.54
MAO 4	-60.1481	-3.1056	Dry	Negro	6.6	2.31	801.9	30.3	8.5	-35.93	-142.5	0.31
MAO 90	-60.0901	-3.1442	Wet	Negro	16	6.97	1017.4	30.3	6.9	-35.05	-153.7	0.27
MAO 05d	-60.0243	-3.2900	Dry	Solimões	22	0.57	165.9	30.0	9.4	-34.53	-156.8	0.33
MAO 08a	-60.1991	-3.2867	Dry	Solimões	16	0.74	199.8	29.9	9.3	-34.89	-162.8	0.34
MAO 08b	-60.2053	-3.2958	Dry	Solimões	13	0.32	295.6	30.1	8.9	-34.71	-152.6	0.37
MAO 09b	-60.2905	-3.2653	Dry	Solimões	25	0.28	119.8	30.0	8.7	-34.40	-152.8	0.30
MAO 11a	-60.3846	-3.2866	Dry	Solimões	21	0.50	61.9	29.9	7.8	-33.05	-164.9	0.40
MAO 11c	-60.3842	-3.3024	Dry	Solimões	3.5	0.90	225.2	30.0	8.5	-34.63	-165.5	0.38
MAO 13b	-59.8791	-3.2957	Dry	Solimões	14	0.84	275.1	30.0	9.3	-34.43	-162.2	0.37
MAO 13c	-59.8847	-3.2037	Dry	Solimões	9	0.77	274.1	29.9	8.5	-34.81	-166.8	0.37
MAO 73	-60.3167	-3.2970	Wet	Solimões	8	0.66	350.5	30.2	9.6	-34.18	-156.1	0.37
MAO 77	-60.0393	-3.3097	Wet	Solimões	40-45	0.39	180.1	30.2	8.5	-33.79	-154.6	0.30
MAO 23a	-59.0771	-3.6753	Dry	Madeira	22.5	0.52	125.6	29.8	6.5	-34.39	-164.8	0.37
MAO 24a	-58.9572	-3.5838	Dry	Madeira	2.5	0.12	9.8	28.8	5.7	-30.88	N/A	0.15
MAO 25a	-58.9023	-3.5313	Dry	Madeira	7.5	0.30	64.5	29.8	9.6	-34.15	N/A	0.20
MAO 25b	-58.9060	-3.5321	Dry	Madeira	22	0.35	88.4	29.9	5.1	-33.93	-167.1	0.31
MAO 25d	-58.9065	-3.5259	Dry	Madeira	17.6	0.14	15.1	28.8	3.6	-31.99	N/A	0.17

Sample	Long.(°E)	Lat.(°N)	Sea-son	River	Water depth (m)	TOC (%)	Conc. nC_{29-31} (ng g^{-1})	ACL	CPI	$\delta^{13}C$ nC_{29-31} (‰)	δD nC_{29-31} (‰)	Al/Si
MAO 25e	-58.9082	-3.5230	Dry	Madeira	10	0.47	92.1	29.8	6.1	-34.08	-160.6	0.31
MAO 28a	-58.7913	-3.4396	Dry	Madeira	4	0.34	54.3	29.2	9.3	-31.94	N/A	0.42
MAO 28d	-58.7985	-3.4379	Dry	Madeira	4	0.52	32.0	29.1	8.8	-32.92	-164.1	0.23
MAO 32	-58.6892	-3.3474	Dry	Madeira	2.5	0.18	25.4	30.0	6.5	-34.25	N/A	0.16
*XA 30	-52.2432	-1.6884	Dry	Xingu	13	0.83	311.2	30.1	7.9	-33.67	-159.4	0.33
*XA 31	-52.2490	-1.7886	Dry	Xingu	11	1.11	273.5	30.1	9.5	-35.23	-155.7	0.30
XA 33	-52.2537	-1.7900	Dry	Xingu	5.1	1.91	780.0	30.1	8.8	-35.33	-149.1	0.40
XA 34	-52.2565	-1.7945	Dry	Xingu	0.5	0.52	182.7	29.9	6.0	-33.90	-154.9	0.14
*XA 25	-51.9702	-2.6446	Dry	Xingu	2.3	3.82	1673.9	30.1	8.1	-35.45	-149.3	0.54
*XA 35	-52.1917	-2.0391	Dry	Xingu	15.2	3.07	1984.6	30.1	8.2	-35.05	-146.9	0.56
XA 36	-52.1323	-2.2217	Dry	Xingu	9.2	3.24	772.5	30.0	6.2	-35.39	-152.7	0.55
XA 38	-52.0158	-2.4659	Dry	Xingu	6	3.63	1820.7	30.4	9.1	-35.56	-150.8	0.49
*XA 38	-52.0158	-2.4659	Dry	Xingu	6	3.52	418.8	30.0	7.6	-35.50	-143.7	0.49
XA 76	-52.0974	-2.4615	Wet	Xingu	4	3.28	1285.3	30.1	8.6	-35.20	-147.0	N/A
*(8) 20/09	-48.9103	-1.5044	Dry	Pará	1.5	0.06	405.4	30.0	8.8	-35.19	-148.5	0.24
*13/05/11BELEM	-48.9191	-1.5342	Wet	Pará	40	1.48	246.3	29.9	7.8	-32.52	-144.7	0.34
*20/09 BELEM	-48.9103	-1.5044	Dry	Pará	1.5	1.32	248.6	30.0	9.2	-34.90	-157.3	0.25
*20/09 BLM MD	-48.9069	-1.5795	Dry	Pará	5	0.72	210.5	30.0	8.9	-34.58	-147.5	N/A
20/09 BLM MD	-48.9069	-1.5795	Dry	Pará	5	0.75	169.7	30.0	8.2	-34.41	-145.6	0.16
*09/05 P99	-50.6076	-0.1692	Wet	Amazon	2-5	0.72	105.4	29.7	7.4	-34.26	-155.5	0.30
*101 9/5	-50.6392	-0.1291	Wet	Amazon	45	0.40	75.7	29.8	8.0	-34.53	-154.5	0.26
*12/03 MCP	-50.0914	-0.0515	Wet	Amazon	3	0.76	221.7	30.1	8.3	-34.55	-151.6	0.26
*14/09 MCP	-50.5809	-0.1978	Dry	Amazon	5	1.29	146.1	30.2	9.4	-34.03	-155.7	0.23
*14/09 MCP	-50.5645	-0.1924	Dry	Amazon	4	0.80	353.5	30.2	9.1	-34.60	-156.0	0.29
*25/9/11	-55.5645	-1.8850	Dry	Amazon	1	0.61	123.7	30.0	8.4	-34.80	-157.7	0.32
*7/5 MACAPA	-51.0876	-0.0636	Wet	Amazon	30	0.13	423.8	30.3	5.3	-33.30	-159.0	0.11
*7/5 P95	-51.0471	-0.0807	Wet	Amazon	20	1.01	261.0	30.1	8.7	-34.74	-165.2	0.36
*9/5 MACAPA	-50.6233	-0.1507	Wet	Amazon	25	0.26	45.7	29.7	6.6	-34.40	-149.1	0.18
*MCP SUL P89	-50.6578	-0.1284	Wet	Amazon	2	0.62	197.2	30.0	8.2	-33.99	-159.6	0.31

4.4.3. Transport

During transport along the Amazon River and its main tributaries, large portions of OM are remineralized to CO_2 (Richey et al., 2002; Ward et al., 2013) and CH_4 (Sawakuchi et al., 2014). Furthermore, the downstream transport of sediments may be interrupted by temporary deposition and storage in flood plains (Dunne et al., 1998; Moreira-Turcq et al., 2013; Moreira-Turcq et al., 2004; Richey et al., 1990). Nevertheless, the δD $nC_{29\text{-}31}$ signal from the Amazon estuary yields values expected for an integrated signal of the major tributaries (Fig. 4.6). This indicates that $nC_{29\text{-}31}$ from upstream the Amazon River are refractory and that remineralisation does not alter the signal to an extent exceeding the sample variability present in the δD $nC_{29\text{-}31}$ data. The observation that core-top δD $nC_{29\text{-}31}$ values from the Amazon Plume are in good agreement with the median value at the estuary and are much more depleted than those from core-tops from northeastern Brazil provides further evidence that transport does not alter δD $nC_{29\text{-}31}$ to a large extent (Figs. 4.6 and 4.10). The refractory behavior of $nC_{29\text{-}31}$ is in contrast to in situ-produced algal organic compounds, which experience fast remineralization (Mayorga et al., 2005). It also contrasts with the observed in-situ overprint of soil-derived lipids, such as branched glycerol dialkyl glycerol tetraethers, during transport (Zell et al., 2013). Since $nC_{29\text{-}31}$ in the Amazon River system are dominantly derived from soil and plant litter, the resistance of $nC_{29\text{-}31}$ toward degradation may be partly due to the close association of plant-wax compounds with mineral surfaces which protects them from remineralisation (Gordon and Goni, 2004; Mayer, 1994).

Seasonal and tidal water level variations may also influence transport and deposition of leaf-waxes in the Amazon River (Archer, 2005; Beardsley et al., 1995). During the wet season, the flooded area in the Amazon Basin more than doubles and extends through the Amazon River valley (Davidson et al., 2012). This results in floodplain deposition particularly along the main-stem Amazon and also in the lower reaches of the lowland tributaries (the *Ria*) through a backflow effect (Archer, 2005). In our study, this effect is apparent in the samples from the Xingu River situated close to its confluence with the Amazon River. These samples have more depleted δD $nC_{29\text{-}31}$ values (~ -156‰) than samples further upstream the Xingu River (~ -148‰) (Fig. 4.8). A similar effect is also apparent for the Fe/K ratio of the same samples. Upstream Xingu samples show elevated Fe/K ratios expected for the heavily weathered Central Brazil Shield rocks they originate from, while samples from the main-stem Amazon and near the confluence show lower Fe/K ratios (Fig. 4.8). The more depleted δD $nC_{29\text{-}31}$ values close to the confluence are within the range of the values found in the Amazon estuary (~ -157‰). Hence, the $nC_{29\text{-}31}$ close to the confluence were likely derived from the Amazon main stem and not from the Xingu River. Apart from the inflow

during river high stands, this may be caused by backflow during lower river stages due to the very low slope of the Amazon close to the Xingu River (i.e. 1.5 cm km^{-1}, Birkett et al. (2002). Such transport likely takes place through small channels which link the main-stem Amazon to the lower reaches of the Xingu River (i.e. the Aquiqui and Urucuricaia Channels) and could be aided by tidal variations of up to 2 meters in the same location (Archer, 2005; Beardsley et al., 1995).

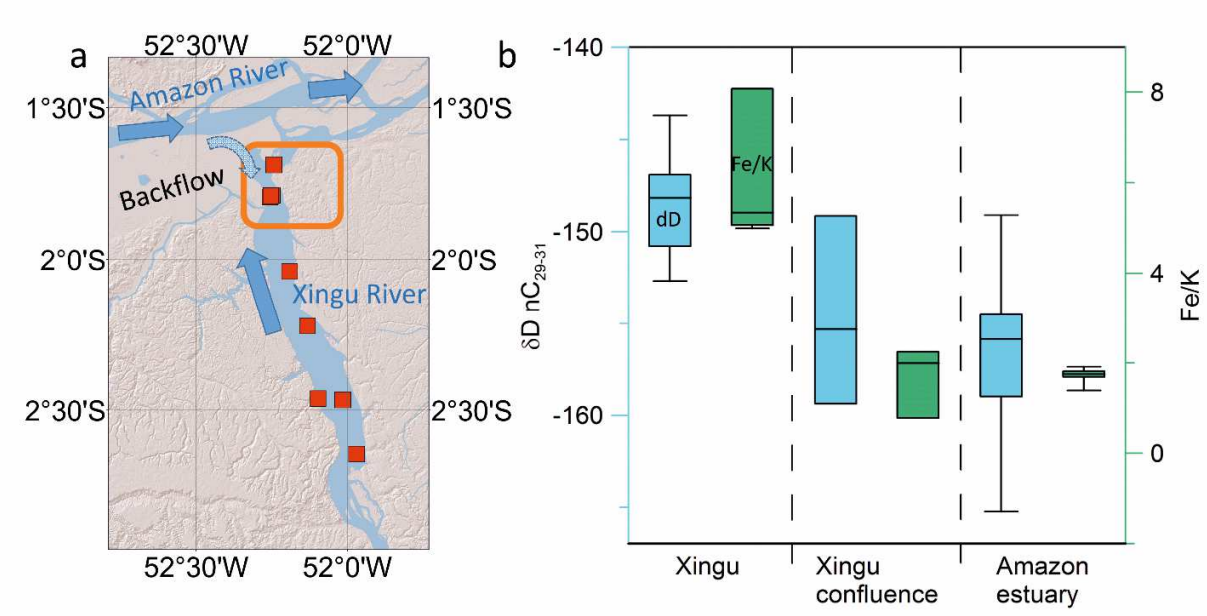

Figure 4.8. a) Samples from the Xingu River are represented by red squares. The samples close to the confluence with the main-stem Amazon are marked by an orange rectangle. Flow directions are marked with blue arrows. b) Boxplots of the δD $nC_{29\text{-}31}$ results (blue) and the Fe/K element ratio (green) for the Xingu River, the Amazon estuary, and samples close to the Xingu River confluence. The figure illustrates that sediment and $nC_{29\text{-}31}$ close to the confluence are mostly Amazon derived.

4.4.4. Deposition

Both marine core-top isotope data sets (i.e. $\delta^{13}C$ $nC_{29\text{-}31}$ and δD $nC_{29\text{-}31}$) show most depleted values in areas underlying the Amazon freshwater plume (Figs. 4.9 and 4.10). Samples outside the influence of the Amazon freshwater plume are isotopically more enriched. The strong contrast in δD $nC_{29\text{-}31}$ can be explained by different $nC_{29\text{-}31}$ sources. In the vicinity of the Amazon freshwater plume, $nC_{29\text{-}31}$ from the Amazon Basin are dominant. Since these compounds are partly sourced from the upper reaches of the Amazon River, they are on average more isotopically depleted than compounds from coastal sources. The values

around -135‰ found off the Parnaíba River mouth are very close to the values expected for a coastal source e.g. from the Parnaíba River catchment (Figs. 4.1 and 4.10, Table 4.3) (Bowen and Revenaugh, 2003). The enriched values found further offshore than the Amazon freshwater plume could have various sources. There could be transport of compounds from north eastern Brazil or other coastal areas in Brazil by the North Brazil Current (NBC) (de Morais et al., 2006). Alternatively, some contribution of dust transported from African sources is possible, which would entrain material enriched in δD $nC_{29\text{-}31}$ from distant sources (Conte and Weber, 2002; Schefuß et al., 2003). The enriched $\delta^{13}C$ $nC_{29\text{-}31}$ values found off north east Brazil are likely caused by an enhanced C4 plant contribution from the Caatinga and Cerrado vegetation. This contrasts with the dominant C3 contribution from the Amazon Basin, which is apparent in the samples collected under the influence of the Amazon freshwater plume. The enriched $\delta^{13}C$ $nC_{29\text{-}31}$ values found in the direction of the open ocean could be caused by compounds delivered by marine or dust transport as described for the enriched δD $nC_{29\text{-}31}$ signals (Maioli et al., 2012; Schefuß et al., 2003).

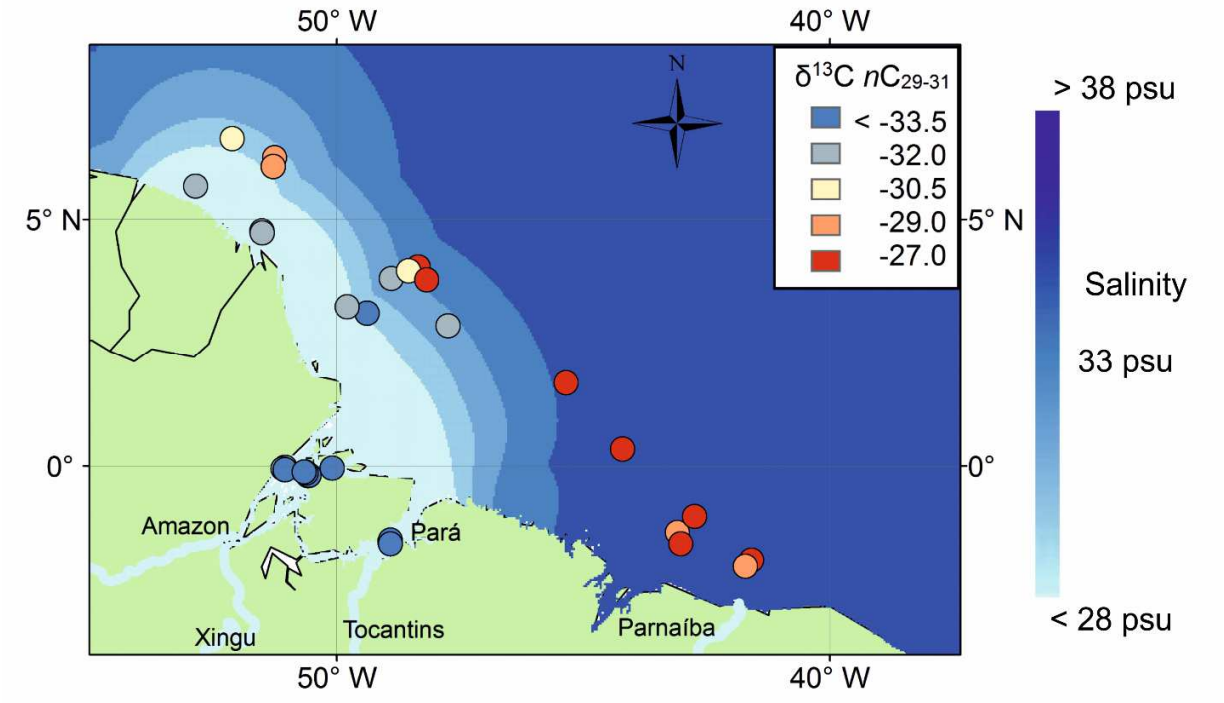

Figure 4.9. $\delta^{13}C$ $nC_{29\text{-}31}$ of marine core-top samples and samples from the Amazon River estuary and the Pará River. Minimal ocean salinity during the annual cycle indicating the maximal extent of the Amazon freshwater plume is marked in shades of blue (Sbrocco and Barber, 2013).

The largest discrepancy between the $\delta^{13}C$ $nC_{29\text{-}31}$ and the δD $nC_{29\text{-}31}$ values can be found in the Pará River. This can be explained by the dominant contribution of *n*-alkanes by the

Tocantins River. While the Tocantins River has more enriched δD $nC_{29\text{-}31}$ values than the Amazon main stem, comparable to the Amazon lowland tributaries, it drains a predominantly C3 vegetated area with a depleted $\delta^{13}C$ $nC_{29\text{-}31}$ signal (Powell et al., 2012).

Overall, our results show that the deposition of organic compounds from suspended load from the Amazon Basin into the present-day Atlantic is limited to the extent of the influence of the Amazon freshwater plume. This supports previous studies, which found similar results for deposition of OM and polar lipids (Chong et al., 2014; Zell et al., 2014). This finding has important implications for the application of proxies associated with leaf-wax biomarkers in paleoclimate studies. During glacial sea-level low-stands when the Amazon freshwater plume was shifted oceanward, the area influenced by Amazon sedimentation also shifted (Damuth and Flood, 1983; Zell et al., 2014). Hence, variability in down-core records may not only be caused by changes in the environmental conditions in the Amazon Basin, but also reflect changes in sediment source area, i.e. Amazon versus coastal or dust sources.

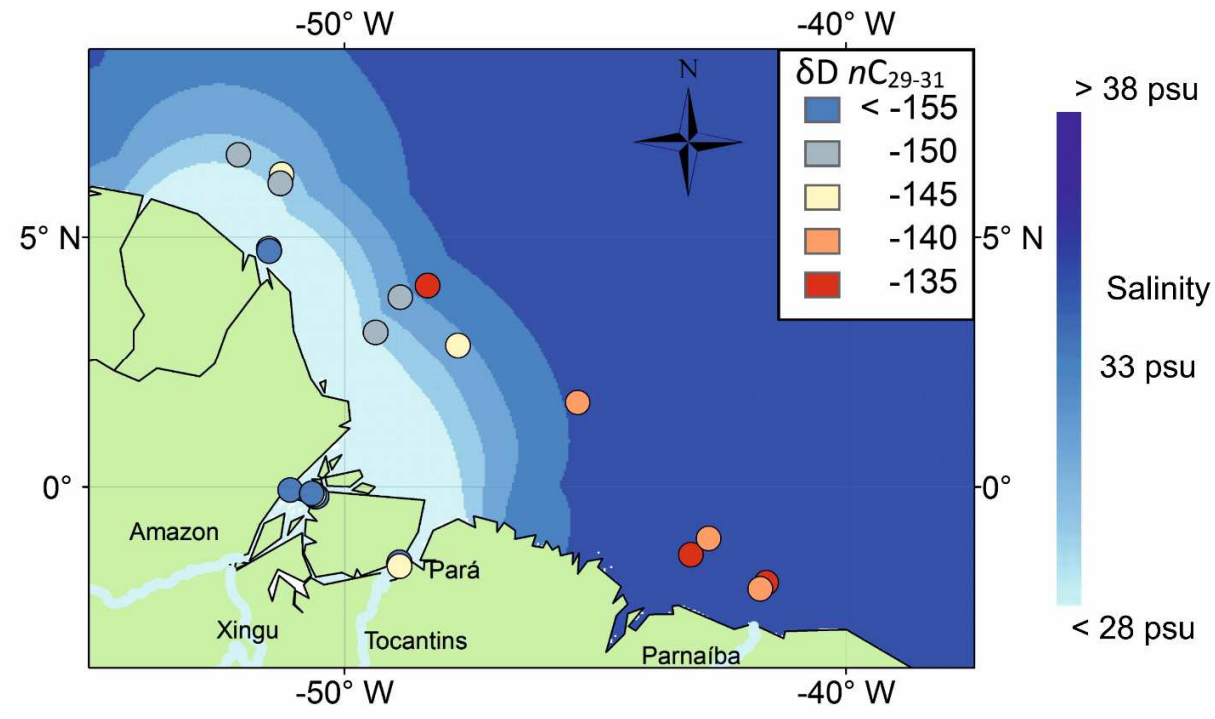

Figure 4.10. δD $nC_{29\text{-}31}$ of marine core-top samples and samples from the Amazon River estuary and the Pará River. Minimal ocean salinity during the annual cycle indicating the maximal extent of the Amazon freshwater plume is marked in shades of blue (Sbrocco and Barber, 2013).

Table 4.3. Position, water depth, core depth, TOC content, *n*$C_{29\text{-}31}$ concentration, ACL, CPI, $\delta^{13}C$ *n*$C_{29\text{-}31}$, δD *n*$C_{29\text{-}31}$ of the core-top samples collected for this study. Positions where no measurements were conducted are marked with N/A. Samples with only one deuterium measurement are marked with [a].

Sample	Long. (°E)	Lat. (°N)	Water depth (m)	Core Depth (cm)	TOC (%)	Conc. *n*$C_{29\text{-}31}$ (ng g^{-1})	ACL	CPI	$\delta^{13}C$ *n*$C_{29\text{-}31}$ (‰)	δD n$C_{29\text{-}31}$ (‰)
GeoB16202	-41.59	-1.91	2247	0-1	0.50	18.48	30.31	3.52	-28.21	-135.7
GeoB16203	-41.72	-2.04	1590	0-1	0.78	59.69	30.47	2.98	-29.12	-141.2[a]
GeoB16205	-43.10	-1.35	1957	0-1	0.54	65.70	30.41	3.56	-29.07	-137.5
GeoB16206	-43.02	-1.58	1367	0-1	0.55	22.80	30.33	2.66	-28.85	N/A
GeoB16212	-49.39	3.10	77	0-1	0.73	70.80	29.99	3.41	-33.53	-154.3
GeoB16216	-51.26	6.24	2851	0-1	0.78	96.26	30.29	3.09	-29.79	-145.8
GeoB16217	-51.29	6.07	2433	0-1	0.49	50.69	30.22	3.43	-30.06	-150.7
GeoB16218	-51.52	4.77	40	0-1	0.76	157.59	30.09	3.79	-32.45	-154.8
GeoB16220	-51.51	4.72	31	0-1	N/A	132.30	30.06	3.92	-33.30	-155.4
GeoB16223	-52.12	6.63	2251	0-1	0.81	84.23	30.16	3.15	-30.82	-150.1
GeoB16225	-52.86	5.67	34	0-1	0.30	13.02	29.58	3.85	-33.27	N/A
Bc17	-48.54	3.96	739	7-8	0.44	55.85	29.89	3.65	-30.77	N/A
Bc24	-48.89	3.80	641	7-9	0.49	79.91	30.26	3.39	-33.25	-153.0
Bc44	-48.17	3.78	1014	8-9	0.44	44.34	29.37	2.90	-28.67	N/A
BC61	-47.74	2.85	609	4-5	0.64	200.21	30.65	3.15	-33.18	-145.6
Bc75	-45.35	1.68	2445	8-9	0.31	64.19	30.18	3.19	-27.88	-140.6
Bc82	-44.21	0.34	3113	5-6	0.35	54.91	30.06	2.19	-28.22	N/A
Bc90	-42.74	-1.03	2847	6-7	0.43	52.40	30.26	2.59	-26.73	-141.2
MC12	-48.35	4.04	1711	5-6	0.67	63.59	29.41	2.75	-28.44	-138.0
MC33	-49.79	3.23	53	8-9	0.74	5.69	29.87	2.84	-33.41	N/A

4.5. Conclusions and outlook

We conclude that long-chain *n*-alkanes from the Amazon estuary represent a mixed signal from the western tributaries (the Solimões and Madeira Rivers) and the eastern tributaries of the Amazon Basin (e.g., the Negro, Tapajos and Xingu Rivers) and are overall mainly lowland sourced. The δD of long-chain *n*-alkanes from the main tributaries is consistent with the values of the average isotopic composition of precipitation for each sub-catchment. The observation that values at the estuary also reflect the average isotopic composition of precipitation over the entire basin, leads to the conclusion that contributions from different geographic sources are integrated in the estuary. This also means that compounds transported from the western sector of the basin do not experience extensive degradation. Compound-specific $\delta^{13}C$ analyses, coupled with TOC contents and ACL results provide evidence that long-chain *n*-alkanes from the Amazon estuary are mostly derived from modern forest plants, with a minor contribution from a petrogenic source. Leaf-waxes derived from the Amazon River clearly impact the δD and $\delta^{13}C$ of long-chain *n*-alkanes deposited off northeastern South America, but their influence in the offshore region is restricted to the extent of the Amazon freshwater plume. These findings should be considered in the interpretation of proxy records based on long-chain *n*-alkanes used in paleo-environmental reconstructions of the Amazon Basin. In order to further increase the understanding of the fate of long-chain *n*-alkanes in the Amazon, future studies should focus on the quantitative assessment of contributions from the different tributaries.

All data presented in this manuscript can be found on pangaea.de.

Acknowledgements

We would like to acknowledge funding through the DFG-Research Center / Cluster of Excellence „The Ocean in the Earth System“ at MARUM - Center for Environmental Sciences. CH thanks GLOMAR – Bremen International Graduate School for Marine Sciences for support. AOS thanks FAPESP for the financial support (grant 2011/06609-1) and CNPq for the research fellowship (grant 309223/2014-8). CMC acknowledges FAPESP (grant 2012/17517-3) for support. HOS acknowledges FAPESP for the financial support (grants 2011/06609-1 and 2011/14502-2). PAB acknowledges support for the KNR/97-4 cruise by NSF-OCE-0823650. Carlos Grohmann, Ingo Wahnfried and Tatiana Pereira are acknowledged for the technical and logistical support during fieldtrips in the Amazon River. We thank the *RV Maria S. Merian* cruise MSM20/3 crew for technical support during core-

top sampling, and Ralph Kreutz and Birk Stern for laboratory support. We acknowledge the GeoB Core Repository at MARUM – University of Bremen for supplying the GeoB core-top samples used in this study. Helpful comments by Sarah J. Feakins and an anonymous reviewer greatly improved the manuscript.

5. Response of the Amazon rainforest to late Pleistocene climate variability

Christoph Häggi[1], Cristiano M. Chiessi[2], Ute Merkel[1], Stefan Mulitza[1], Matthias Prange[1], Michael Schulz[1], Enno Schefuß[1]

[1] MARUM – Center for Marine Environmental Sciences, University of Bremen, Leobener Str. 8, 28359 Bremen, Germany.

[2] School of Arts, Sciences and Humanities, University of São Paulo, Av. Arlindo Bettio 1000, 03828-000 São Paulo SP, Brazil.

Abstract

Late Pleistocene climate and vegetation history of lowland Amazonia is controversially debated. Here we use the isotopic composition of plant-waxes from a marine sediment core to reconstruct the high-resolution integrated precipitation and vegetation history of lowland Amazonia for the late Pleistocene (50-12.8 ka BP). Our results show that humid conditions comparable to modern climate persisted through much of the late Pleistocene, and that moderate drying was limited to full glacial conditions. Dominant forest cover prevailed through the late Pleistocene and was only reduced during Heinrich Stadials. This implies that forest vegetation was resilient to glacial climate conditions in lowland Amazonia and rather affected by savanna intrusions in the northern sector of the Amazon basin during Heinrich Stadials.

5.1. Main Text

Lowland Amazonia is covered by the largest and most biodiverse rainforest on Earth and is one of the major centers of deep tropical convection (Olson et al., 2001; Werth and Avissar, 2002). Hence, environmental changes in lowland Amazonia have major implications for the global carbon and hydrologic cycles (Brienen et al., 2015; Werth and Avissar, 2002). To understand the stability of Amazonian vegetation and precipitation to global climate shifts, a firm comprehension of past variability is critical. So far, there are conflicting scenarios regarding vegetation and climate history of lowland Amazonia (Colinvaux et al., 1996; D'Apolito et al., 2013). On the one hand, it was suggested that forest vegetation persisted under wet, albeit cooler, conditions throughout the last glacial maximum (LGM) (Colinvaux et al., 1996; Haberle and Maslin, 1999). On the other hand, significantly drier climate conditions during the LGM were proposed to have led to changes in the forest structure, potentially even to partially open savanna landscapes (D'Apolito et al., 2013; Haffer, 1969; van der Hammen and Hooghiemstra, 2000). These different views are linked to hypotheses on the history and distribution of neotropical biodiversity. While the refugia hypothesis proposing speciation in isolated forest refugia surrounded by glacial savanna (Haffer, 1969) has been refuted from a phylogenetic (Smith et al., 2014) as well as paleobotanic perspective (Behling et al., 2009), changes in the extent and structure of the Amazon rainforest are still thought to play a major role in shaping biodiversity and species distribution patterns in the Neotropics. Stable forest vegetation in the western sector of the basin is thought to have led to the exceptionally high species richness (Hoorn et al., 2010; Smith et al., 2014), but expansion and contraction of forest and savanna vegetation in eastern Amazonia were suggested to have led to increased extinction, but potentially also opened corridors connecting otherwise separated biomes (Behling et al., 2009; Cheng et al., 2013; Da Silva and Bates, 2002).

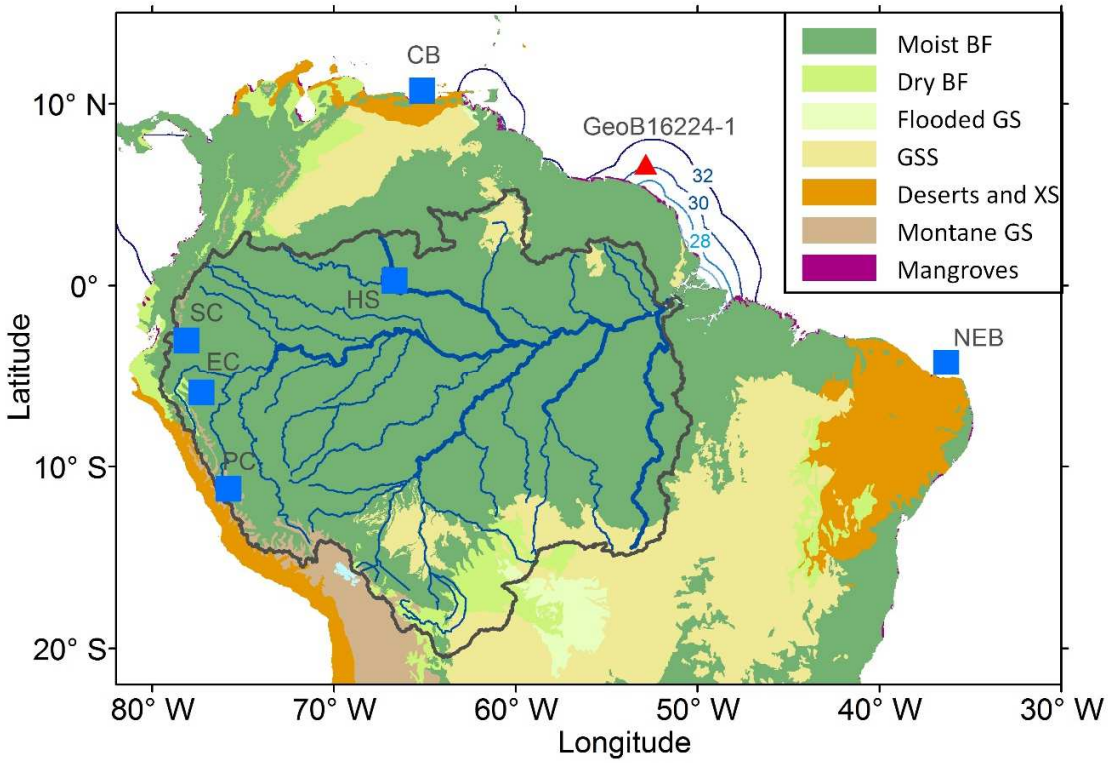

Fig. 5.1. Map of the Amazon Basin and the adjacent Atlantic Ocean. Color shading represents the major modern biomes in tropical South America (Olson et al., 2001) (BF: Broad leaf forest; GS: Grassland and savanna; GSS: Grassland savanna and shrub land; XS: Xeric shrub land). The Amazon Basin is marked with a black line. Blue contour lines in the Atlantic Ocean represent sea surface salinity indicating the northward flow of Amazonian freshwater (Sbrocco and Barber, 2013). The location of core GeoB16224-1 is marked with a red triangle. The location of the other paleoclimate records from the Cariaco basin (CB) (Deplazes et al., 2013), the Santiago (SC) (Mosblech et al., 2012), El Condor (EC) (Cheng et al., 2013) and Pacupahuain (PC) (Kanner et al., 2012) caves, the Hill of Six Lakes (HS) (Colinvaux et al., 1996) and northeastern Brazil (NEB) (Jaeschke et al., 2007) discussed in this study are marked with blue squares.

The uncertainty regarding the late Pleistocene vegetation and climate history is owed to the circumstance that almost all available climate records from lowland Amazonia are derived from the fringes of the rainforest area, while the late Pleistocene conditions in the interior lowland basin are largely unknown (Baker and Fritz, 2015; Behling et al., 2009). The understanding of past vegetation and climate variability in the central Amazon Basin is mainly based on records from lacustrine sediment cores from the Hill of Six Lakes (Colinvaux et al., 1996; D'Apolito et al., 2013) and offshore sediment cores recording a basin integrated but low-temporal resolution signal (Haberle and Maslin, 1999). From both the lacustrine

and marine archives, wet conditions with a constant forest cover have been inferred for the LGM (Colinvaux et al., 1996; Haberle and Maslin, 1999). However, the detection of a sediment hiatus during the LGM in the Hill of Six Lakes record has recently challenged these findings (D'Apolito et al., 2013), highlighting the need for continuous high-resolution proxy records reflecting the lowland Amazonian vegetation and climate conditions.

Here we provide high-resolution plant-wax isotope records from a marine sediment core to reconstruct the climate and vegetation conditions in the lowland Amazon Basin (Häggi et al., 2016) (see supplementary materials for the methodology description). The sediment core was retrieved from the continental margin off French Guiana (GeoB16224-1; 6°39.38'N, 52°04.99'W, 2510 m water depth, Fig. 5.1). The core site received continuous sedimentation by the Amazon Plume from 50 ka BP until the end of the Bølling-Allerød (12.8 ka BP) when rising sea levels shifted the depositional areas onto the shelf (Fig. S1, S2) (Zhang et al., 2015). The δD of plant-waxes, such as long-chain *n*-alkanes, predominantly reflects the isotopic composition of precipitation (Sachse et al., 2012), which is mainly controlled by the amount effect in the tropics (Dansgaard, 1964). Hence, variations in *n*-alkane δD were used to reconstruct variations in the amount of precipitation. The $\delta^{13}C$ of *n*-alkanes is controlled by the photosynthetic pathway and allows differentiation between biomes with dominant C3 and C4 vegetation (i.e. forest vs. savanna vegetation) (Castañeda and Schouten, 2011). Therefore, we used the $\delta^{13}C$ to reconstruct potential shifts in dominant vegetation type. Unlike inorganic sedimentary components, which mainly originate from the Andes, organic matter, including plant-waxes, is primarily sourced from the lowland Amazon Basin (Bouchez et al., 2014; Häggi et al., 2016). Since the isotopic composition of precipitation in the Amazon reflects large-scale changes in precipitation (Brienen et al., 2012), a potential bias towards a signal from gallery forests would only have limited influence on the reconstructed *n*-alkane δD. Moreover, our approach allows to independently assess changes in vegetation and precipitation on the same compounds.

Our vegetation reconstruction based on the $\delta^{13}C$ of nC_{29} and nC_{31} alkanes ($\delta^{13}C$ $nC_{29\text{-}31}$) shows values between -31.5 ‰ and -34 ‰ vs. VPDB (Fig. 5.2B). The most depleted values of -34 ‰ are found during the LGM and in the period before 45 ka BP. There is a small long-term trend to more enriched values of around -32.5 ‰ from 45 to 42 ka BP and a trend back towards more depleted values from 38 to 20 ka BP. Compared to the values found in the modern outflow (Häggi et al., 2016), most of the $\delta^{13}C$ $nC_{29\text{-}31}$ record is only slightly more enriched suggesting that lowland Amazonia remained largely forest covered from 50 to 12.8 ka BP (Fig 5.2B, Fig. S3, S4, S5) A shift to full savanna vegetation would have led to values around -22 ‰ (Castañeda and Schouten, 2011), and even a shift to a mixed vegetation with gallery forests as found today over Northeastern Brazil would have led to more enriched values between -27 ‰ and -29 ‰ (Häggi et al., 2016). The most enriched $\delta^{13}C$ $nC_{29\text{-}31}$ values in our record indicating savanna expansions are found in distinct peaks of up to -31.5 ‰

coinciding with Heinrich Stadials 1-4 and Greenland Stadial 11 (Fig. 5.2B). Since these values are intermediate between the present-day Amazon rainforest and Northeastern Brazil, this indicates only a partial replacement of the Amazon rainforest by mixed vegetation types or savanna.

The average δD for the dominant nC$_{29}$ and nC$_{31}$ *n*-alkanes corrected for ice volume changes (δD nC$_{29-31}$) found in core GeoB16224-1 during marine isotope stage (MIS) 3 shows values similar to samples from the modern Amazon estuary (-155 to -160 ‰ vs. VSMOW) (Fig. 5.2C, Fig. S3) (Häggi et al., 2016). Towards the LGM there is a gradual enrichment of 15 ‰ indicating a drying trend. During the deglaciation, δD nC$_{29-31}$ became again more depleted, but remained more enriched compared to modern values. On shorter, millennial time-scales the δD record shows only limited variability. Our finding that humid conditions persisted through much of the late Pleistocene, while drying occurred only under full glacial conditions is corroborated by experiments with a comprehensive climate model (Merkel et al., 2010) which showed the same trends (Fig. 5.3, Fig. S6, see supplementary material for model description). The magnitude of modelled basin-wide precipitation changes between the LGM and preindustrial are only moderate (0.4 mm/day). This is in line with the δD nC$_{29-31}$ variability which is low compared to speleothem isotope records from the fringes of the Amazon Basin (Cheng et al., 2013) (Fig. S7).

Our combined vegetation and precipitation reconstructions indicate that the LGM drying was insufficient to result in large-scale replacement of forest by savanna vegetation. This underscores the resilience of tropical vegetation towards drier climate. The distinct peaks in savanna vegetation during Heinrich Stadials were most likely caused by a meridional southward shift of the tropical convection center evident in climate records to the north (Cariaco basin) (Deplazes et al., 2013) and south (Northeastern Brazil) (Jaeschke et al., 2007) of the Amazon Basin (Fig. 5.2A, D). As a consequence of a southward shift of the convection center, savanna expansion most likely occurred in the northern sector of the Amazon Basin. The small long-term trend potentially reflects a development similar to the Cariaco basin record that also shows some of the driest sections around HS4 (Fig. 5.2A). Alternatively the long-term trend could be influenced by shifts in savanna vegetation in the south of the basin (Mayle et al., 2000)

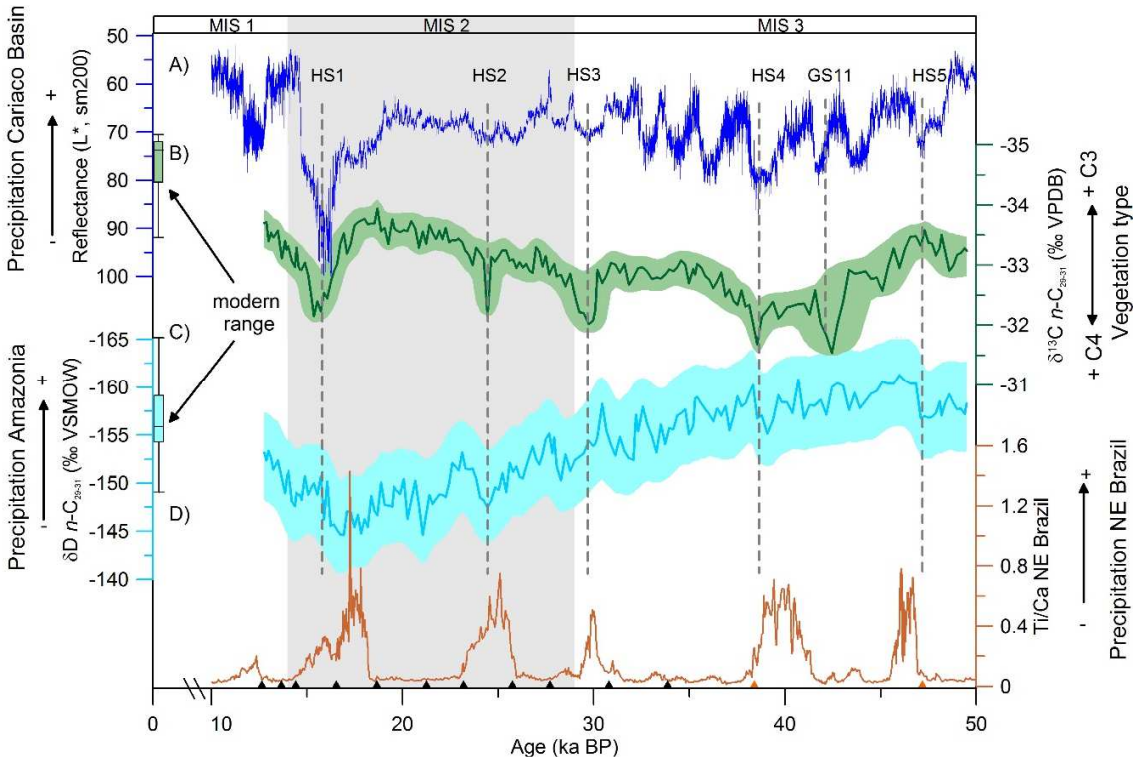

Fig. 5.2. Precipitation and vegetation reconstructions for lowland Amazonia and other hydroclimate records from tropical South America. A) Color reflectance from the Cariaco basin indicating the relative amount of terrestrial sediment input and the position of the tropical convection center in northern South America (Deplazes et al., 2013). B) $\delta^{13}C$ $nC_{29\text{-}31}$ of core GeoB16224-1 indicating the dominant vegetation type over lowland Amazonia (this study). The range of modern values from the Amazon estuary are shown as box-whisker plot on the left of the figure (Häggi et al., 2016). C) δD $nC_{29\text{-}31}$ of core GeoB16224-1 representing precipitation evolution over Amazonia (this study). The range of modern values is also given as box-whisker plot (Häggi et al., 2016). D) Ti/Ca data from GeoB3910-2 indicating the relative amount of terrestrial sediment input and the position of the tropical convection center south of the Amazon Basin (Jaeschke et al., 2007). The grey bar indicates the duration of marine isotope stage 2 (MIS2). The timing of Heinrich Stadials (HS) 1-5 and Greenland Stadial (GS) 11 is given with dashed lines. Black triangles indicate the calibrated ^{14}C AMS ages constraining the age model of core GeoB16224-1 (Zhang et al., 2015). Orange triangles represent tie points to the U/Th dated El Condor speleothem record (Cheng et al., 2013). Shaded areas in the isotope records indicate the 2σ uncertainty envelope calculated with the BACON software (Blaauw and Christen, 2011).

In contrast to the $\delta^{13}C$ $nC_{29\text{-}31}$ record, millennial-scale variations appear to be muted in the δD $nC_{29\text{-}31}$ record (Fig. 5.2C). Here, drying in the north was likely offset by wetter conditions in the southern and western sectors of the basin (Cheng et al., 2013). Instead, our basin-wide integrated δD $nC_{29\text{-}31}$ record features a dominant long-term mode of variability with humid conditions during MIS3 and drying during MIS2. Since proxy records to the north and the south of the Amazon Basin show little variation from MIS3 to MIS2 (Fig. 5.2A, D), a meridional movement of the convection center is unlikely to be the cause for this pattern (Deplazes et al., 2013; Jaeschke et al., 2007). Based on CCSM3 model simulations (Merkel et al., 2010), we suggest that LGM rainfall reduction was caused by a combination of reduced atmospheric water vapor, decreasing the available moisture supply, and dynamical circulation change associated with reduced convective mass flux. The climate model runs show a decrease of total precipitable water (TPW), i.e. column-integrated water vapor, for all late Pleistocene time slices compared to the preindustrial (Fig. 5.3), primarily controlled by sea surface a temperature decrease and the reduced moisture-holding capacity of colder air (Chadwick et al., 2016). Convective mass flux is correlated with tropospheric vertical velocity (Vecchi and Soden, 2007). The intensity of vertical velocity at the 500 hPa level ($\omega500$) only decreased during Heinrich Stadial 1 and the LGM but increased during MIS3 leading to precipitation amounts comparable to the preindustrial despite drier air masses (Fig. 5.3). The decrease (increase) of $\omega500$ during MIS2 (MIS3) was partly related to the different ice sheet heights during MIS3 and MIS2 which induced high-to-low latitude atmospheric wave trains of upper-tropospheric zonal wind anomalies of opposite signs over our study area, thereby interfering with regional circulation in suppressing (enforcing) convection. The finding that tropical convection decreased only during full glacial conditions is in line with a suggested non-linear effect of changes in ice sheet topography on tropical precipitation (Lee et al., 2014).

The LGM drying in our lowland record contrasts with speleothem isotope records from the Andes and the Andean foothills in the western Amazon Basin (Fig. 5.1), which showed continuously wet conditions during MIS3 and MIS2, and mostly varied on millennial time-scales (Fig. S7) (Cheng et al., 2013; Kanner et al., 2012; Mosblech et al., 2012). This offset to our findings indicates that the LGM drying inferred from our record does not extend to the westernmost sector of the basin and was probably more pronounced in the central and eastern parts. Conversely, climate patterns with humid conditions during MIS3 and drying during full glacial conditions have been reported from other major centers of tropical deep convection in Africa and Indonesia (Fig. S8) (Russell et al., 2014; Tierney et al., 2008). This suggests that the climate conditions in the centers of deep tropical convection are dominantly influenced by northern hemisphere ice sheet evolution (Russell et al., 2014).

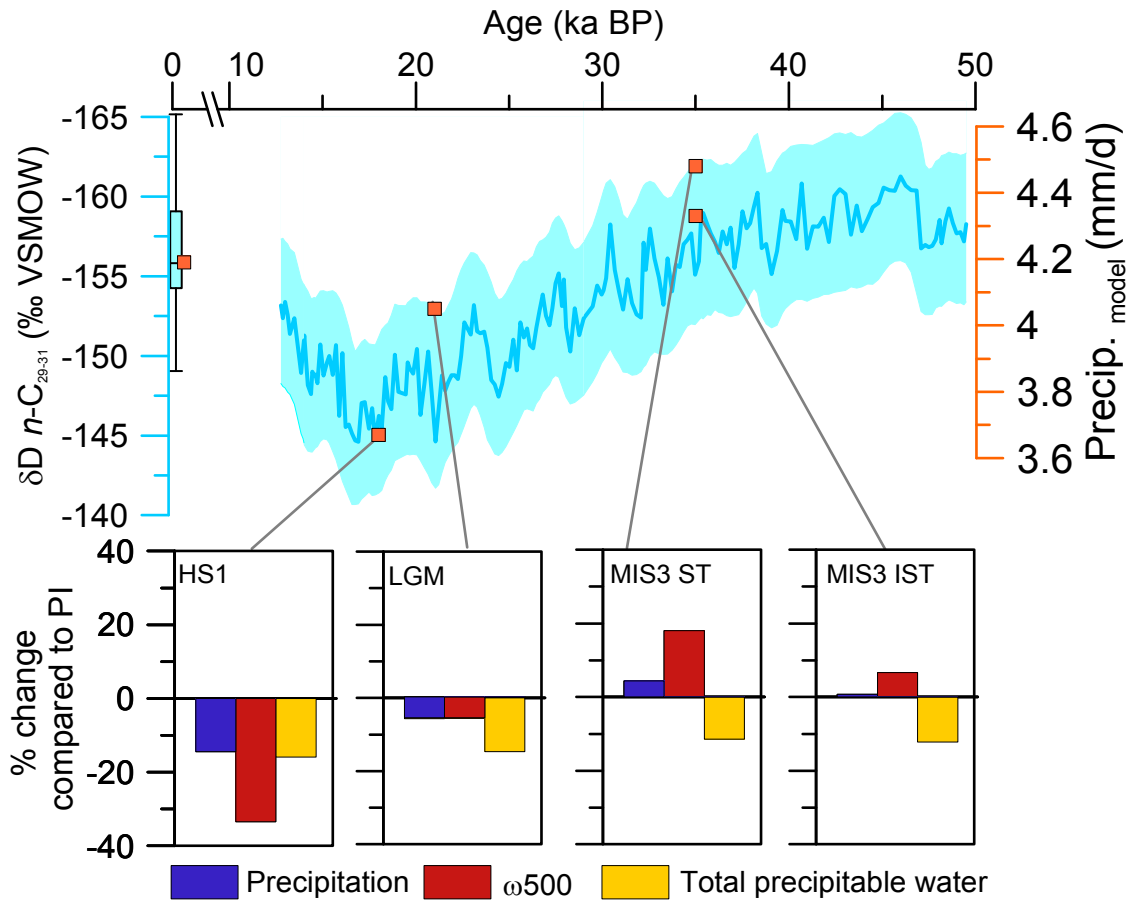

Fig. 5.3. Modelled precipitation, convection and total precipitable water over the Amazon Basin (72°W to 48°W; 12°S to 3°N). δD $nC_{29\text{-}31}$ in blue as in Fig. 5.2C indicating precipitation intensity. Orange squares represent simulated annual mean precipitation (in mm/day) averaged over the Amazon Basin for the preindustrial, Heinrich Stadial 1 (HS1), the last glacial maximum (LGM) and MIS3 stadial and interstadial conditions at 35 ka BP (22). Bar-charts for each time slice represent relative changes (in %) with respect to preindustrial conditions for simulated precipitation, atmospheric vertical velocity at the 500 hPa level (ω500) as an indicator for convection intensity and total precipitable water as an indicator of atmospheric moisture content averaged over the Amazon Basin. Model results are long-term annual means based on the last 100 years of each simulation.

Even though glacial drying did not lead to extensive expansion of savanna vegetation in Amazonia, it might have been responsible for changes in forest structure leading to replacement of humid rainforest by drier forest types (Behling et al., 2009; D'Apolito et al., 2013). During the humid MIS3 conditions, changes in forest structure observed in some pollen records probably reflect the influence of lower glacial temperatures (Behling et al., 2009; Mayle et al., 2000). Contrary to studies which inferred savanna expansion during the LGM (Haffer, 1969; van der Hammen and Hooghiemstra, 2000), we find that savanna expansions were associated with Heinrich Stadials. While these limited savanna expansions lasted probably not long enough to lead to speciation as suggested by the refugia hypothesis (Haffer, 1969), it is conceivable that shifts in vegetation cover during Heinrich Stadials led to the connection of otherwise separated biomes. Phylogenetic and biogeographic studies suggest that the savanna regions to the north and the south of the Amazon Basin were repeatedly connected during the Pleistocene (Da Silva and Bates, 2002; Quijada-Mascareñas et al., 2007). This pattern has been attributed to the formation of an open forest corridor through the Amazon during glacials (Behling et al., 2009). We suggest that the opening of migration routes was further influenced by vegetation shifts during Heinrich Stadials. While savanna intrusions from the north occurred during Heinrich Stadials, the southern edge of the Amazon rainforest was displaced northwards during glacial periods (Mayle et al., 2000). This may not necessarily have led to a continuous connection, but could also have involved stepwise migration along savanna patches in the Amazon interior.

In conclusion our study shows that lowland Amazon vegetation and climate were relatively stable during the late Pleistocene. This supports the hypothesis that the Amazonian biodiversity is not a result of forest refugia during glacial droughts, but was rather favored by stable conditions (Cheng et al., 2013; Hoorn et al., 2010; Smith et al., 2014). The finding that the most pronounced vegetation shifts were associated with Heinrich Stadials rather than glacial drying opens new perspectives in understanding the connection of biomes in the Neotropics.

Acknowledgments:

We acknowledge funding through the DFG-Research Center / Cluster of Excellence „The Ocean in the Earth System“ at MARUM - Center for Environmental Sciences. CH thanks GLOMAR – Bremen International Graduate School for Marine Sciences for support. CMC acknowledges FAPESP (grant 2012/17517-3) and CAPES (grants 1976/2014 and 564/2015) for support. We thank the RV Maria S. Merian cruise MSM20/3 crew for support during sampling, and Ralph Kreutz and Birk Stern for laboratory support. We acknowledge the GeoB Core Repository at MARUM – University of Bremen for supplying the samples used in this study.

Author contributions: SM, CMC and ES conceived the study and led the sampling effort. CH conducted the laboratory work and wrote the manuscript. UM, MP and MS conducted the climate model experiments. All authors contributed to the interpretation of the results.

All data presented in this manuscript is permanently archived on pangaea.de.

5.2. Supplementary Material

5.2.1. Materials and Methods

5.2.1.1 Materials

Sample material for this study was taken from core GeoB16224-1 (6°39.38´N, 52° 04.99´W; 760 cm core length; 2510 m water depth). The core was retrieved from the continental margin off French Guiana during *RV MS Merian* cruise MSM20/3 in February 2012 (Mulitza et al., 2013). A previous study (Zhang et al., 2015) using Nd isotope measurements showed that the core received continuous sedimentation from the Amazon during the late Pleistocene. To produce the age model for core GeoB16224-1, we used 15 ^{14}C AMS ages of planktonic foraminifera from Zhang et al. (2015) (Tab. S1). Since there is a large gap in ages between 50 and 66 cm, suggesting the presence of a hiatus, we did not use the upper 66 cm of the core. For the lowermost part of the core, where radiocarbon dating reached the limits of its applicability, the age model was amended by tying the published GeoB16224-1 XRF data from Zhang et al. (2015) to the absolutely U/Th dated speleothem chronology of speleothem ELC-B from El Condor Cave in the western Amazon Basin (Cheng et al., 2013). Both records show distinct peaks during Heinrich Stadials allowing for a precise correlation (Fig. S1). Since the tying to the speleothem record led to an improved precision, the lowermost two radiocarbon ages were not used in the final age model and replaced by tie points to the speleothem U/Th chronology (Fig. S1, Tab. S1).

The age model was established using Bayesian modelling conducted with the R-script BACON (Blaauw and Christen, 2011). Calibrated ^{14}C ages were adapted from Zhang et al. (2015), where calibration was achieved with the Marine2013 calibration curve (Reimer et al., 2013). Errors for the tie points to the speleothem U/Th chronology were used without modifications from Cheng et al. (2013). The Bacon script was used with default parameters, except for *acc.mean*, which was changed to 50 y cm^{-1}, which closer reflects the average accumulation than the default setting of 20 y cm^{-1}. Of a total of 15,000 iterations, the last 10,000 age-depth iterations were used to calculate the median age and the 2σ error envelope (Fig. S2). Uncertainty estimates for the δ^{13}C and δD proxies were calculated by combining the BACON age models with 10,000 Monte Carlo proxy time series realizations based on a 1σ-error estimate of 2.8‰ for δD and 0.15‰ for δ^{13}C (see Methods).

Aliquots for compound specific δ^{13}C and δD analyses of *n*-alkanes were collected on a 4 cm interval, yielding an average temporal resolution of approximately 250 years. A total of 180 samples with a dry weight between 8 and 12 g were collected for proxy analysis.

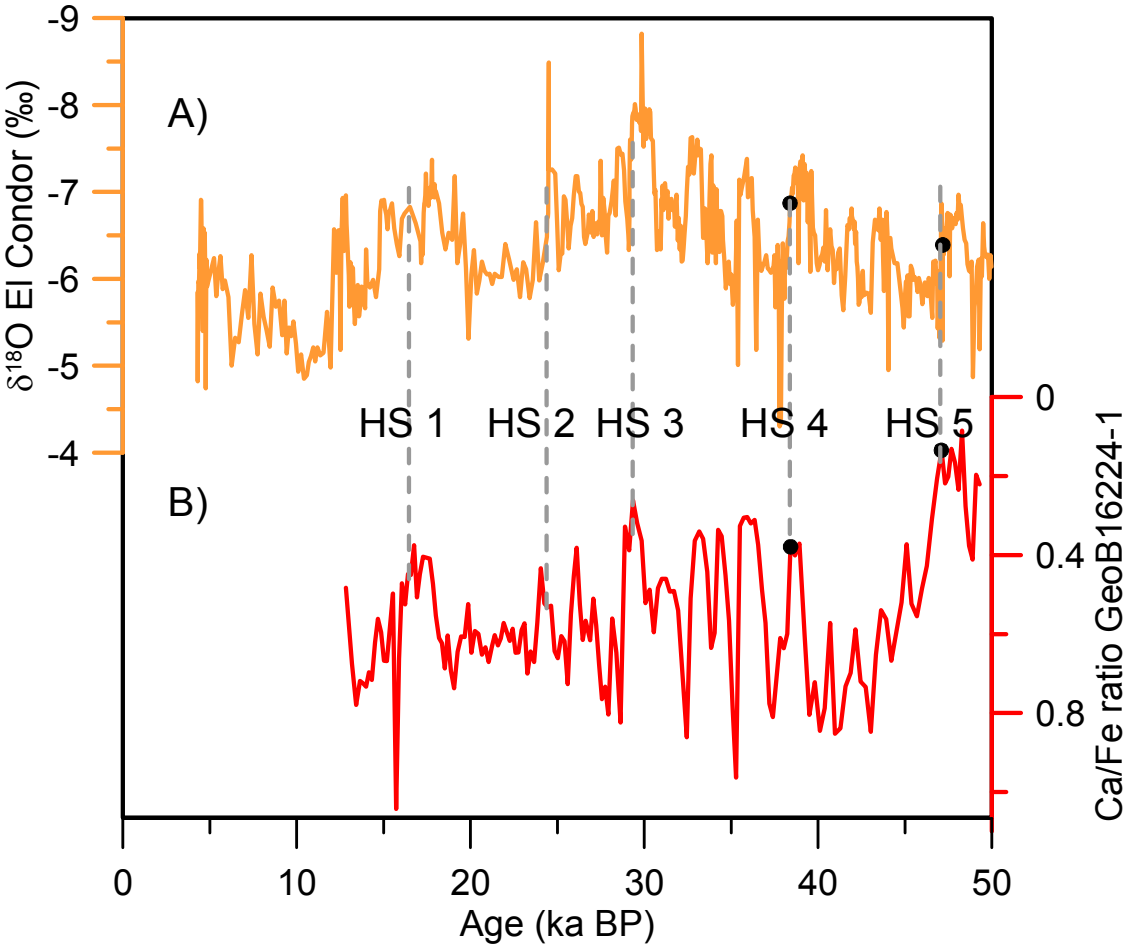

Fig. S1. Tie points of the age model to the El Condor Cave speleothem record. A) El Condor speleothem δ18O record (Cheng et al., 2013). B) Ca/Fe ratio from GeoB16224-1 (Zhang et al., 2015). Heinrich Stadials 1-5 are marked with grey dashed lines. The tie points for HS4 and HS5 are marked with a black dot in all three plots.

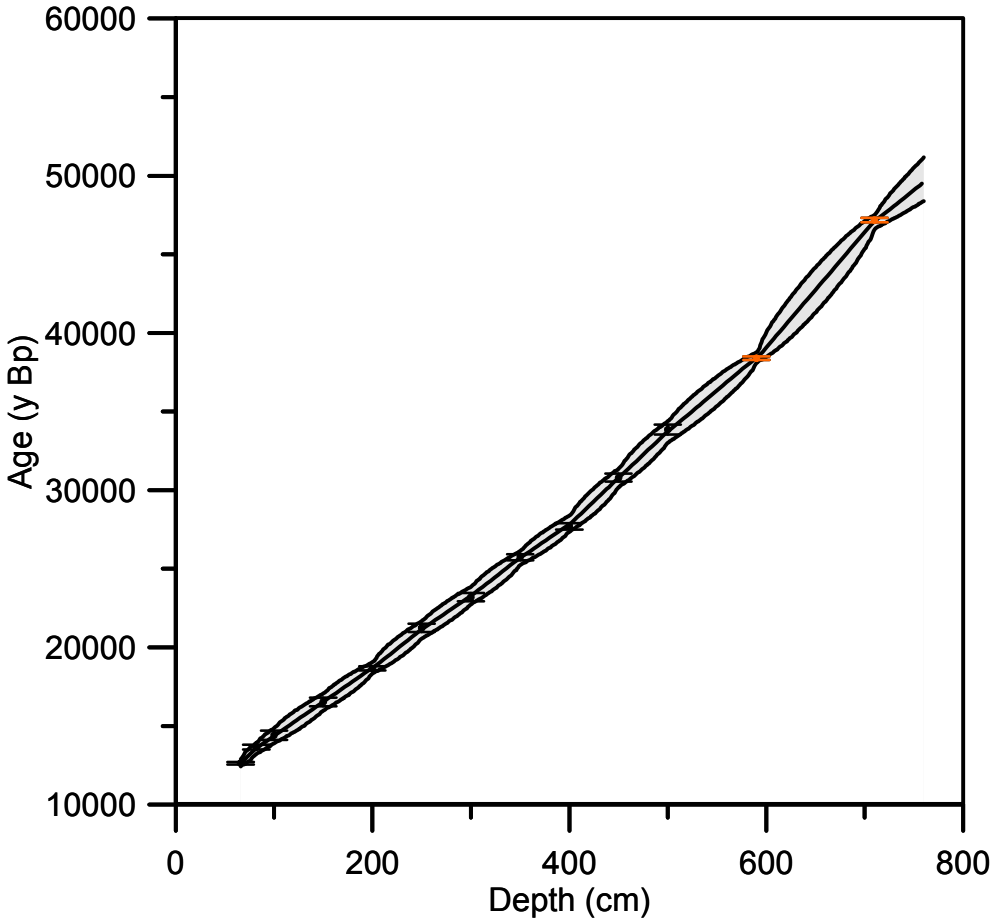

Fig. S2. Age model of core GeoB16224-1. Black points represent radiocarbon ages (Zhang et al., 2015). Orange points mark the tie points of the XRF record of core GeoB16224-1 to the Andean speleothem chronology (Cheng et al., 2013). The grey envelope and error bars indicate the 2σ uncertainty interval.

Table S1. List of ages used to produce the age model of core GeoB16224-1. AMS radiocarbon ages are from Zhang et al. (2015).The ages at 590 and 710 cm depth are based on matching of the XRF record of core GeoB16224-1 (Zhang et al., 2015) to the El Condor speleothem chronology (Cheng et al., 2013). The radiocarbon ages marked with an asterisk were excluded for the age model.

Depth (cm)	Species	^{14}C AMS ages ± 1σ error (yr BP)	Calibrated ages ± 2σ error (yr BP)
6*	*G. sacculifer, G. ruber*	4,910 ± 35	5,126 ± 80
50*	*G. sacculifer, G. ruber*	5,920 ± 30	6,318 ± 38
66	Mixed planktonic foraminifera	11,110 ± 30	12,635 ± 77
82	Mixed planktonic foraminifera	12,220 ± 40	13,667 ± 152
100	*G. sacculifer, G. ruber*	12,760 ± 50	14,420 ± 300
150	Mixed planktonic foraminifera	14,090 ± 70	16,537 ± 277
200	*G. sacculifer, G. ruber*	15,790 ± 60	18,660 ± 137
250	*G. sacculifer, G. ruber*	17,980 ± 70	21,245 ± 267
300	*G. sacculifer, G. ruber*	19,640 ± 80	23,193 ± 272
350	*G. sacculifer, G. ruber*	21,820 ± 90	25,740 ± 189
400	*G. sacculifer, G. ruber*	23,980 ± 120	27,700 ± 204
450	Mixed planktonic foraminifera	26,930 ± 140	30,792 ± 254
500	Mixed planktonic foraminifera	30,110 ± 180	33,854 ± 310
550*	Mixed planktonic foraminifera	31950 ± 180	35,428 ± 463
600*	Mixed planktonic foraminifera	37,070 ± 320	41,222 ± 634
590	Tied to speleothem chronology		38,390 ± 110
710	Tied to speleothem chronology		47,180 ± 140

5.2.1.2 Methods

Lipid extraction and separation procedures followed the same protocol in described in Häggi et al. (2016). Quantification of long-chain *n*-alkanes was achieved using a ThermoFisher Scientific Focus gas chromatograph equipped with an Rxi-5 ms 30x column (30 m, 0.25 mm, 0.25 lm) and a flame ionization detector. Compound-specific δD analysis was conducted in duplicates on a ThermoFisher Scientific MAT 253 isotope ratio mass spectrometer (IRMS) coupled via a GC Isolink operated at 1420°C to a ThermoFisher Scientific Trace GC equipped with a HP-5ms column (30 m, 0.25 mm, 1 µm). δD compositions were measured against calibrated H_2 reference gas and accuracy was controlled by *n*-alkane standards of known isotopic composition calibrated against VSMOV. The H^+_3 factor was determined daily and varied between 5.3 and 5.9 over the measurement period. Long-term mean absolute deviation based on the external *n*-alkane standard was 2.8 ‰. Compound-specific stable carbon isotope analyses were carried out in duplicates on a ThermoFisher Scientific MAT 252 isotope ratio mass spectrometer coupled via a GCC combustion interface with a nickel catalyzer operated at 1000°C to a ThermoFisher Scientific Trace GC equipped with a HP-5ms column (30 m, 0.25 mm, 0.25 µm). $\delta^{13}C$ values were calibrated against CO_2 reference gas of known isotopic composition and accuracy was controlled by measuring *n*-alkane standards of known isotopic composition every six measurements. Long-term mean absolute deviation of external standards was 0.15 ‰.

5.2.1.3 Climate model experiments

A detailed description of the model setup and experimental design is given in Merkel et al. (2010). Here we provide a short description of the numerical climate model experiments. We used the fully-coupled general circulation model CCSM3 (Community Climate System Model version 3) in the low-resolution setup (Yeager et al., 2006). In this configuration, the atmospheric component has a 3.75° (T31) horizontal resolution with 26 layers in the vertical and is coupled to an ocean model with nominal 3° horizontal resolution and 25 levels. For the different experiments, boundary conditions for the pre-industrial, the Last Glacial Maximum (LGM), and the 35 ka time slice (MIS3) were applied. These boundary conditions take atmospheric greenhouse gas concentrations, ice-sheet configurations, astronomical parameters, and land-sea distribution due to sea level changes into account. Preindustrial and LGM boundary conditions follow the guidelines of the Paleoclimate Modelling Intercomparison Project phase 2 (Braconnot et al., 2007). The HS1 (Heinrich Stadial 1) experiment uses the LGM setup with an additional constant freshwater hosing of 0.2 Sv (1

Sv = 10^6 m^3/s) into the northern North Atlantic to disturb the Atlantic Meridional Overturning Circulation (AMOC). A smaller and negative freshwater forcing (-0.1 Sv) was applied to the MIS3 simulation in order to obtain two different MIS3 climate states, a weak-AMOC stadial (MIS3 ST) and a strong-AMOC interstadial (MIS3 IST) state. All simulations were run into quasi-equilibria and long-term means were used for the analysis of climate variables. The AMOC strengths (as measured by the Atlantic overturning stream function at 25°S) in these experiments is 11.6 (preindustrial), 2.7 (HS1), 10.1 (LGM), 6.6 (MIS3 ST), and 14.1 Sv (MIS3 IST).

5.2.2. Supplementary text

5.2.2.1 Factors controlling the δD composition of plant-wax *n*-alkanes

The δD of plant-waxes such as long-chain *n*-alkanes is mainly influenced by the δD of meteoric water (Sachse et al., 2012). There are, however, secondary effects that can overprint the effect of precipitation. In arid regions, the δD of plant-waxes is reported to be additionally controlled by evapotranspirative enrichment of soil and leaf waters (Feakins and Sessions, 2010). Different vegetation types also show a wide range of different fractionation factors (Sachse et al., 2012). Since our data show that forest cover persisted through the late Pleistocene, evapotranspirative enrichment and changes in vegetation cover likely did not play a dominant role in defining the δD of plant-waxes in the Amazon rainforest. Even if a small-scale evapotranspirative enrichment would have taken place, this would have enhanced the enrichment caused by the lower precipitation amount and thus acted in the same direction.

In the Amazon Basin, previous studies showed that the source region of plant-waxes is distributed throughout the lowland basin (Häggi et al., 2016; Ponton et al., 2014). This contrasts the dominant Andean sourcing of inorganic sediments (Meade et al., 1985). Since the present-day signal integrates compounds with varying isotope composition from different regions at the estuary (Häggi et al., 2016), changes in the source region could also have a considerable impact on our δD record. Given that the δD of precipitation in the eastern sector is more δD enriched than in the western sector of the basin (Bowen and Revenaugh, 2003), more enriched values in our δD record could indicate an enhanced input from the eastern basin. However, such an interpretation of our record is at odds with previous studies which indicate that precipitation in the Andes was high during the LGM (Cheng et al., 2013; Kanner et al., 2012; Mosblech et al., 2012). An enhanced input of material from the western part of the basin would have resulted in an increased input of more depleted compounds, which would contradict the more enriched values in our δD

record. Likewise, climate records from the eastern portion of the Amazon rainforest show dry conditions during the LGM (Absy, 1991; van der Hammen and Hooghiemstra, 2000), which makes an enhanced input of isotopically enriched compounds from the eastern basin unlikely.

Due to the accumulation of the lighter hydrogen isotope (^{1}H) in continental ice sheets during the last glacial, the mean isotopic composition of hydrogen in the rest of the global hydrological cycle became more ^{2}H-enriched (by 8‰ on average) compared to present day conditions. This ice volume effect was accounted for by applying the following ice volume correction (IVC) (Tierney and deMenocal, 2013):

$$\delta D_{\mathrm{wax-IVC}} = \frac{1000+\delta D_{wax}}{8*0.001*\delta^{18}isoice+1} - 1000 \quad (5.1)$$

Where $\delta D_{wax\text{-}IVC}$ represents the ice volume corrected isotope values, δD_{wax} the measured δD of plant-waxes and $\delta^{18}O_{isoice}$ the effect of ice volume on the benthic $\delta^{18}O$ variation (Bintanja et al., 2005).

5.2.2.2 Factors controlling the $\delta^{13}C$ in plant-wax *n*-alkanes

$\delta^{13}C$ of plant-waxes reflects the $\delta^{13}C$ of plant organic matter and is mainly controlled by the dominant photosynthetic pathway and $\delta^{13}C$ of source CO_2. C4 plants synthesize compounds with isotopically enriched values, while C3 plants produce ^{13}C depleted compounds (Castañeda and Schouten, 2011). Apart from the relation to the plant photosynthetic pathway, there are other effects that can change the carbon isotope composition of long-chain *n*-alkanes. Petrogenic *n*-alkanes derived from mature sedimentary rocks are also enriched in $\delta^{13}C$ (Bouchez et al., 2014). In the Amazon Basin, this effect is especially visible in coarse-grained, low TOC samples from Andean tributaries (Bouchez et al., 2014; Häggi et al., 2016). In our sediment record there is, however, no indication for enhanced petrogenic input. The carbon preference index (CPI) and the average chain length (ACL) of long-chain *n*-alkanes, which can be used to trace degraded material (Cranwell, 1981; Häggi et al., 2016), are both relatively constant over the entire record (Fig. S4, formulas can be found in ref. (Häggi et al., 2016)). Even though our record shows $\delta^{13}C$ enrichment during Heinrich Stadials, when the likelihood of enhanced input of petrogenic material from the Andes would be highest (Zhang et al., 2015), the timing of events makes a dominant influence of petrogenic material implausible. During Heinrich Stadial 1, enhanced sediment input begins

at 18 ka BP and declines again at around 16 ka BP (Fig. S5 A), while the $\delta^{13}C$ enrichment peaks at 15.5 ka BP coinciding with the southward displacement of the tropical rain belt over northern South America (Deplazes et al., 2013) (Fig. S5 B, C). Furthermore, the canopy effect can lead to changes of the $\delta^{13}C$ composition of plant organic matter. The canopy effect describes the observation that $\delta^{13}C$ values in dense forest systems can show very depleted values due to the uptake of recycled CO_2 from degraded biomass on the forest floor (van der Merwe and Medina, 1991). Since a decrease in the canopy effect due to a more open forest vegetation would lead to more enriched values it would act in the same direction as shifts from C3 to C4 vegetation types. Variations in atmospheric $\delta^{13}C$ are also unlikely to have influenced our record, since this parameter was relatively stable during the studied time period (Eggleston et al., 2016).

Studies using riverine sediment for the reconstruction of dominant vegetation in river catchments, are often regarded to be disproportionally influenced by gallery forest that could mask savannah contributions in the hinterland. Even though gallery forests could lead to a bias in $\delta^{13}C$ values towards forest vegetation, they are unlikely to fully mask potential savanna contribution. In the Paranaiba River basin, present-day vegetation features a mix of C3 and C4 species (Caatinga and Cerrado vegetation types) (Pennington et al., 2000), with gallery forests along the rivers. Data from marine core tops offshore the Paranaiba basin show a clear $\delta^{13}C$ enrichment (Häggi et al., 2016) and thus indicate that a mixed C3/C4 vegetation in the hinterland leads to a $\delta^{13}C$ enrichment even if gallery forests are present.

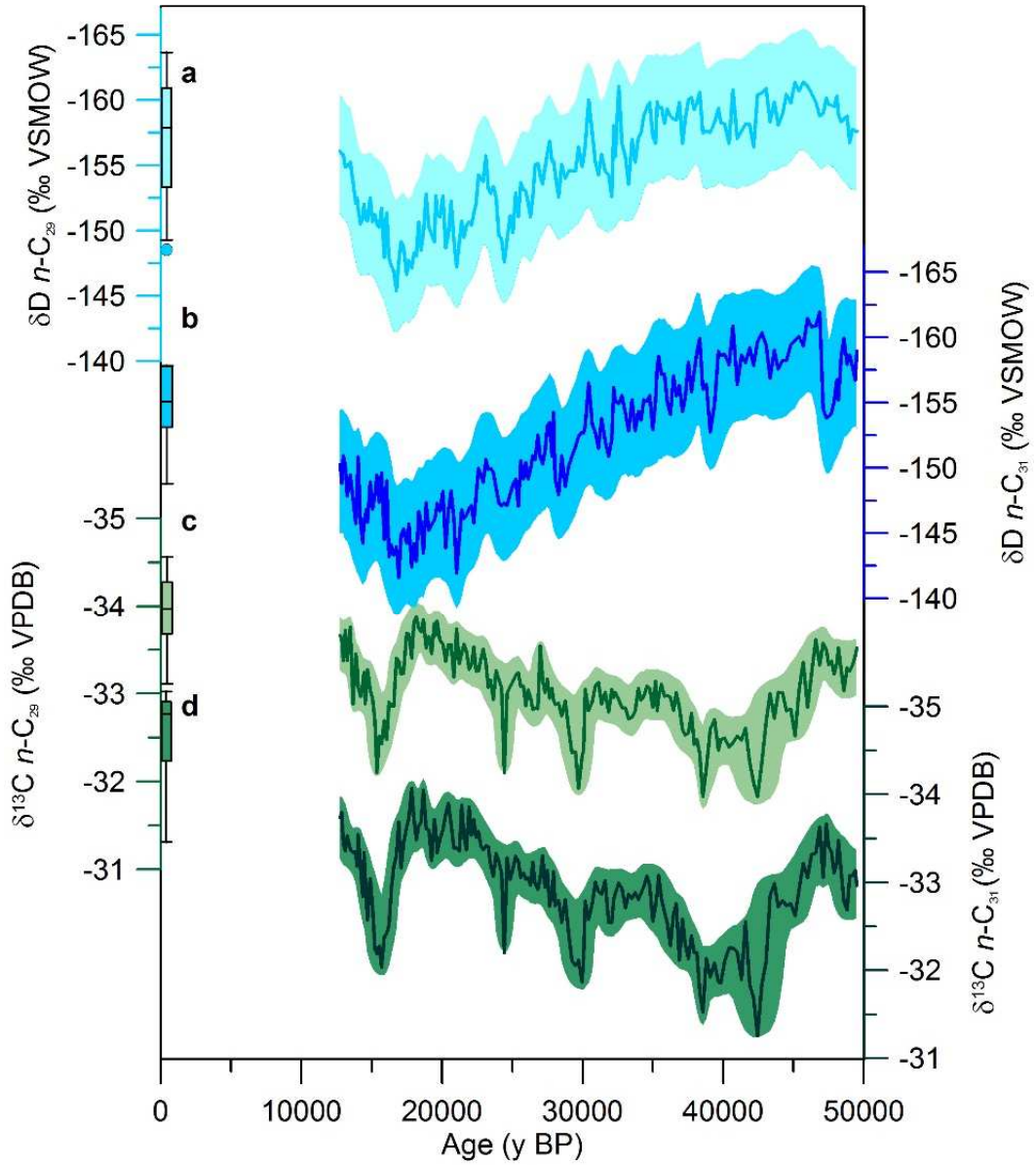

Fig. S3. Separate isotope data from the nC_{29} and nC_{31} *n*-alkanes. A) δD of the nC_{29} *n*-alkane. B) δD of the C_{31} *n*-alkane. C) $\delta^{13}C$ of the nC_{29} *n*-alkane. D) $\delta^{13}C$ of the nC_{31} *n*-alkane.

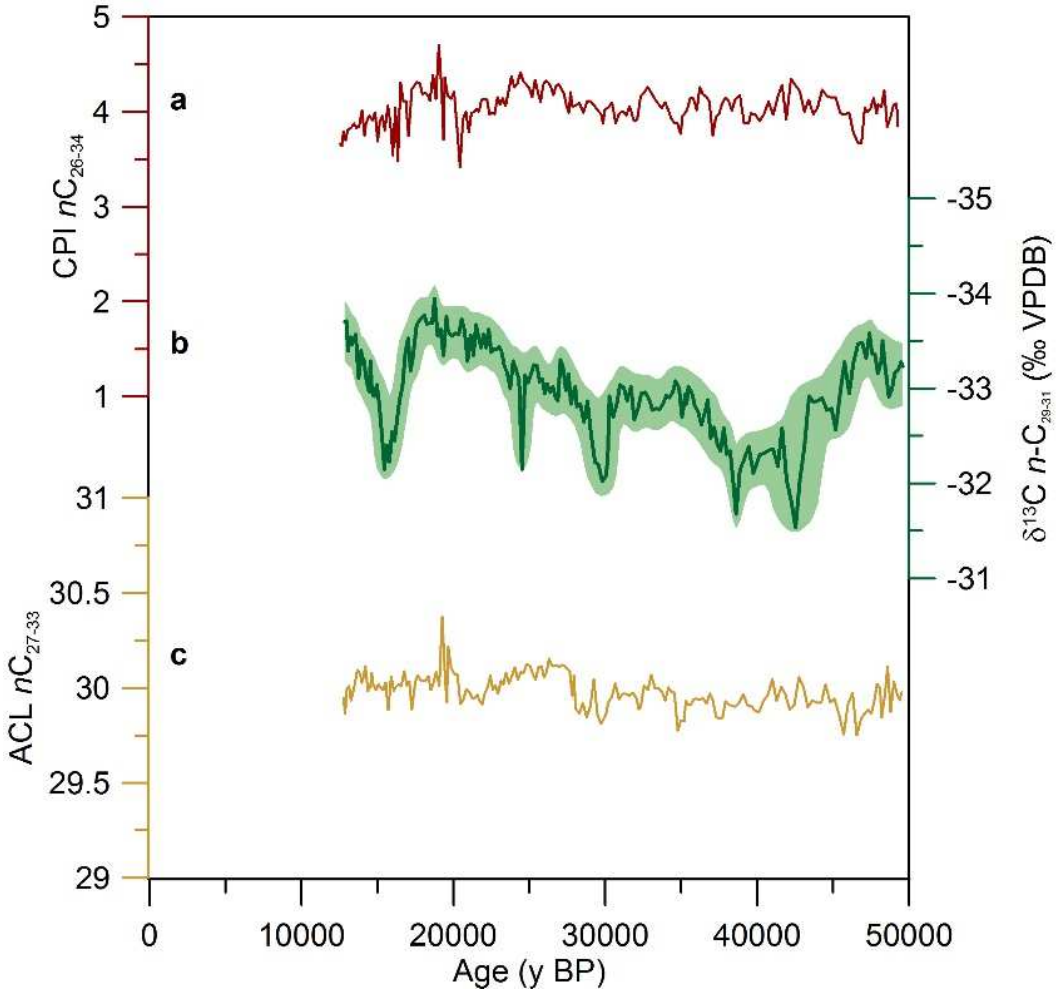

Fig. S4. Variations in CPI and ACL compared to $\delta^{13}C$ nC_{29-31} in GeoB16224-1. A) CPI of the nC_{26} to nC_{34} *n*-alkanes (CPI_{26-34}) representing the degree of degradation. *n*-Alkanes of fully degraded, mature organic matter would be expected to have a CPI of 1 (Lichtfouse and Eglinton, 1995), B) $\delta^{13}C$ nC_{29-31}. The more enriched values during HS are interpreted to be caused by savannah expansion in the northern part of the basin. C) ACL of the nC_{27} to nC_{33} *n*-alkanes (ACL_{27-33}). ACL values below 29 would indicate a high input of petrogenic material (Häggi et al., 2016).

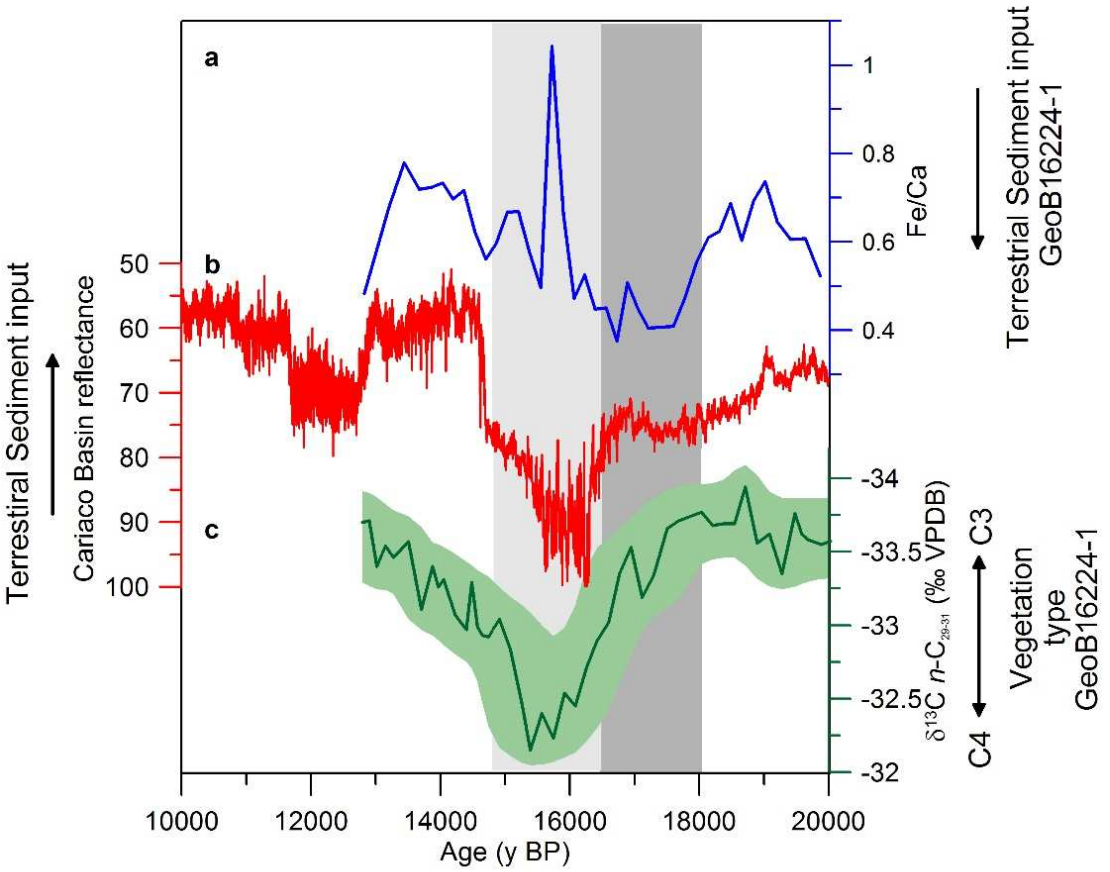

Fig. S5. Timing of climate shifts during HS1. A) Ca/ Fe XRF data from GeoB16224-1 (Zhang et al., 2015) indicating the relative input of terrestrial to marine sedimentation (Govin et al., 2012). B) Colour reflectance data from the Cariaco Basin reflecting the position of the tropical rain belt during boreal summer (Deplazes et al., 2013). C) $\delta^{13}C$ $nC_{29\text{-}31}$ from GeoB16224-1 (this study).

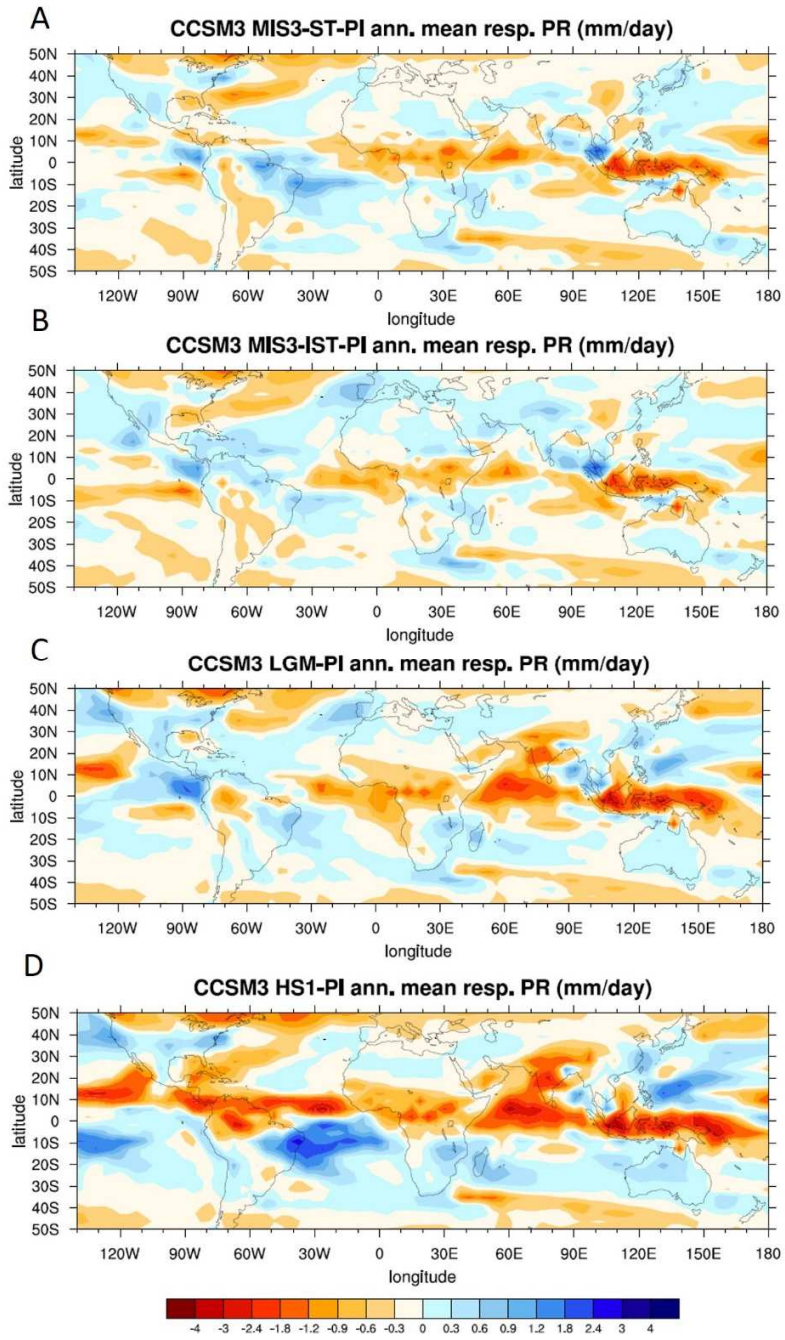

Fig. S6. Annual mean precipitation changes (in mm/day) simulated by CCSM3 model runs for differences between preindustrial (PI) and late Pleistocene time slices (Merkel et al., 2010). Model results are based on long-term annual means from the last 100 years of each simulation. Difference with respect to preindustrial (PI) for A) MIS3 stadial conditions at 35ka BP, B) MIS3 interstadial conditions at 35ka BP, C) LGM, and D) HS1.

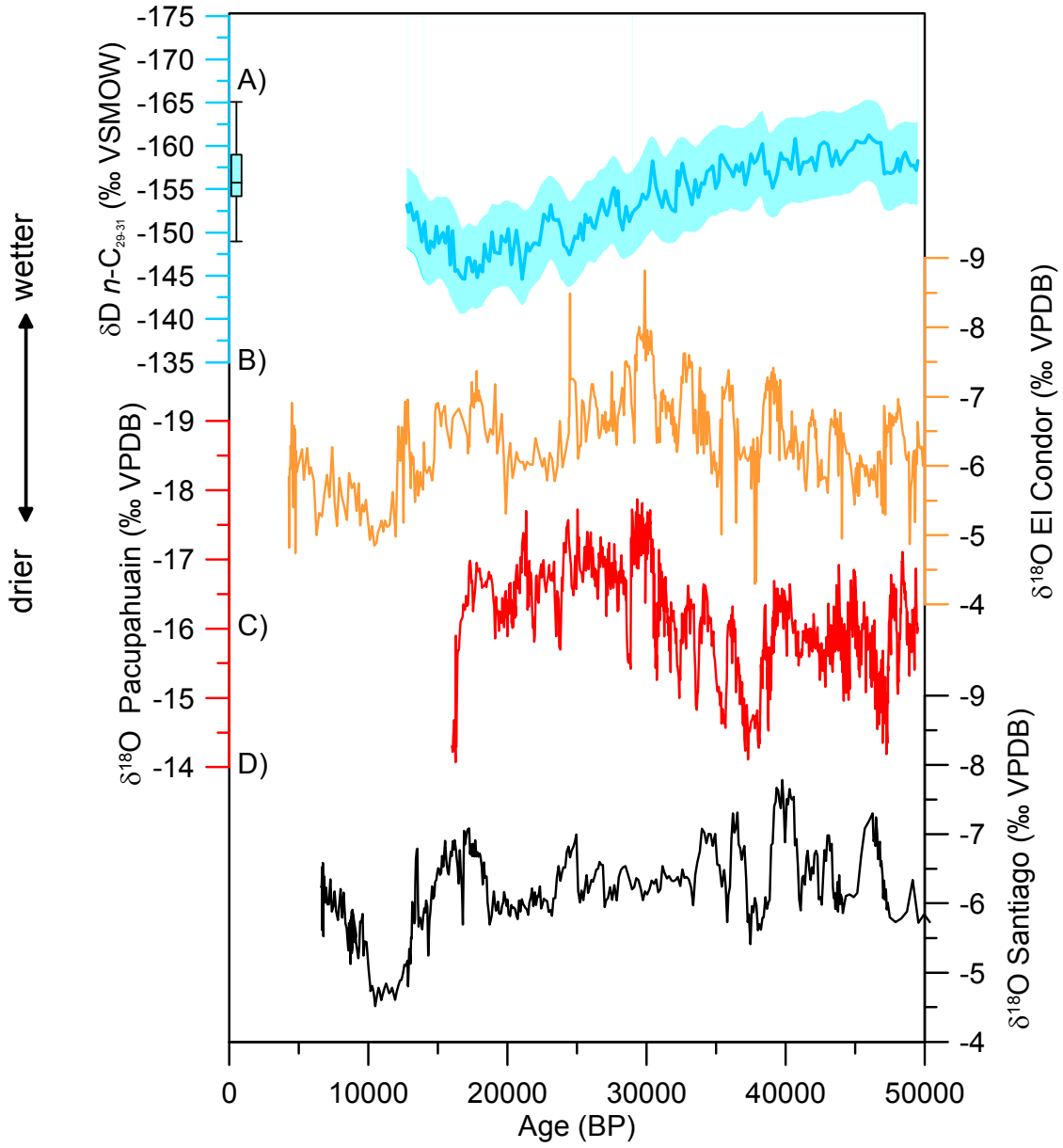

Fig. S7. Comparison of the δD $nC_{29\text{-}31}$ record from GeoB16224-1 to speleothem records from the western Amazon Basin. The y-axes of the plots are scaled for the meteoric water line with the relationship δD = 8* $\delta^{18}O$ (Craig, 1961). A) δD $nC_{29\text{-}31}$ from GeoB16224-1. B) $\delta^{18}O$ data from El Condor cave (Cheng et al., 2013). C) $\delta^{18}O$ data from Pacupahuain cave (Kanner et al., 2012). D) $\delta^{18}O$ data from Santiago cave (Mosblech et al., 2012).

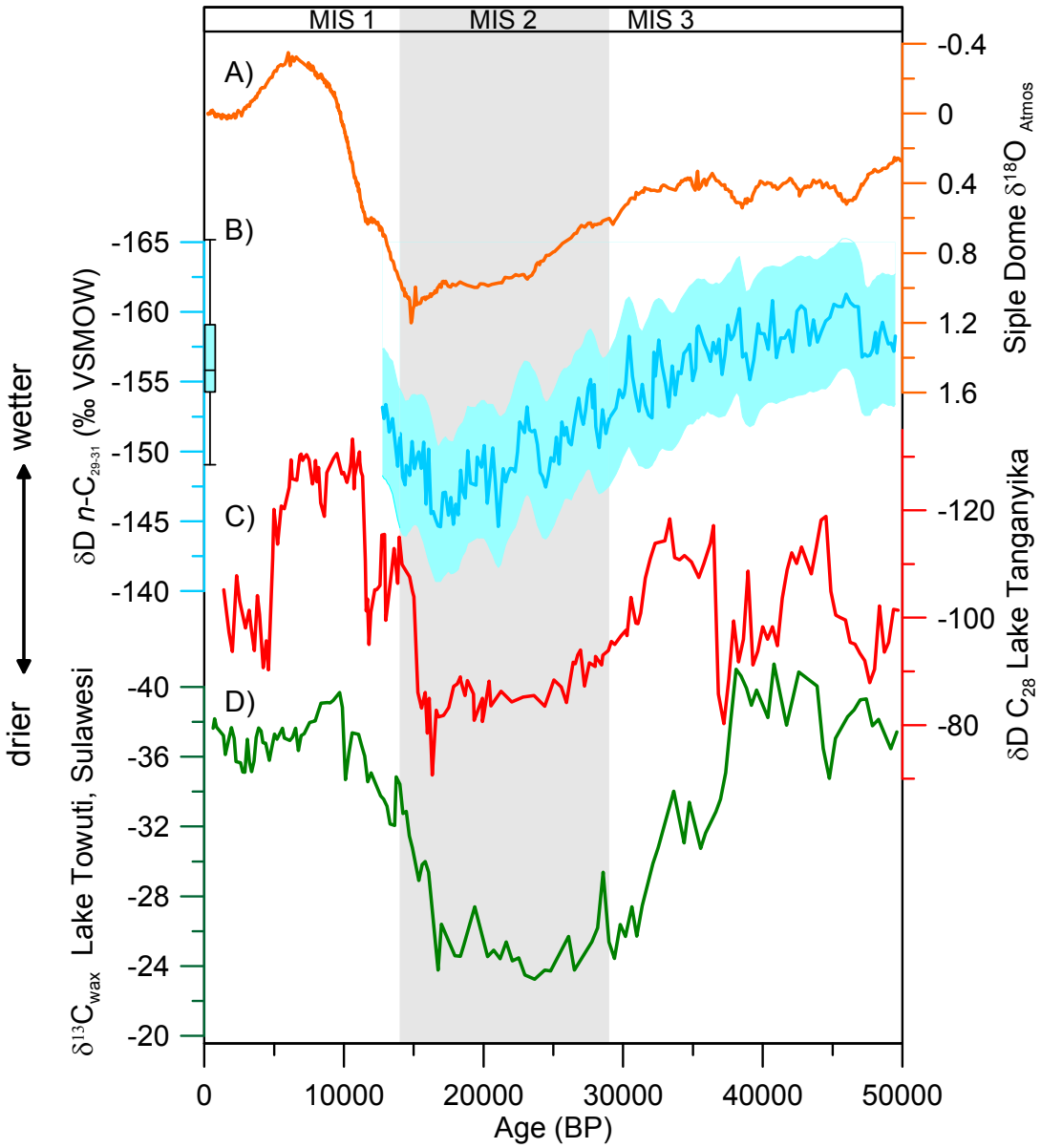

Fig. S8. Comparison to records from other tropical convection centers. A) Atmospheric $\delta^{18}O$ from the Siple Dome (Severinghaus et al., 2009), reflecting the strength of the Dole effect (i.e. primary productivity in monsoonal regions and the tropics). B) δD of nC_{29} and nC_{31} *n*-alkanes from lowland Amazonia (this study). C) δD of the C_{28} *n*-carboxylic acid from Lake Tanganyika (Tierney et al., 2008). D) $\delta^{13}C$ of the $C_{26,}$ $C_{28,}$ and C_{30} *n*-carboxylic acids from Lake Towuti, Sulawesi, indicating large-scale savanna expansion during the LGM (Russell et al., 2014).

6. Synthesis and Outlook

The primary goals of this thesis were

i) to test δD of alkenones and palmitic acid as proxies for ocean salinity to reconstruct past changes in the Amazon Plume
ii) to test δD and $\delta^{13}C$ of long-chain *n*-alkanes as proxies to reconstruct past Amazonian climate and vegetation variability
iii) to apply these proxies to reconstruct the Amazonian climate and vegetation of the late Pleistocene

In the following, the outcomes of the calibration studies concerning goals i) and ii) and the reconstruction of the Amazonian paleoclimate concerning goal iii) are addressed separately.

6.1. Proxy calibration

The two proxy calibration studies presented in this thesis evaluate the use of the isotope composition of lipid biomarker as paleoenvironmental proxies. These studies demonstrate the applicability of some of these proxies. There are, however, several shortfalls that either inhibit the use in certain situations or require further investigation.

In case of the application of the δD composition of biomarkers as salinity proxies, we found that δD of alkenones did not record sea surface salinity in the Amazon Plume. The main complication for the application of this proxy likely arises from the sensitivity of alkenone-producing haptophytes to sediment-rich Amazonian freshwater. This problem was circumvented by successfully applying the δD of the ubiquitous molecule palmitic acid as proxy. However, this marker has the disadvantage of easier degradation and of being potentially produced deeper in the water column. Hence, its application is limited to regions with high sedimentation rates that guarantee fast sealing and thereby protection from potential degradation. In consequence, a new marker that is neither sensitive to changes in riverine input nor susceptible to degradation could prove pivotal in future paleo salinity studies. The establishment of further δD-based biomarker proxies is highly desirable since they have the potential to significantly improve present day reconstructions in combination with the classical $\delta^{18}O$ approach (Rohling, 2007).

The $\delta^{13}C$ and δD composition of plant-wax *n*-alkanes have shown to be a useful tool for the reconstruction of the isotopic composition of precipitation and the dominant vegetation

type in lowland Amazonia. The data presented in this thesis confirmed that long-chain *n*-alkanes are extremely resistant towards degradation during transport in the Amazon River. Especially in tropical environments, this is a rare advantage. Other soil derived molecular proxies like branched glycerol dialkyl glycerol tetraethers (brGDGTs) are overprinted by riverine *in situ* production during transport (Zell et al., 2013) and plant-wax biomarkers, like long-chain fatty acids, are also less resistant towards degradation (Cranwell, 1981). A potential problem in the use of long-chain *n*-alkanes as a paleoenvironmental proxy is the presence of petrogenic *n*-alkanes that could influence the signal of pristine plant derived compounds. The influence of petrogenic material can be detected by analyzing the relative contribution of the different homologues and can hence be controlled. The largest uncertainty in the application of long-chain *n*-alkanes in the Amazon Basin remains the precise geographic source of these compounds. While this thesis was able to qualitatively assign the source areas to be distributed in lowland Basin with a potential bias towards floodplains, a more quantitative approach could further constrain the source region of the paleoclimate signal recorded in offshore sediment cores. To this end, detailed measurements of biomarker fluxes in the Amazon and its tributaries would be needed. Given that there are large regional and seasonal variations in organic matter transport, a precise understanding of seasonal fluctuation would also be necessary to fully understand the sourcing of plant-waxes in the Amazon Basin.

6.2. Reconstruction of Amazonian paleoclimate

The paleoenvironmental reconstructions showed that the climate and vegetation conditions in lowland Amazonia were relatively stable during the late Pleistocene. During MIS2, moderate drying took place, but was insufficient to lead to forest retreat and savanna expansion. The reconstructions also showed that local variations in precipitation intensity during millennial climate shifts were likely leveled out on a basin-wide scale, even though they led to strong regional variations. Most prominently the southward shift of the tropical convection center during Heinrich Stadials led to savanna expansion in the north of the basin. Together with the observation that Heinrich Stadials were an important controlling factor of climate and vegetation conditions in northeastern Brazil, this finding suggest that climate shifts during Heinrich Stadials were likely one of the dominant factors in controlling the extent of different biomes in tropical South America (Hessler et al., 2010). This raises also the question how these shifts in vegetation patterns influenced the species distribution in tropical South America by opening and closing migration routes between different biomes. To fully constrain the precise location and extent of such migration routes, local

high resolution vegetation records from lakes from the lowland Amazon Basin would be needed.

Since the paleoclimate record presented in this thesis only covers a limited time window (i.e. 12-50 ka BP), further investigations are needed to fully comprehend the climate variations in Amazonia on a basin-wide scale. One aspect is for instance the climate and vegetation variability during the Holocene, where previous studies have inferred a strong influence of El Niño Southern Oscillation (Bush et al., 2007; Moy et al., 2002). Another highly debated aspect of the Holocene climate and vegetation history is the question to what degree it was influenced by human presence in the Amazon Basin (e.g. Bush et al., 2007; Carson et al., 2014). The picture of a pristine pre-Columbian Amazon rainforest has been increasingly challenged by the hypothesis of widespread cultivation (e.g. Clement and Junqueira, 2010; Heckenberger et al., 2003).

To understand the forcing mechanisms of Pleistocene climate in Amazonia, sediment records should be extended further back in time. To comprehend the influence of glacial cycles on the Amazonian hydroclimate, the reconstruction of climate over at least one full glacial cycle is paramount. To understand the origin of the Amazon rainforest and the biodiversity in western Amazonia, the evolution of the Amazon needs to be studied even further back through the Cenozoic. For the establishment of a complete history of the Amazon Basin and the current tributary system, a full understanding of the still contested timing of the Andean uplift is also needed.

One of the key complications to reconstruct a continuous history of the Amazon Basin from its beginning to the current times is the detection of suitable archives. As noted in this thesis, sea-level changes on glacial-interglacial timescales led to shifts in the depositional areas, which makes the detection of continuous archives of Amazonian sedimentation challenging. This is further complicated by the constant remobilization of sediments on the present day shelf and on the Amazon delta during the Pleistocene. A promising approach to study the history of Amazon further back in time is the current “Trans-Amazon Drilling Project” that aims to retrieve long sediment cores from the shelf margin (Baker et al., 2015). Furthermore, the project also aims to obtain continental sediment cores from the interior lowland Amazon Basin on a transect from the Andes to the Atlantic Ocean. These cores are expected to yield an almost continuous record of Cenozoic sedimentation in the Amazon Basin.

With regard to future climate and vegetation variability in the lowland Amazon Basin, our reconstructions show that the Amazon climate and forest are remarkably persistent during of large global climate shifts. The finding that savannah expansion was most pronounced during shifts in the meridional position of the tropical rain belt indicates that the most vulnerable parts of the Amazon forest are situated on the southern and northern edge of

the forest. In the wake of current climate warming, the northern hemisphere is expected to experience stronger warming than the southern hemisphere due to its larger landmass (Friedman et al., 2013). This is expected to lead to a northward shift of the thermal equator and thereby a northward shift of the tropical rain belt (e.g. Schneider et al., 2014). This interpretation is supported by current shifts in the Amazon hydrology. Recent studies found that precipitation decreased in the south western parts of the basin (Fu et al., 2013), while it increased in the northern parts (Gloor et al., 2013). Moreover, models regarding the resilience of the forest vegetation to drier conditions indicate that the vulnerability of the in the southwestern parts of the basin to savanna expansion is highest (Hirota et al., 2011). The finding that lower temperatures during the late Pleistocene led to a decrease precipitable water in the Amazon Basin and drier LGM conditions implicates that higher temperatures could lead to increased moisture and precipitation in lowland Amazonia. This view was advanced in a recent paper by Gloor et al. (2015) who conjectured that the recent discharge history of the Amazon River was related to an increase in tropical sea surface temperature. Nevertheless, it remains contested how precipitation in the Amazon Basin is going to change and if there is going to be an increase in climate variability with more droughts and flood events (Duffy et al., 2015). Predictions on the future development of the forest structure also depend on the different scenarios regarding precipitation variability. While continuously humid conditions would favor intact rainforest vegetation (Gloor et al., 2015), increases in climate variability could lead to transitions to drier forest types (Levine et al., 2016). This has also major implications for the carbon cycle. A resilient Amazon rainforest under continuously humid conditions would continue to act as a carbon sink (Huntingford et al., 2013). Conversely, large scale drying and an increase in droughts could turn lead to a carbon release (Cox et al., 2013).

Even though the forest vegetation in the lowland Amazon Basin is probably robust towards future climate variability, deforestation may play a major role in defining the future forest extent in lowland Amazonia. A reduction in forest area due to deforestation may in turn influence the local climate (Davidson et al., 2012). Since deforestation has so far mainly affected the south of the basin, drier conditions induced by changes in land cover could enhance drying due to a northward shift of the tropical rain belt (Malhi et al., 2008). How deforestation in lowland Amazonia and the resulting impact on local precipitation regimes are relevant for global hydrologic changes remains also debated (e.g. Lorenz et al., 2016; Werth and Avissar, 2002).

In conclusion, the late Pleistocene Amazonian climate and vegetation records showed that the integrated approach chosen in this thesis is suitable to study the climate and vegetation signal of a riverine catchment. In contrast to previous studies based on local records, this approach was for instance able to detect signals that were either not observed due to low temporal resolution (e.g. Heinrich Stadials) or contested due to doubts about the

representability of the records (e.g. glacial drying). In combination with the proxy calibration conducted in this thesis, the paleoclimate and vegetation records lay the groundwork for future studies that are going to extend the climate records of Amazonia further back in time.

7. References

Absy M. L. (1991) Mise en evidence de quatre phases d'ouverture de la foret dense dans le sud-est de l'Amazonie au cours des 60 000 dernieres annees. *Comptes Rendus - Academie des Sciences, Serie II* **312**, 673-678.

Absy M. L.and Van Der Hammen T. (1976) Some paleoecological data from Rondonia, southern part of the Amazon Basin. *Acta Amazon.* **6**, 293-299.

Agassiz L., 1840, Études sur les Glaciers, Neuchâtel, Switzerland, Jent & Gassman.

Archer A. W. (2005) Review of Amazonian Depositional Systems. In *Fluvial Sedimentology VII.* (Eds. M. D. Blum, S. B. Marriott,S. Leclair). Blackwell Publishing Ltd. pp. 17-39.

Auler A. S., Wang X. F., Edwards R. L., Cheng H., Cristalli P. S., Smart P. L.and Richards D. A. (2004) Quaternary ecological and geomorphic changes associated with rainfall events in presently semi-arid northeastern Brazil. *Journal of Quaternary Science* **19**, 693-701.

Baker P. A.and Fritz S. C. (2015) Nature and causes of Quaternary climate variation of tropical South America. *Quat. Sci. Rev.* **124**, 31-47.

Baker P. A., Fritz S. C., Silva C. G., Rigsby C. A., Absy M. L., Almeida R. P., Caputo M., Chiessi C. M., Cruz F. W., Dick C. W., Feakins S. J., Figueiredo J., Freeman K. H., Hoorn C., Jaramillo C., Kern A. K., Latrubesse E. M., Ledru M. P., Marzoli A., Myrbo A., Noren A., Piller W. E., Ramos M. I. F., Ribas C. C., Trnadade R., West A. J., Wahnfried I.and Willard D. A. (2015) Trans-Amazon Drilling Project (TADP): origins and evolution of the forests, climate, and hydrology of the South American tropics. *Sci. Dril.* **20**, 41-49.

Bard E., Rostek F.and Sonzogni C. (1997) Interhemispheric synchrony of the last deglaciation inferred from alkenone palaeothermometry. *Nature* **385**, 707-710.

Batalha-Filho H., Fjeldså J., Fabre P.-H.and Miyaki C. Y. (2013) Connections between the Atlantic and the Amazonian forest avifaunas represent distinct historical events. *Journal of Ornithology* **154**, 41-50.

Beardsley R. C., Candela J., Limeburner R., Geyer W. R., Lentz S. J., Castro B. M., Cacchione D.and Carneiro N. (1995) The M2 tide on the Amazon Shelf. *Journal of Geophysical Research: Oceans* **100**, 2283-2319.

Behling H., Bush M.and Hooghiemstra H. (2009) Biotic Development of Quaternary Amazonia: A Palynological Perspective. In *Amazonia: Landscape and Species Evolution.* Wiley-Blackwell Publishing Ltd. pp. 335-345.

Benthien A.and Müller P. J. (2000) Anomalously low alkenone temperatures caused by lateral particle and sediment transport in the Malvinas Current region, western Argentine Basin. *Deep-Sea Res. Part I-Oceanogr. Res. Pap.* **47**, 2369-2393.

Berger A.and Loutre M. F. (1991) Insolation values for the climate of the last 10000000 years. *Quat. Sci. Rev.* **10**, 297-317.

Berrio J. C., Hooghiemstra H., Behling H.and van der Borg K. (2000) Late Holocene history of savanna gallery forest from Carimagua area, Colombia. *Review of Palaeobotany and Palynology* **111**, 295-308.

Bintanja R., van de Wal R. S. W.and Oerlemans J. (2005) Modelled atmospheric temperatures and global sea levels over the past million years. *Nature* **437**, 125-128.

Bird M. I., Summons R. E., Gagan M. K., Roksandic Z., Dowling L., Head J., Keith Fifield L., Cresswell R. G.and Johnson D. P. (1995) Terrestrial vegetation change inferred from n-alkane σ13C analysis in the marine environment. *Geochim. Cosmochim. Acta* **59**, 2853-2857.

Birkett C. M., Mertes L. A. K., Dunne T., Costa M. H.and Jasinski M. J. (2002) Surface water dynamics in the Amazon Basin: Application of satellite radar altimetry. *Journal of Geophysical Research: Atmospheres* **107**, 8059–8080.

Birks H. J. B., Felde V. A., Bjune A. E., Grytnes J.-A., Seppä H.and Giesecke T. (2016) Does pollen-assemblage richness reflect floristic richness? A review of recent developments and future challenges. *Review of Palaeobotany and Palynology* **228**, 1-25.

Blaauw M.and Christen J. A. (2011) Flexible Paleoclimate Age-Depth Models Using an Autoregressive Gamma Process. *Bayesian Analysis* **6**, 457-474.

Bond G., Broecker W., Johnsen S., McManus J., Labeyrie L., Jouzel J.and Bonani G. (1993) Correlations between climate records from North Atlantic sediments and Greenland ice. *Nature* **365**, 143-147.

Bookhagen B.and Strecker M. R. (2009) Modern Andean Rainfall Variation during ENSO Cycles and its Impact on the Amazon Drainage Basin. In *Amazonia: Landscape and Species Evolution.* Wiley-Blackwell Publishing Ltd. pp. 223-241.

Boot C. S., Ettwein V. J., Maslin M. A., Weyhenmeyer C. E.and Pancost R. D. (2006) A 35,000 year record of terrigenous and marine lipids in Amazon Fan sediments. *Org. Geochem.* **37**, 208-219.

Bouchez J., Gaillardet J., France-Lanord C., Maurice L.and Dutra-Maia P. (2011) Grain size control of river suspended sediment geochemistry: Clues from Amazon River depth profiles. *Geochem. Geophys. Geosyst.* **12**, 24.

Bouchez J., Galy V., Hilton R. G., Gaillardet J., Moreira-Turcq P., Perez M. A., France-Lanord C.and Maurice L. (2014) Source, transport and fluxes of Amazon River particulate organic carbon: Insights from river sediment depth-profiles. *Geochim. Cosmochim. Acta* **133**, 280-298.

Bowen G. J.and Revenaugh J. (2003) Interpolating the isotopic composition of modern meteoric precipitation. *Water Resour. Res.* **39**, 1299–1312.

Braconnot P., Otto-Bliesner B., Harrison S., Joussaume S., Peterchmitt J. Y., Abe-Ouchi A., Crucifix M., Driesschaert E., Fichefet T., Hewitt C. D., Kageyama M., Kitoh A., Laîné A., Loutre M. F., Marti O., Merkel U., Ramstein G., Valdes P., Weber S. L., Yu Y.and Zhao Y. (2007) Results of PMIP2 coupled simulations of the Mid-Holocene and Last Glacial Maximum - Part 1: experiments and large-scale features. *Clim. Past* **3**, 261-277.

Brienen R. J. W., Helle G., Pons T. L., Guyot J. L.and Gloor M. (2012) Oxygen isotopes in tree rings are a good proxy for Amazon precipitation and El Nino-Southern Oscillation variability. *Proc. Natl. Acad. Sci. U. S. A.* **109**, 16957-16962.

Brienen R. J. W., Phillips O. L., Feldpausch T. R., Gloor E., Baker T. R., Lloyd J., Lopez-Gonzalez G., Monteagudo-Mendoza A., Malhi Y., Lewis S. L., Vasquez Martinez R., Alexiades M., Alvarez Davila E., Alvarez-Loayza P., Andrade A., Aragao L. E. O. C., Araujo-Murakami A., Arets E. J. M. M., Arroyo L., Aymard C G. A., Banki O. S., Baraloto C., Barroso J., Bonal D., Boot R. G. A., Camargo J. L. C., Castilho C. V., Chama V., Chao K. J., Chave J., Comiskey J. A., Cornejo Valverde F., da Costa L., de Oliveira E. A., Di Fiore A., Erwin T. L., Fauset S., Forsthofer M., Galbraith D. R., Grahame E. S., Groot N., Herault B., Higuchi N., Honorio Coronado E. N., Keeling H., Killeen T. J., Laurance W. F., Laurance S., Licona J., Magnussen W. E., Marimon B. S., Marimon-Junior B. H., Mendoza C., Neill D. A., Nogueira E. M., Nunez P., Pallqui Camacho N. C., Parada A., Pardo-Molina G., Peacock J., Pena-Claros M., Pickavance G. C., Pitman N. C. A., Poorter L., Prieto A., Quesada C. A., Ramirez F., Ramirez-Angulo H., Restrepo Z., Roopsind A., Rudas A., Salomao R. P., Schwarz M., Silva N., Silva-Espejo J. E., Silveira M., Stropp J., Talbot J., ter Steege H., Teran-Aguilar J., Terborgh J., Thomas-Caesar R., Toledo M., Torello-Raventos M., Umetsu R. K., van der Heijden G. M. F., van der Hout P., Guimaraes Vieira I. C., Vieira S. A., Vilanova E., Vos V. A.and Zagt R. J. (2015) Long-term decline of the Amazon carbon sink. *Nature* **519**, 344-348.

Bush M. B., De Oliveira P. E., Colinvaux P. A., Miller M. C.and Moreno J. E. (2004a) Amazonian paleoecological histories: one hill, three watersheds. *Palaeogeography, Palaeoclimatology, Palaeoecology* **214**, 359-393.

Bush M. B., Silman M. R., de Toledo M. B., Listopad C., Gosling W. D., Williams C., de Oliveira P. E.and Krisel C. (2007) Holocene fire and occupation in Amazonia: records from two lake districts. *Philos. Trans. R. Soc. B-Biol. Sci.* **362**, 209-218.

Bush M. B., Silman M. R.and Urrego D. H. (2004b) 48,000 Years of Climate and Forest Change in a Biodiversity Hot Spot. *Science* **303**, 827-829.

Bush R. T.and McInerney F. A. (2015) Influence of temperature and C4 abundance on n-alkane chain length distributions across the central USA. *Org. Geochem.* **79**, 65-73.

Campbell Jr K. E., Frailey C. D.and Romero-Pittman L. (2006) The Pan-Amazonian Ucayali Peneplain, late Neogene sedimentation in Amazonia, and the birth of the modern Amazon River system. *Palaeogeography, Palaeoclimatology, Palaeoecology* **239**, 166-219.

Carson J. F., Whitney B. S., Mayle F. E., Iriarte J., Prümers H., Soto J. D.and Watling J. (2014) Environmental impact of geometric earthwork construction in pre-Columbian Amazonia. *Proceedings of the National Academy of Sciences* **111**, 10497-10502.

Carvalho L. M. V., Jones C.and Liebmann B. (2004) The South Atlantic convergence zone: Intensity, form, persistence, and relationships with intraseasonal to interannual activity and extreme rainfall. *J. Clim.* **17**, 88-108.

Castañeda I. S.and Schouten S. (2011) A review of molecular organic proxies for examining modern and ancient lacustrine environments. *Quat. Sci. Rev.* **30**, 2851-2891.

Chadwick R., Good P.and Willett K. (2016) A Simple Moisture Advection Model of Specific Humidity Change over Land in Response to SST Warming. *J. Clim.* **29**, 7613-7632.

Cheng H., Edwards R. L., Sinha A., Spötl C., Yi L., Chen S., Kelly M., Kathayat G., Wang X., Li X., Kong X., Wang Y., Ning Y.and Zhang H. (2016) The Asian monsoon over the past 640,000 years and ice age terminations. *Nature* **534**, 640-646.

Cheng H., Sinha A., Cruz F. W., Wang X. F., Edwards R. L. A., d'Horta F. M., Ribas C. C., Vuille M., Stott L. D.and Auler A. S. (2013) Climate change patterns in Amazonia and biodiversity. *Nat. Commun.* **4**, 1411.

Chivall D., M'Boule D., Heinzelmann S. M., Kasper S., Sinke-Schoen D., Sinninghe-Damsté J. S., Schouten S.and van der Meer M. T. J. (2014a) Towards a palaeosalinity proxy: hydrogen isotopic fractionation between source water and lipids produced via different biosynthetic pathways in haptophyte algae. *Geophysical Research Abstracts* **16**, 12066.

Chivall D., M'Boule D., Sinke-Schoen D., Sinninghe Damsté J. S., Schouten S.and van der Meer M. T. J. (2014b) The effects of growth phase and salinity on the hydrogen isotopic composition of alkenones produced by coastal haptophyte algae. *Geochim. Cosmochim. Acta* **140**, 381-390.

Chong L. S., Berelson W. M., McManus J., Hammond D. E., Rollins N. E.and Yager P. L. (2014) Carbon and biogenic silica export influenced by the Amazon River Plume: Patterns of remineralization in deep-sea sediments. *Deep-Sea Res. Part I-Oceanogr. Res. Pap.* **85**, 124-137.

Chu G. Q., Sun Q., Li S. Q., Zheng M. P., Jia X. X., Lu C. F., Liu J. Q.and Liu T. S. (2005) Long-chain alkenone distributions and temperature dependence in lacustrine surface sediments from China. *Geochim. Cosmochim. Acta* **69**, 4985-5003.

Clark K. E., Malhi Y., New M., Hilton R. G., West A. J., Grocke D. R., Bryant C. L., Ascough P. L.and Caceres A. R. (2013) New views on "old" carbon in the Amazon River: Insight from the source of organic carbon eroded from the Peruvian Andes. *Geochem. Geophys. Geosyst.* **14**, 1644-1659.

Clement C. R.and Junqueira A. B. (2010) Between a Pristine Myth and an Impoverished Future. *Biotropica* **42**, 534-536.

Cohen K. M., Finney S. C., Gibbard P. L.and Fan J. X. (2013) The ICS International Chronostratigraphic Chart. *Episodes* **36**, 199-204.

Colinvaux P. A., DeOliveira P. E., Moreno J. E., Miller M. C.and Bush M. B. (1996) A long pollen record from lowland Amazonia: Forest and cooling in glacial times. *Science* **274**, 85-88.

Collister J. W., Rieley G., Stern B., Eglinton G.and Fry B. (1994) Compound-specific δ 13C analyses of leaf lipids from plants with differing carbon dioxide metabolisms. *Org. Geochem.* **21**, 619-627.

Conte M. H., Thompson A., Lesley D.and Harris R. P. (1998) Genetic and physiological influences on the alkenone/alkenoate versus growth temperature relationship in Emiliania huxleyi and Gephyrocapsa oceanica. *Geochim. Cosmochim. Acta* **62**, 51-68.

Conte M. H.and Weber J. C. (2002) Long-range atmospheric transport of terrestrial biomarkers to the western North Atlantic. *Glob. Biogeochem. Cycle* **16**, 1142.

Cox P. M., Pearson D., Booth B. B., Friedlingstein P., Huntingford C., Jones C. D.and Luke C. M. (2013) Sensitivity of tropical carbon to climate change constrained by carbon dioxide variability. *Nature* **494**, 341-344.

Craig H. (1961) Isotopic Variations in Meteoric Waters. *Science* **133**, 1702-1703.

Cranwell P. A. (1981) Diagenesis of free and bound lipids in terrestrial detritus deposited in a lacustrine sediment. *Org. Geochem.* **3**, 79-89.

Cranwell P. A., Eglinton G.and Robinson N. (1987) Lipids of aquatic organisms as potential contributors to lacustrine sediments—II. *Org. Geochem.* **11**, 513-527.

Cruz F. W., Burns S. J., Karmann I., Sharp W. D., Vuille M., Cardoso A. O., Ferrari J. A., Dias P. L. S.and Viana O. (2005) Insolation-driven changes in atmospheric circulation over the past 116,000 years in subtropical Brazil. *Nature* **434**, 63-66.

D'Apolito C., Absy M. L.and Latrubesse E. M. (2013) The Hill of Six Lakes revisited: new data and re-evaluation of a key Pleistocene Amazon site. *Quat. Sci. Rev.* **76**, 140-155.

Da Silva J. M. C.and Bates J. M. (2002) Biogeographic patterns and conservation in the South American Cerrado: A tropical Savanna hotspot. *Bioscience* **52**, 225-233.

Da Silva J. M. C., Rylands A. B.and Da Fonseca G. A. B. (2005) The Fate of the Amazonian Areas of Endemism. *Conservation Biology* **19**, 689-694.

Dai A.and Trenberth K. E. (2002) Estimates of freshwater discharge from continents: Latitudinal and seasonal variations. *J. Hydrometeorol.* **3**, 660-687.

Damuth J. E.and Flood R. D. (1983) Morphology, sedimentation processes, and growth pattern of the Amazon Deep-Sea Fan. *Geo-Mar. Lett.* **3**, 109-117.

Dansgaard W. (1964) Stable isotopes in precipitation. *Tellus* **16**, 436-468.

Dansgaard W., Johnsen S. J., Clausen H. B., Dahl-Jensen D., Gundestrup N. S., Hammer C. U., Hvidberg C. S., Steffensen J. P., Sveinbjornsdottir A. E., Jouzel J.and Bond G. (1993) Evidence for general instability of past climate from a 250-kyr ice-core record. *Nature* **364**, 218-220.

Davidson E. A., de Araujo A. C., Artaxo P., Balch J. K., Brown I. F., Bustamante M. M. C., Coe M. T., DeFries R. S., Keller M., Longo M., Munger J. W., Schroeder W., Soares B. S., Souza C. M.and Wofsy S. C. (2012) The Amazon basin in transition *Nature* **483**, 232-232.

de Morais J. O., Tintelnot M., Irion G.and Pinheiro L. S. (2006) Pathways of clay mineral transport in the coastal zone of the Brazilian continental shelf from Ceara to the mouth of the Amazon River. *Geo-Mar. Lett.* **26**, 16-22.

Deplazes G., Luckge A., Peterson L. C., Timmermann A., Hamann Y., Hughen K. A., Rohl U., Laj C., Cane M. A., Sigman D. M.and Haug G. H. (2013) Links between tropical rainfall and North Atlantic climate during the last glacial period. *Nat. Geosci.* **6**, 213-217.

Duffy P. B., Brando P., Asner G. P.and Field C. B. (2015) Projections of future meteorological drought and wet periods in the Amazon. *Proceedings of the National Academy of Sciences* **112**, 13172-13177.

Dunne T., Mertes L. A. K., Meade R. H., Richey J. E.and Forsberg B. R. (1998) Exchanges of sediment between the flood plain and channel of the Amazon River in Brazil. *Geol. Soc. Am. Bull.* **110**, 450-467.

Eggleston S., Schmitt J., Bereiter B., Schneider R.and Fischer H. (2016) Evolution of the stable carbon isotope composition of atmospheric CO2 over the last glacial cycle. *Paleoceanography* **31**, 434-452.

Eglinton G.and Hamilton R. J. (1963) The Distribution of Alkanes. In *Chemical Plant Taxonomy.* (Ed. T. Swain). Academic Press pp. 187-217.

- (1967) Leaf epicuticular waxes. *Science* **156**, 1322-1335.

Eglinton T. I.and Eglinton G. (2008) Molecular proxies for paleoclimatology. *Earth Planet. Sci. Lett.* **275**, 1-16.

Englebrecht A. C.and Sachs J. P. (2005) Determination of sediment provenance at drift sites using hydrogen isotopes and unsaturation ratios in alkenones. *Geochim. Cosmochim. Acta* **69**, 4253-4265.

Epstein B. L., D'Hondt S., Quinn J. G., Zhang J. P.and Hargraves P. E. (1998) An effect of dissolved nutrient concentrations on alkenone-based temperature estimates. *Paleoceanography* **13**, 122-126.

Epstein S.and Mayeda T. (1953) Variation of O18 content of waters from natural sources. *Geochim. Cosmochim. Acta* **4**, 213-224.

Fairchild I. J., Smith C. L., Baker A., Fuller L., Spotl C., Mattey D., McDermott F.and Eimp (2006) Modification and preservation of environmental signals in speleothems. *Earth-Sci. Rev.* **75**, 105-153.

Farquhar G. D., Cernusak L. A.and Barnes B. (2007) Heavy water fractionation during transpiration. *Plant Physiol.* **143**, 11-18.

Feakins S. J., Bentley L. P., Salinas N., Shenkin A., Blonder B., Goldsmith G. R., Ponton C., Arvin L. J., Wu M. S., Peters T., West A. J., Martin R. E., Enquist B. J., Asner G. P.and Malhi Y. (2016) Plant leaf wax biomarkers capture gradients in hydrogen isotopes of precipitation from the Andes and Amazon. *Geochim. Cosmochim. Acta* **182**, 155-172.

Feakins S. J.and Sessions A. L. (2010) Controls on the D/H ratios of plant leaf waxes in an arid ecosystem. *Geochim. Cosmochim. Acta* **74**, 2128-2141.

Ficken K. J., Li B., Swain D. L.and Eglinton G. (2000) An n-alkane proxy for the sedimentary input of submerged/floating freshwater aquatic macrophytes. *Org. Geochem.* **31**, 745-749.

Fornace K. L., Hughen K. A., Shanahan T. M., Fritz S. C., Baker P. A.and Sylva S. P. (2014) A 60,000-year record of hydrologic variability in the Central Andes from the hydrogen isotopic composition of leaf waxes in Lake Titicaca sediments. *Earth Planet. Sci. Lett.* **408**, 263-271.

Friedman A. R., Hwang Y.-T., Chiang J. C. H.and Frierson D. M. W. (2013) Interhemispheric Temperature Asymmetry over the Twentieth Century and in Future Projections. *J. Clim.* **26**, 5419-5433.

Fu R., Yin L., Li W., Arias P. A., Dickinson R. E., Huang L., Chakraborty S., Fernandes K., Liebmann B., Fisher R.and Myneni R. B. (2013) Increased dry-season length over southern Amazonia in recent decades and its implication for future climate projection. *Proceedings of the National Academy of Sciences* **110**, 18110-18115.

Galy V., Eglinton T., France-Lanord C.and Sylya S. (2011) The provenance of vegetation and environmental signatures encoded in vascular plant biomarkers carried by the Ganges-Brahmaputra rivers. *Earth Planet. Sci. Lett.* **304**, 1-12.

Garcin Y., Schwab V. F., Gleixner G., Kahmen A., Todou G., Sene O., Onana J. M., Achoundong G.and Sachse D. (2012) Hydrogen isotope ratios of lacustrine sedimentary n-alkanes as proxies of tropical African hydrology: Insights from a calibration transect across Cameroon. *Geochim. Cosmochim. Acta* **79**, 106-126.

Garreaud R. D., Vuille M., Compagnucci R.and Marengo J. (2009) Present-day South American climate. *Paleogeogr. Paleoclimatol. Paleoecol.* **281**, 180-195.

Gat J. R. (1996) Oxygen and hydrogen isotopes in the hydrologic cycle. *Annual Review of Earth and Planetary Sciences* **24**, 225-262.

Geyer W. R., Beardsley R. C., Lentz S. J., Candela J., Limeburner R., Johns W. E., Castro B. M.and Soares I. D. (1996) Physical oceanography of the Amazon shelf. *Cont. Shelf Res.* **16**, 575-616.

Gibbs R. J. (1967) Amazon River: Environmental Factors That Control Its Dissolved and Suspended Load. *Science* **156**, 1734-1737.

Giosan L., Coolen M. J. L., Kaplan J. O., Constantinescu S., Filip F., Filipova-Marinova M., Kettner A. J.and Thom N. (2012) Early Anthropogenic Transformation of the Danube-Black Sea System. *Sci. Rep.* **2**.

Gloor M., Barichivich J., Ziv G., Brienen R., Schöngart J., Peylin P., Ladvocat Cintra B. B., Feldpausch T., Phillips O.and Baker J. (2015) Recent Amazon climate as background for possible ongoing and future changes of Amazon humid forests. *Glob. Biogeochem. Cycle* **29**, 2014GB005080.

Gloor M., Brienen R. J. W., Galbraith D., Feldpausch T. R., Schöngart J., Guyot J. L., Espinoza J. C., Lloyd J.and Phillips O. L. (2013) Intensification of the Amazon hydrological cycle over the last two decades. *Geophys. Res. Lett.* **40**, 1729-1733.

Gonfiantini R., Roche M.-A., Olivry J.-C., Fontes J.-C.and Zuppi G. M. (2001) The altitude effect on the isotopic composition of tropical rains. *Chemical Geology* **181**, 147-167.

Gordon E. S.and Goni M. A. (2004) Controls on the distribution and accumulation of terrigenous organic matter in sediments from the Mississippi and Atchafalaya river margin. *Marine Chemistry* **92**, 331-352.

Gosse J. C.and Phillips F. M. (2001) Terrestrial in situ cosmogenic nuclides: theory and application. *Quat. Sci. Rev.* **20**, 1475-1560.

Govin A., Chiessi C. M., Zabel M., Sawakuchi A. O., Heslop D., Horner T., Zhang Y.and Mulitza S. (2014) Terrigenous input off northern South America driven by changes in Amazonian climate and the North Brazil Current retroflection during the last 250 ka. *Clim. Past.* **10**, 843-862.

Govin A., Holzwarth U., Heslop D., Keeling L. F., Zabel M., Mulitza S., Collins J. A.and Chiessi C. M. (2012) Distribution of major elements in Atlantic surface sediments (36 degrees N-49 degrees S): Imprint of terrigenous input and continental weathering. *Geochem. Geophys. Geosyst.* **13**, 23.

Haberle S. G.and Maslin M. A. (1999) Late Quaternary vegetation and climate change in the Amazon basin based on a 50,000 year pollen record from the Amazon fan, ODP site 932. *Quat. Res.* **51**, 27-38.

Haffer J. (1969) Speciation in Amazonian forest birds. *Science* **165**, 131-137.

Häggi C., Chiessi C. M.and Schefuß E. (2015) Testing the D / H ratio of alkenones and palmitic acid as salinity proxies in the Amazon Plume. *Biogeosciences* **12**, 7239-7249.

Häggi C., Sawakuchi A. O., Chiessi C. M., Mulitza S., Mollenhauer G., Sawakuchi H. O., Baker P. A., Zabel M.and Schefuß E. (2016) Origin, transport and deposition of leaf-wax biomarkers in the Amazon Basin and the adjacent Atlantic. *Geochim. Cosmochim. Acta* **192**, 149-165.

Hall D. M.and Jones R. L. (1961) Physiological Significance of Surface Wax on Leaves. *Nature* **191**, 95-96.

Hamilton S. K., Sippel S. J.and Melack J. M. (2004) Seasonal inundation patterns in two large savanna floodplains of South America: the Llanos de Moxos (Bolivia) and the Llanos del Orinoco (Venezuela and Colombia). *Hydrol. Process.* **18**, 2103-2116.

Harada N., Shin K. H., Murata A., Uchida M.and Nakatani T. (2003) Characteristics of alkenones synthesized by a bloom of Emiliania huxleyi in the Bering Sea. *Geochim. Cosmochim. Acta* **67**, 1507-1519.

Hays J. D., Imbrie J.and Shackleton N. J. (1976) Variations in the Earth's Orbit: Pacemaker of the Ice Ages. *Science* **194**, 1121-1132.

Heckenberger M. J., Kuikuro A., Kuikuro U. T., Russell J. C., Schmidt M., Fausto C.and Franchetto B. (2003) Amazonia 1492: Pristine Forest or Cultural Parkland? *Science* **301**, 1710-1714.

Hedges J. I., Mayorga E., Tsamakis E., McClain M. E., Aufdenkampe A., Quay P., Richey J. E., Benner R., Opsahl S., Black B., Pimentel T., Quintanilla J.and Maurice L. (2000) Organic matter in Bolivian tributaries of the Amazon River: A comparison to the lower mainstream. *Limnol. Oceanogr.* **45**, 1449-1466.

Heinrich H. (1988) Origin and consequences of cyclic ice rafting in the Northeast Atlantic Ocean during the past 130,000 years. *Quat. Res.* **29**, 142-152.

Hessler I., Dupont L., Bonnefille R., Behling H., Gonzalez C., Helmens K. F., Hooghiemstra H., Lebamba J., Ledru M. P., Lezine A. M., Maley J., Marret F.and Vincens A. (2010) Millennial-scale changes in vegetation records from tropical Africa and South America during the last glacial. *Quat. Sci. Rev.* **29**, 2882-2899.

Hijmans R. J., Cameron S. E., Parra J. L., Jones P. G.and Jarvis A. (2005) Very high resolution interpolated climate surfaces for global land areas. *Int. J. Climatol.* **25**, 1965-1978.

Hirota M., Holmgren M., Van Nes E. H.and Scheffer M. (2011) Global Resilience of Tropical Forest and Savanna to Critical Transitions. *Science* **334**, 232-235.

Hoorn C., Wesselingh F. P., ter Steege H., Bermudez M. A., Mora A., Sevink J., Sanmartin I., Sanchez-Meseguer A., Anderson C. L., Figueiredo J. P., Jaramillo C., Riff D., Negri F. R., Hooghiemstra H., Lundberg J., Stadler T., Sarkinen T.and Antonelli A. (2010) Amazonia Through Time: Andean Uplift, Climate Change, Landscape Evolution, and Biodiversity. *Science* **330**, 927-931.

Hou J. Z., D'Andrea W. J.and Huang Y. S. (2008) Can sedimentary leaf waxes record D/H ratios of continental precipitation? Field, model, and experimental assessments. *Geochim. Cosmochim. Acta* **72**, 3503-3517.

Houghton R. A., Lawrence K. T., Hackler J. L.and Brown S. (2001) The spatial distribution of forest biomass in the Brazilian Amazon: a comparison of estimates. *Glob. Change Biol.* **7**, 731-746.

Huang Y., Street-Perrott F. A., Metcalfe S. E., Brenner M., Moreland M.and Freeman K. H. (2001) Climate Change as the Dominant Control on Glacial-Interglacial Variations in C3 and C4 Plant Abundance. *Science* **293**, 1647-1651.

Huang Y. S., Shuman B., Wang Y.and Webb T. (2002) Hydrogen isotope ratios of palmitic acid in lacustrine sediments record late Quaternary climate variations. *Geology* **30**, 1103-1106.

- (2004) Hydrogen isotope ratios of individual lipids in lake sediments as novel tracers of climatic and environmental change: a surface sediment test. *J. Paleolimn.* **31**, 363-375.

Hughen K. A., Eglinton T. I., Xu L.and Makou M. (2004) Abrupt tropical vegetation response to rapid climate changes. *Science* **304**, 1955-1959.

Huntingford C., Zelazowski P., Galbraith D., Mercado L. M., Sitch S., Fisher R., Lomas M., Walker A. P., Jones C. D., Booth B. B. B., Malhi Y., Hemming D., Kay G., Good P., Lewis S. L., Phillips O. L., Atkin O. K., Lloyd J., Gloor E., Zaragoza-Castells J., Meir P., Betts R., Harris P. P., Nobre C., Marengo J.and Cox P. M. (2013) Simulated resilience of tropical rainforests to CO2-induced climate change. *Nature Geosci* **6**, 268-273.

Ishiwatari R., Uzaki M.and Yamada K. (1994) Carbon isotope composition of individual n-alkanes in recent sediments. *Org. Geochem.* **21**, 801-808.

Jaeschke A., Rühlemann C., Arz H., Heil G.and Lohmann G. (2007) Coupling of millennial-scale changes in sea surface temperature and precipitation off northeastern Brazil with high-latitude climate shifts during the last glacial period. *Paleoceanography* **22**, 2006PA001391.

Jeng W.-L. (2006) Higher plant n-alkane average chain length as an indicator of petrogenic hydrocarbon contamination in marine sediments. *Marine Chemistry* **102**, 242-251.

Jenkins C. N., Pimm S. L.and Joppa L. N. (2013) Global patterns of terrestrial vertebrate diversity and conservation. *Proceedings of the National Academy of Sciences* **110**, 2602-2610.

Jiménez-Muñoz J. C., Mattar C., Barichivich J., Santamaría-Artigas A., Takahashi K., Malhi Y., Sobrino J. A.and Schrier G. v. d. (2016) Record-breaking warming and extreme drought in the Amazon rainforest during the course of El Niño 2015–2016. *Scientific Reports* **6**, 33130.

Kahmen A., Simonin K., Tu K. P., Merchant A., Callister A., Siegwolf R., Dawson T. E.and Arndt S. K. (2008) Effects of environmental parameters, leaf physiological properties and leaf water relations on leaf water delta(18)O enrichment in different Eucalyptus species. *Plant Cell Environ.* **31**, 738-751.

Kanner L. C., Burns S. J., Cheng H.and Edwards R. L. (2012) High-Latitude Forcing of the South American Summer Monsoon During the Last Glacial. *Science* **335**, 570-573.

Karr J. D.and Showers W. J. (2002) Stable oxygen and hydrogen isotopic tracers in Amazon shelf waters during Amasseds. *Oceanol. Acta* **25**, 71-78.

Kasper S., van der Meer M. T. J., Castañeda I. S., Tjallingii R., Brummer G.-J. A., Sinninghe Damsté J. S.and Schouten S. (2015) Testing the alkenone D/H ratio as a paleo indicator of sea surface salinity in a coastal ocean margin (Mozambique Channel). *Org. Geochem.* **78**, 62-68.

Kineke G. C.and Sternberg R. W. (1995) Distribution of fluid muds on the Amazon continental shelf. *Marine Geology* **125**, 193-233.

Konhauser K. O., Fyfe W. S.and Kronberg B. I. (1994) Multi-element chemistry of some Amazonian waters and soils. *Chemical Geology* **111**, 155-175.

Kourounioti R. L. A., Band L. R., Fozard J. A., Hampstead A., Lovrics A., Moyroud E., Vignolini S., King J. R., Jensen O. E.and Glover B. J. (2013) Buckling as an origin of ordered cuticular patterns in flower petals. *Journal of The Royal Society Interface* **10**, 20120847.

Kucera M. (2007) Planktonic foraminifera as tracers of past oceanic environments. *Developments in marine geology* **1**, 213-262.

Lea D. W., Pak D. K.and Spero H. J. (2000) Climate impact of late Quaternary equatorial Pacific sea surface temperature variations. *Science* **289**, 1719-1724.

Lee S.-Y., Chiang J. C. H.and Chang P. (2014) Tropical Pacific response to continental ice sheet topography. *Clim. Dyn.* **44**, 2429-2446.

Lentz S. J.and Limeburner R. (1995) The Amazon River Plume during AMASSEDS - Spatial characteristics and salinity variability. *J. Geophys. Res.-Oceans* **100**, 2355-2375.

Levine N. M., Zhang K., Longo M., Baccini A., Phillips O. L., Lewis S. L., Alvarez-Dávila E., Segalin de Andrade A. C., Brienen R. J. W., Erwin T. L., Feldpausch T. R., Monteagudo Mendoza A. L., Nuñez Vargas P., Prieto A., Silva-Espejo J. E., Malhi Y.and Moorcroft P. R. (2016) Ecosystem heterogeneity determines the ecological resilience of the Amazon to climate change. *Proceedings of the National Academy of Sciences* **113**, 793-797.

Li C., Sessions A. L., Kinnaman F. S.and Valentine D. L. (2009) Hydrogen-isotopic variability in lipids from Santa Barbara Basin sediments. *Geochim. Cosmochim. Acta* **73**, 4803-4823.

Li C., Sessions A. L., Valentine D. L.and Thiagarajan N. (2011a) D/H variation in terrestrial lipids from Santa Barbara Basin over the past 1400 years: A preliminary assessment of paleoclimatic relevance. *Org. Geochem.* **42**, 15-24.

Li W. H., Zhang P. F., Ye J. S., Li L. F.and Baker P. A. (2011b) Impact of two different types of El Nino events on the Amazon climate and ecosystem productivity. *J. Plant Ecol.* **4**, 91-99.

Lichtfouse É.and Eglinton T. I. (1995) 13C and 14C evidence of pollution of a soil by fossil fuel and reconstruction of the composition of the pollutant. *Org. Geochem.* **23**, 969-973.

Lisiecki L. E.and Raymo M. E. (2005) A Pliocene-Pleistocene stack of 57 globally distributed benthic delta O-18 records. *Paleoceanography* **20**, PA1003.

Lorenz R., Pitman A. J.and Sisson S. A. (2016) Does Amazonian deforestation cause global effects; can we be sure? *J. Geophys. Res.-Atmos.* **121**, 5567-5584.

Lüthi D., Le Floch M., Bereiter B., Blunier T., Barnola J.-M., Siegenthaler U., Raynaud D., Jouzel J., Fischer H., Kawamura K.and Stocker T. F. (2008) High-resolution carbon dioxide concentration record 650,000-800,000 years before present. *Nature* **453**, 379-382.

M'Boule D., Chivall D., Sinke-Schoen D., Sinninghe-Damsté J. S., Schouten S.and van der Meer M. T. J. (2014) Salinity dependent hydrogen isotope fractionation in alkenones produced by coastal and open ocean haptophyte algae. *Geochim. Cosmochim. Acta* **130**, 126-135.

Maffei M. (1996) Chemotaxonomic significance of leaf wax alkanes in the gramineae. *Biochem. Syst. Ecol.* **24**, 53-64.

Maioli O. L. G., de Oliveira C. R., Dal Sasso M. A., Madureira L. A. d. S., Azevedo D. d. A.and de Aquino Neto F. R. (2012) Evaluation of the organic matter sources using the δ13C composition of individual n-alkanes in sediments from Brazilian estuarine systems by GC/C/IRMS. *Estuarine, Coastal and Shelf Science* **114**, 140-147.

Malhi Y., Roberts J. T., Betts R. A., Killeen T. J., Li W. H.and Nobre C. A. (2008) Climate change, deforestation, and the fate of the Amazon. *Science* **319**, 169-172.

Marengo J. A., Soares W. R., Saulo C.and Nicolini M. (2004) Climatology of the low-level jet east of the Andes as derived from the NCEP-NCAR reanalyses: Characteristics and temporal variability. *J. Clim.* **17**, 2261-2280.

Marlowe I. T., Brassell S. C., Eglinton G.and Green J. C. (1990) Long-Chain Alkenones and Alkyl Alkenoates and the Fossil Coccolith Record of Marine Sediments. *Chemical Geology* **88**, 349-375.

Marlowe I. T., Green J. C., Neal A. C., Brassell S. C., Eglinton G.and Course P. A. (1984) Long-Chain (n-C37-C39) Alkenones in the Prymnesiophyceae - Distribution of Alkenones and other Lipids and their Taxonomic Significance. *British Phycological Journal* **19**, 203-216.

Maslin M. A., Ettwein V. J., Boot C. S., Bendle J.and Pancost R. D. (2012) Amazon Fan biomarker evidence against the Pleistocene rainforest refuge hypothesis? *Journal of Quaternary Science* **27**, 451-460.

Mayer L. M. (1994) Relationships between mineral surfaces and organic carbon concentrations in soils and sediments. *Chemical Geology* **114**, 347-363.

Mayle F. E., Burbridge R.and Killeen T. J. (2000) Millennial-scale dynamics of southern Amazonian rain forests. *Science* **290**, 2291-2294.

Mayorga E., Aufdenkampe A. K., Masiello C. A., Krusche A. V., Hedges J. I., Quay P. D., Richey J. E.and Brown T. A. (2005) Young organic matter as a source of carbon dioxide outgassing from Amazonian rivers. *Nature* **436**, 538-541.

McCarroll D.and Loader N. J. (2004) Stable isotopes in tree rings. *Quat. Sci. Rev.* **23**, 771-801.

McClain M. E.and Naiman R. J. (2008) Andean influences on the biogeochemistry and ecology of the Amazon River. *Bioscience* **58**, 325-338.

McConnell M. C., Thunell R. C., Lorenzoni L., Astor Y., Wright J. D.and Fairbanks R. (2009) Seasonal variability in the salinity and oxygen isotopic composition of seawater from the Cariaco Basin, Venezuela: Implications for paleosalinity reconstructions. *Geochemistry, Geophysics, Geosystems* **10**, Q06019.

Meade R. H., Dunne T., Richey J. E., De M. Santos U.and Salati E. (1985) Storage and Remobilization of Suspended Sediment in the Lower Amazon River of Brazil. *Science* **228**, 488-490.

Merkel U., Prange M.and Schulz M. (2010) ENSO variability and teleconnections during glacial climates. *Quat. Sci. Rev.* **29**, 86-100.

Milankovitch M., 1920, Théorie mathématique des phénomènes thermiques produits par la radiation solaire, Paris, Gauthier Villars.

Molleri G. S. F., Novo E.and Kampel M. (2010) Space-time variability of the Amazon River plume based on satellite ocean color. *Cont. Shelf Res.* **30**, 342-352.

Moreira-Turcq P., Bonnet M. P., Amorim M., Bernardes M., Lagane C., Maurice L., Perez M.and Seyler P. (2013) Seasonal variability in concentration, composition, age, and fluxes of particulate organic carbon exchanged between the floodplain and Amazon River. *Glob. Biogeochem. Cycle* **27**, 119-130.

Moreira-Turcq P., Jouanneau J. M., Turcq B., Seyler P., Weber O.and Guyot J. L. (2004) Carbon sedimentation at Lago Grande de Curuai, a floodplain lake in the low Amazon region: insights into sedimentation rates. *Palaeogeography, Palaeoclimatology, Palaeoecology* **214**, 27-40.

Moreira-Turcq P., Seyler P., Guyot J. L.and Etcheber H. (2003) Exportation of organic carbon from the Amazon River and its main tributaries. *Hydrol. Process.* **17**, 1329-1344.

Mosblech N. A. S., Bush M. B., Gosling W. D., Hodell D., Thomas L., van Calsteren P., Correa-Metrio A., Valencia B. G., Curtis J.and van Woesik R. (2012) North Atlantic forcing of Amazonian precipitation during the last ice age. *Nat. Geosci.* **5**, 817-820.

Moy C. M., Seltzer G. O., Rodbell D. T.and Anderson D. M. (2002) Variability of El Nino/Southern Oscillation activity at millennial timescales during the Holocene epoch. *Nature* **420**, 162-165.

Mulitza S., Chiessi C. M., Cruz A. P. S., Frederichs T., Gomes J. G., Gurgel M. H., Haberkern J., Huang E., Jovane L., Kuhnert H., Pittauerová D., Reiners S.-J., Roud S. C., Schefuß E., Schewe F., Schwenk T. A., Sicoli Seoane J. C., Sousa S. H. M., Wagner D. J.and Wiers S. (2013) Response of Amazon sedimentation to deforestation, land use and climate variability – Cruise No. MSM20/3 - February 19 - March 11, 2012 - Recife (Brazil) - Bridgetown (Barbados). Berichte, Fachbereich Geowissenschaften, Universität Bremen, Bremen, Germany, 2013, 1-86.

Muller-Karger F. E., McClain C. R.and Richardson P. L. (1988) The dispersal of the Amazon's water. *Nature* **333**, 56-59.

Müller P. J., Kirst G., Ruhland G., von Storch I.and Rosell-Mele A. (1998) Calibration of the alkenone paleotemperature index U-37(K ') based on core-tops from the eastern South Atlantic and the global ocean (60 degrees N-60 degrees S). *Geochim. Cosmochim. Acta* **62**, 1757-1772.

Nelson D. B.and Sachs J. P. (2014) The influence of salinity on D/H fractionation in dinosterol and brassicasterol from globally distributed saline and hypersaline lakes. *Geochim. Cosmochim. Acta* **133**, 325-339.

NGRIP Project members (2004) High-resolution record of Northern Hemisphere climate extending into the last interglacial period. *Nature* **431**, 147-151.

Nogueira A. C. R., Silveira R.and Guimarães J. T. F. (2013) Neogene–Quaternary sedimentary and paleovegetation history of the eastern Solimões Basin, central Amazon region. *J. South Am. Earth Sci.* **46**, 89-99.

O'Leary M. H. (1981) Carbon isotope fractionation in plants. *Phytochemistry* **20**, 553-567.

Olson D. M., Dinerstein E., Wikramanayake E. D., Burgess N. D., Powell G. V. N., Underwood E. C., D'Amico J. A., Itoua I., Strand H. E., Morrison J. C., Loucks C. J., Allnutt T. F., Ricketts T. H.,

Kura Y., Lamoreux J. F., Wettengel W. W., Hedao P.and Kassem K. R. (2001) Terrestrial ecoregions of the worlds: A new map of life on Earth. *Bioscience* **51**, 933-938.

Ono M., Sawada K., Kubota M.and Shiraiwa Y. (2009) Change of the unsaturation degree of alkenone and alkenoate during acclimation to salinity change in Emiliania huxleyi and Gephyrocapsa oceanica with reference to palaeosalinity indicator. *Res. Org. Geochem* **25**, 53-60.

Pahnke K., Sachs J. P., Keigwin L., Timmermann A.and Xie S. P. (2007) Eastern tropical Pacific hydrologic changes during the past 27,000 years from D/H ratios in alkenones. *Paleoceanography* **22**, PA4214.

Pancost R. D.and Boot C. S. (2004) The palaeoclimatic utility of terrestrial biomarkers in marine sediments. *Marine Chemistry* **92**, 239-261.

Pearson A., McNichol A. P., Benitez-Nelson B. C., Hayes J. M.and Eglinton T. I. (2001) Origins of lipid biomarkers in Santa Monica Basin surface sediment: A case study using compound-specific Delta C-14 analysis. *Geochim. Cosmochim. Acta* **65**, 3123-3137.

Peel M. C., Finlayson B. L.and McMahon T. A. (2007) Updated world map of the Köppen-Geiger climate classification. *Hydrol. Earth Syst. Sci.* **11**, 1633-1644.

Pennington R. T., Lavin M., Prado D. E., Pendry C. A., Pell S. K.and Butterworth C. A. (2004) Historical climate change and speciation: neotropical seasonally dry forest plants show patterns of both Tertiary and Quaternary diversification. *Philos. Trans. R. Soc. B-Biol. Sci.* **359**, 515-537.

Pennington R. T., Prado D. E.and Pendry C. A. (2000) Neotropical seasonally dry forests and Quaternary vegetation changes. *J. Biogeogr.* **27**, 261-273.

Perry G. J., Volkman J. K., Johns R. B.and Bavor Jr H. J. (1979) Fatty acids of bacterial origin in contemporary marine sediments. *Geochim. Cosmochim. Acta* **43**, 1715-1725.

Peterson L. C., Haug G. H., Hughen K. A.and Rohl U. (2000) Rapid changes in the hydrologic cycle of the tropical Atlantic during the last glacial. *Science* **290**, 1947-1951.

Phillips O. L., Aragao L., Lewis S. L., Fisher J. B., Lloyd J., Lopez-Gonzalez G., Malhi Y., Monteagudo A., Peacock J., Quesada C. A., van der Heijden G., Almeida S., Amaral I., Arroyo L., Aymard G., Baker T. R., Banki O., Blanc L., Bonal D., Brando P., Chave J., de Oliveira A. C. A., Cardozo N. D., Czimczik C. I., Feldpausch T. R., Freitas M. A., Gloor E., Higuchi N., Jimenez E., Lloyd G., Meir P., Mendoza C., Morel A., Neill D. A., Nepstad D., Patino S., Penuela M. C., Prieto A., Ramirez F., Schwarz M., Silva J., Silveira M., Thomas A. S., ter Steege H., Stropp J., Vasquez R., Zelazowski P., Davila E. A., Andelman S., Andrade A., Chao K. J., Erwin T., Di Fiore A., Honorio E., Keeling H., Killeen T. J., Laurance W. F., Cruz A. P., Pitman N. C. A., Vargas P. N., Ramirez-Angulo H., Rudas A., Salamao R., Silva N., Terborgh J.and Torres-Lezama A. (2009) Drought Sensitivity of the Amazon Rainforest. *Science* **323**, 1344-1347.

Polissar P. J.and Freeman K. H. (2010) Effects of aridity and vegetation on plant-wax δD in modern lake sediments. *Geochim. Cosmochim. Acta* **74**, 5785-5797.

Ponton C., West A. J., Feakins S. J.and Galy V. (2014) Leaf wax biomarkers in transit record river catchment composition. *Geophys. Res. Lett.* **41**, 6420–6427.

Powell R. L., Yoo E. H.and Still C. J. (2012) Vegetation and soil carbon-13 isoscapes for South America: integrating remote sensing and ecosystem isotope measurements. *Ecosphere* **3**, 109.

Prahl F. G., Muehlhausen L. A.and Zahnle D. L. (1988) Further Evalutation of Long-Chain Alkenones as Indicators of Paleoceanographic Conditions. *Geochim. Cosmochim. Acta* **52**, 2303-2310.

Prahl F. G.and Wakeham S. G. (1987) Calibration of unsaturation patterns in long-chain ketone compositions or paleotemperature assessment. *Nature* **330**, 367-369.

Putzer H. (1984) The geological evolution of the Amazon basin and its mineral resources. In *The Amazon: Limnology and landscape ecology of a mighty tropical river and its basin.* (Ed. H. Sioli). Springer Netherlands, Dordrecht pp. 15-46.

Quay P. D., Wilbur D. O., Richey J. E., Hedges J. I., Devol A. H.and Victoria R. (1992) Carbon Cycling in the Amazon River: Implicatons from the C-13 Compositions of Particles and Solutes. *Limnol. Oceanogr.* **37**, 857-871.

Quijada-Mascareñas J. A., Ferguson J. E., Pook C. E., Salomão M. D. G., Thorpe R. S.and Wüster W. (2007) Phylogeographic patterns of trans-Amazonian vicariants and Amazonian biogeography: the Neotropical rattlesnake (Crotalus durissus complex) as an example. *J. Biogeogr.* **34**, 1296-1312.

Rasmussen T. L., Oppo D. W., Thomsen E.and Lehman S. J. (2003) Deep sea records from the southeast Labrador Sea: Ocean circulation changes and ice-rafting events during the last 160,000 years. *Paleoceanography* **18**.

Raymo M. E.and Huybers P. (2008) Unlocking the mysteries of the ice ages. *Nature* **451**, 284-285.

Reimer P. J., Bard E., Bayliss A., Beck J. W., Blackwell P. G., Ramsey C. B., Buck C. E., Cheng H., Edwards R. L., Friedrich M., Grootes P. M., Guilderson T. P., Haflidason H., Hajdas I., Hatte C., Heaton T. J., Hoffmann D. L., Hogg A. G., Hughen K. A., Kaiser K. F., Kromer B., Manning S. W., Niu M., Reimer R. W., Richards D. A., Scott E. M., Southon J. R., Staff R. A., Turney C. S. M.and van der Plicht J. (2013) INTCAL13 and MARINE13 Radiocarbon age calibration curves 0-50000 years cal BP. *Radiocarbon* **55**, 1869-1887.

Ribas C. C., Aleixo A., Nogueira A. C. R., Miyaki C. Y.and Cracraft J. (2012) A palaeobiogeographic model for biotic diversification within Amazonia over the past three million years. *Proceedings of the Royal Society B: Biological Sciences* **279**, 681-689.

Ribeiro V., Werneck F. P.and Machado R. B. (2016) Distribution dynamics of South American savanna birds in response to Quaternary climate change. *Austral Ecology* **41**, 768–777.

Richey J. E., Hedges J. I., Devol A. H., Quay P. D., Victoria R., Martinelli L.and Forsberg B. R. (1990) Biogeochemistry of carbon in the Amazon River. *Limnol. Oceanogr.* **35**, 352-371.

Richey J. E., Melack J. M., Aufdenkampe A. K., Ballester V. M.and Hess L. L. (2002) Outgassing from Amazonian rivers and wetlands as a large tropical source of atmospheric CO2. *Nature* **416**, 617-620.

Rieley G., Collier R. J., Jones D. M., Eglinton G., Eakin P. A.and Fallick A. E. (1991) Sources of sedimentary lipids deduced from stable carbon-isotope analyses of individual compounds. *Nature* **352**, 425-427.

Rohling E. J. (2007) Progress in paleosalinity: Overview and presentation of a new approach. *Paleoceanography* **22**, PA3215.

Rohling E. J.and Bigg G. R. (1998) Paleosalinity and δ18O: A critical assessment. *Journal of Geophysical Research: Oceans* **103**, 1307-1318.

Rommerskirchen F., Eglinton G., Dupont L., Güntner U., Wenzel C.and Rullkötter J. (2003) A north to south transect of Holocene southeast Atlantic continental margin sediments: Relationship between aerosol transport and compound-specific δ13C land plant biomarker and pollen records. *Geochemistry, Geophysics, Geosystems* **4**, 1101–1128.

Rosell-Mele A., Carter J.and Eglinton G. (1994) Distributions of long-chain alkenones and alkyl alkenoates in marine surface sediments from the North-East Atlantic. *Org. Geochem.* **22**, 501-509.

Rostek F., Ruhland G., Bassinot F. C., Muller P. J., Labeyrie L. D., Lancelot Y.and Bard E. (1993) Reconstructing Sea-Surface Temperature and Salinity using Delta-O-18 and Alkenone Records. *Nature* **364**, 319-321.

Rühlemann C.and Butzin M. (2006) Alkenone temperature anomalies in the Brazil-Malvinas Confluence area caused by lateral advection of suspended particulate material. *Geochem. Geophys. Geosyst.* **7**, Q10015.

Rühlemann C., Mulitza S., Muller P. J., Wefer G.and Zahn R. (1999) Warming of the tropical Atlantic Ocean and slowdown of thermohaline circulation during the last deglaciation. *Nature* **402**, 511-514.

Russell J. M., Vogel H., Konecky B. L., Bijaksana S., Huang Y. S., Melles M., Wattrus N., Costa K.and King J. W. (2014) Glacial forcing of central Indonesian hydroclimate since 60,000 y BP. *Proc. Natl. Acad. Sci. U. S. A.* **111**, 5100-5105.

Rustan A. C.and Drevon C. A. (2001) Fatty Acids: Structures and Properties. In *Encyclopedia of Life Sciences.* John Wiley & Sons, Ltd.

Sachse D., Billault I., Bowen G. J., Chikaraishi Y., Dawson T. E., Feakins S. J., Freeman K. H., Magill C. R., McInerney F. A., van der Meer M. T. J., Polissar P., Robins R. J., Sachs J. P., Schmidt H. L., Sessions A. L., White J. W. C., West J. B.and Kahmen A. (2012) Molecular Paleohydrology: Interpreting the Hydrogen- Isotopic Composition of Lipid Biomarkers from Photosynthesizing Organisms. *Annu. Rev. Earth. Planet. Sci.* **40**, 221-249.

Sachse D., Radke J.and Gleixner G. (2004) Hydrogen isotope ratios of recent lacustrine sedimentary n-alkanes record modern climate variability. *Geochim. Cosmochim. Acta* **68**, 4877-4889.

Sachse D.and Sachs J. P. (2008) Inverse relationship between D/H fractionation in cyanobacterial lipids and salinity in Christmas Island saline ponds. *Geochim. Cosmochim. Acta* **72**, 793-806.

Salati E., Dall'Olio A., Matsui E.and Gat J. R. (1979) Recycling of water in the Amazon Basin: An isotopic study. *Water Resour. Res.* **15**, 1250-1258.

Santos M. L. S., Muniz K., Barros-Neto B.and Araujo M. (2008) Nutrient and phytoplankton biomass in the Amazon River shelf waters. *An. Acad. Bras. Cienc.* **80**, 703-717.

Sauer P. E., Eglinton T. I., Hayes J. M., Schimmelmann A.and Sessions A. L. (2001) Compound-specific D/H ratios of lipid biomarkers from sediments as a proxy for environmental and climatic conditions. *Geochim. Cosmochim. Acta* **65**, 213-222.

Sawakuchi H. O., Bastviken D., Sawakuchi A. O., Krusche A. V., Ballester M. V. R.and Richey J. E. (2014) Methane emissions from Amazonian Rivers and their contribution to the global methane budget. *Glob. Change Biol.* **20**, 2829-2840.

Sbrocco E. J.and Barber P. H. (2013) MARSPEC: ocean climate layers for marine spatial ecology. *Ecology* **94**, 979-979.

Schefuß E., Ratmeyer V., Stuut J.-B. W., Jansen J. H. F.and Sinninghe Damsté J. S. (2003) Carbon isotope analyses of n-alkanes in dust from the lower atmosphere over the central eastern Atlantic. *Geochim. Cosmochim. Acta* **67**, 1757-1767.

Schefuß E., Schouten S.and Schneider R. R. (2005) Climatic controls on central African hydrology during the past 20,000 years. *Nature* **437**, 1003-1006.

Schimmelmann A., Sessions A. L.and Mastalerz M. (2006) Hydrogen Isotopic (D/H) composition of organic matter during diagensis and thermal maturation. *Annual Review of Earth and Planetary Sciences* **34**, 501-533.

Schmidt F., Oberhansli H.and Wilkes H. (2014) Biocoenosis response to hydrological variability in Southern Africa during the last 84 ka BP: A study of lipid biomarkers and compound-specific stable carbon and hydrogen isotopes from the hypersaline Lake Tswaing. *Glob. Planet. Change* **112**, 92-104.

Schneider T., Bischoff T.and Haug G. H. (2014) Migrations and dynamics of the intertropical convergence zone. *Nature* **513**, 45-53.

Schouten S., Hopmans E. C., Schefuss E.and Damste J. S. S. (2002) Distributional variations in marine crenarchaeotal membrane lipids: a new tool for reconstructing ancient sea water temperatures? *Earth Planet. Sci. Lett.* **204**, 265-274.

Schouten S., Ossebaar J., Schreiber K., Kienhuis M. V. M., Langer G., Benthien A.and Bijma J. (2006) The effect of temperature, salinity and growth rate on the stable hydrogen isotopic composition of long chain alkenones produced by Emiliania huxleyi and Gephyrocapsa oceanica. *Biogeosciences* **3**, 113-119.

Schwab V. F.and Sachs J. P. (2009) The measurement of D/H ratio in alkenones and their isotopic heterogeneity. *Org. Geochem.* **40**, 111-118.

Schwab V. F.and Sachs J. P. (2011) Hydrogen isotopes in individual alkenones from the Chesapeake Bay estuary. *Geochim. Cosmochim. Acta* **75**, 7552-7565.

Sessions A. L., Burgoyne T. W., Schimmelmann A.and Hayes J. M. (1999) Fractionation of hydrogen isotopes in lipid biosynthesis. *Org. Geochem.* **30**, 1193-1200.

Severinghaus J. P., Beaudette R., Headly M. A., Taylor K.and Brook E. J. (2009) Oxygen-18 of O-2 Records the Impact of Abrupt Climate Change on the Terrestrial Biosphere. *Science* **324**, 1431-1434.

Shuman B., Huang Y. S., Newby P.and Wang Y. (2006) Compound-specific isotopic analyses track changes in seasonal precipitation regimes in the Northeastern United States at ca 8200cal yrBP. *Quat. Sci. Rev.* **25**, 2992-3002.

Smith B. T., McCormack J. E., Cuervo A. M., Hickerson M. J., Aleixo A., Cadena C. D., Perez-Eman J., Burney C. W., Xie X., Harvey M. G., Faircloth B. C., Glenn T. C., Derryberry E. P., Prejean J., Fields S.and Brumfield R. T. (2014) The drivers of tropical speciation. *Nature* **515**, 406-409.

Smith F. A.and Freeman K. H. (2006) Influence of physiology and climate on δD of leaf wax n-alkanes from C3 and C4 grasses. *Geochim. Cosmochim. Acta* **70**, 1172-1187.

Smith W. O.and Demaster D. J. (1996) Phytoplankton biomass and productivity in the Amazon River plume: Correlation with seasonal river discharge. *Cont. Shelf Res.* **16**, 291-319.

Smittenberg R. H., Saenger C., Dawson M. N.and Sachs J. P. (2011) Compound-specific D/H ratios of the marine lakes of Palau as proxies for West Pacific Warm Pool hydrologic variability. *Quat. Sci. Rev.* **30**, 921-933.

Sternberg L. D. L. (1988) D/H ratios of environmental water recorded by D/H ratios of plant lipids. *Nature* **333**, 59-61.

Sun M. Y.and Wakeham S. G. (1994) Molecular evidence for degradation and preservation of organic matter in the anoxic Black-Sea Basin. *Geochim. Cosmochim. Acta* **58**, 3395-3406.

Sun Q., Chu G. Q., Liu G. X., Li S.and Wang X. H. (2007) Calibration of alkenone unsaturation index with growth temperature for a lacustrine species, Chrysotila lamellosa (Haptophyceae). *Org. Geochem.* **38**, 1226-1234.

Tierney J. E.and deMenocal P. B. (2013) Abrupt Shifts in Horn of Africa Hydroclimate Since the Last Glacial Maximum. *Science* **342**, 843-846.

Tierney J. E., Russell J. M., Huang Y., Sinninghe Damsté J. S., Hopmans E. C.and Cohen A. S. (2008) Northern Hemisphere Controls on Tropical Southeast African Climate During the Past 60,000 Years. *Science* **322**, 252-255.

Tipple B. J.and Pagani M. (2007) The early origins of terrestrial C(4) photosynthesis. In *Annual Review of Earth and Planetary Sciences.* Annual Reviews, Palo Alto pp. 435-461.

Townsend-Small A., Noguera J. L., McClain M. E.and Brandes J. A. (2007) Radiocarbon and stable isotope geochemistry of organic matter in the Amazon headwaters, Peruvian Andes. *Glob. Biogeochem. Cycle* **21**, GB2029.

van der Hammen T.and Absy M. L. (1994) Amazonia during the last glacial. *Palaeogeography, Palaeoclimatology, Palaeoecology* **109**, 247-261.

van der Hammen T.and Hooghiemstra H. (2000) Neogene and Quaternary history of vegetation, climate, and plant diversity in Amazonia. *Quat. Sci. Rev.* **19**, 725-742.

van der Meer M. T. J., Baas M., Rijpstra W. I. C., Marino G., Rohling E. J., Sinninghe Damsté J. S.and Schouten S. (2007) Hydrogen isotopic compositions of long-chain alkenones record freshwater flooding of the Eastern Mediterranean at the onset of sapropel deposition. *Earth Planet. Sci. Lett.* **262**, 594-600.

van der Meer M. T. J., Benthien A., Bijma J., Schouten S.and Sinninghe Damsté J. S. (2013) Alkenone distribution impacts the hydrogen isotopic composition of the C-37:2 and C-37:3 alkan-2-ones in Emiliania huxleyi. *Geochim. Cosmochim. Acta* **111**, 162-166.

van der Meer M. T. J., Sangiorgi F., Baas M., Brinkhuis H., Sinninghe Damsté J. S.and Schouten S. (2008) Molecular isotopic and dinoflagellate evidence for Late Holocene freshening of the Black Sea. *Earth Planet. Sci. Lett.* **267**, 426-434.

van der Merwe N. J.and Medina E. (1991) The canopy effect, carbon isotope ratios and foodwebs in amazonia. *Journal of Archaeological Science* **18**, 249-259.

Vecchi G. A.and Soden B. J. (2007) Global Warming and the Weakening of the Tropical Circulation. *J. Clim.* **20**, 4316-4340.

Venetz I. (1833) Mémoire sur les variations de la temperature dans les Alps de la Suisse. *Denkschriften der Allgemeinen Schweizerischen Gesellschaft für die Gesamte Natur* **1**, 1–38.

Versteegh G. J. M., Riegman R., de Leeuw J. W.and Jansen J. H. F. (2001) U(37)(K ')values for Isochrysis galbana as a function of culture temperature, light intensity and nutrient concentrations. *Org. Geochem.* **32**, 785-794.

Vogts A., Schefuß E., Badewien T.and Rullkötter J. (2012) n-Alkane parameters from a deep sea sediment transect off southwest Africa reflect continental vegetation and climate conditions. *Org. Geochem.* **47**, 109-119.

Vuille M., Bradley R. S., Werner M., Healy R.and Keimig F. (2003) Modeling δ18O in precipitation over the tropical Americas: 1. Interannual variability and climatic controls. *Journal of Geophysical Research: Atmospheres* **108**, 4174,.

Wang X. F., Auler A. S., Edwards R. L., Cheng H., Cristalli P. S., Smart P. L., Richards D. A.and Shen C. C. (2004) Wet periods in northeastern Brazil over the past 210 kyr linked to distant climate anomalies. *Nature* **432**, 740-743.

Wang Y. J., Cheng H., Edwards R. L., An Z. S., Wu J. Y., Shen C.-C.and Dorale J. A. (2001) A High-Resolution Absolute-Dated Late Pleistocene Monsoon Record from Hulu Cave, China. *Science* **294**, 2345-2348.

Ward N. D., Keil R. G., Medeiros P. M., Brito D. C., Cunha A. C., Dittmar T., Yager P. L., Krusche A. V.and Richey J. E. (2013) Degradation of terrestrially derived macromolecules in the Amazon River. *Nat. Geosci.* **6**, 530-533.

Werneck F. P., Nogueira C., Colli G. R., Sites J. W.and Costa G. C. (2012) Climatic stability in the Brazilian Cerrado: implications for biogeographical connections of South American savannas, species richness and conservation in a biodiversity hotspot. *J. Biogeogr.* **39**, 1695-1706.

Werth D.and Avissar R. (2002) The local and global effects of Amazon deforestation. *J. Geophys. Res.-Atmos.* **107**, 8087.

Wolhowe M. D., Prahl F. G., Langer G., Oviedo A. M.and Ziveri P. (2015) Alkenone δD as an ecological indicator: A culture and field study of physiologically-controlled chemical and hydrogen-isotopic variation in C37 alkenones. *Geochim. Cosmochim. Acta* **162**, 166-182.

Wolhowe M. D., Prahl F. G., Probert I.and Maldonado M. (2009) Growth phase dependent hydrogen isotopic fractionation in alkenone-producing haptophytes. *Biogeosciences* **6**, 1681-1694.

Wright J. S. (2002) Plant diversity in tropical forests: a review of mechanisms of species coexistence. *Oecologia* **130**, 1-14.

Yeager S. G., Shields C. A., Large W. G.and Hack J. J. (2006) The low-resolution CCSM3. *J. Clim.* **19**, 2545-2566.

Zachos J., Pagani M., Sloan L., Thomas E.and Billups K. (2001) Trends, Rhythms, and Aberrations in Global Climate 65 Ma to Present. *Science* **292**, 686-693.

Zell C., Kim J.-H., Hollander D., Lorenzoni L., Baker P., Silva C. G., Nittrouer C.and Sinninghe Damsté J. S. (2014) Sources and distributions of branched and isoprenoid tetraether lipids on the Amazon shelf and fan: Implications for the use of GDGT-based proxies in marine sediments. *Geochim. Cosmochim. Acta* **139**, 293-312.

Zell C., Kim J. H., Moreira-Turcq P., Abril G., Hopmans E. C., Bonnet M. P., Sobrinho R. L.and Sinnignhe Damsté J. S. (2013) Disentangling the origins of branched tetraether lipids and crenarchaeol in the lower Amazon River: Implications for GDGT-based proxies. *Limnol. Oceanogr.* **58**, 343-353.

Zhang X., Lohmann G., Knorr G.and Purcell C. (2014) Abrupt glacial climate shifts controlled by ice sheet changes. *Nature* **512**, 290-294.

Zhang Y. C., Chiessi C. M., Mulitza S., Zabel M., Trindade R. I. F., Hollanda M., Dantas E. L., Govin A., Tiedemann R.and Wefer G. (2015) Origin of increased terrigenous supply to the NE South American continental margin during Heinrich Stadial 1 and the Younger Dryas. *Earth Planet. Sci. Lett.* **432**, 493-500.

Zhang Z., Sachs J. P.and Marchetti A. (2009) Hydrogen isotope fractionation in freshwater and marine algae: II. Temperature and nitrogen limited growth rate effects. *Org. Geochem.* **40**, 428-439.

Zhang Z. H.and Sachs J. P. (2007) Hydrogen isotope fractionation in freshwater algae: I. Variations among lipids and species. *Org. Geochem.* **38**, 582-608.